12-2014

Adaptive Control for Power System Voltage and Frequency Regulation

Yao Xu
University of Tennessee - Knoxville, yxu25@vols.utk.edu

To the Graduate Council:

I am submitting herewith a dissertation written by Yao Xu entitled "Adaptive Control for Power System Voltage and Frequency Regulation." I have examined the final electronic copy of this dissertation for form and content and recommend that it be accepted in partial fulfillment of the requirements for the degree of Doctor of Philosophy, with a major in Electrical Engineering.

Fangxing Li, Major Professor

We have read this dissertation and recommend its acceptance:

Leon Tolbert, Kevin Tomsovic, Mingzhou Jin

Accepted for the Council:
Carolyn R. Hodges

Vice Provost and Dean of the Graduate School

(Original signatures are on file with official student records.)

Adaptive Control for Power System Voltage and Frequency Regulation

A Dissertation Presented for the

Doctor of Philosophy

Degree

The University of Tennessee, Knoxville

Yao Xu

December 2014

DEDICATION

I dedicate my work to my beloved parents, my dear husband Quan Yuan, and my so loved son Elvis Xu Yuan.

ACKNOWLEDGEMENTS

First and foremost, I thank my advisor, Dr. Fangxing Li, for his continuous guidance and support for this and all other research works during my PhD study at the University of Tennessee.

I also thank my committee members: Dr. Leon M. Tolbert, Dr. Kevin Tomsovic and Dr. Mingzhou Jin for their time and valuable comments on my work.

I also thank to Dr. Stanley McDaniel for editing my dissertation. In addition, I want to thank all students in UT CURENT Lab, including the former alumni from the UT Power Lab. Their efforts and help make my research life colorful here.

Last but not the least, I am greatly indebted to my parents and my husband, for their unconditional love and support which made it possible for me to finish this work.

ABSTRACT

Variable and uncertain wind power output introduces new challenges to power system voltage and frequency stability. To guarantee the safe and stable operation of power systems, the control for voltage and frequency regulation is studied in this work.

Static Synchronous Compensator (STATCOM) can provide fast and efficient reactive power support to regulate system voltage. In the literature, various STATCOM control methods have been discussed, including many applications of proportional–integral (PI) controllers. However, these previous works obtain the PI gains via a trial and error approach or extensive studies with a tradeoff of performance and applicability. Hence, control parameters for the optimal performance at a given operating point may not be effective at a different operating point. To improve the controller's performance, this work proposes a new control model based on adaptive PI control, which can self-adjust the control gains during disturbance, such that the performance always matches a desired response in relation to operating condition changes. Further, a new method called the flatness-based adaptive control (FBAC), for STATCOM is also proposed. By this method, the nonlinear STATCOM variables can easily and exactly be controlled by controlling the flat output without solving differential equations. Further, the control gains can be dynamically tuned to satisfy the time-varying operation condition requirement.

In addition to the voltage control, frequency control is also investigated in this work. Automatic generation control (AGC) is used to regulate the system frequency in power systems. Various control methods have been discussed in order to design control gains and obtain good frequency response performances. However, the control gains obtained by

existing control methods are usually fixed and designed for specific scenarios in the studied power system. The desired response may not be obtained when variable wind power is integrated into power systems. To address these challenges, an adaptive gain-tuning control (AGTC) for AGC with effects of wind resources is presented in this dissertation. By AGTC, the PI control parameters can be automatically and dynamically calculated during the disturbance to make AGC consistently provide excellent performance under variable wind power. Simulation result verifies the advantages of the proposed control strategy.

TABLE OF CONTENTS

LIST OF TABLES

LIST OF FIGURES

CHAPTER 1

INTRODUCTION AND GENERAL INFORMATION

1.1 Power System Stability

1.1.1 Definitions and Classification of Power System Stability

Renewable energy resources have significantly increased in power systems recently. Renewable energy provides 19% of the electricity generation worldwide, and renewable power generators spread in many countries [1]. The report on annual energy outlook in [2] shown in Figure 1.1 indicates that the share of U.S. electricity generation from renewable sources (including conventional hydropower) grew from 9% in 2000 to 12% in 2012, and will grow to 16% in 2040. Unfortunately, renewable energy, especially wind, tends to be variable and uncertain because the wind depends on natural and meteorological conditions [3-4]. This variability introduces many new challenges for power system frequency stability. For example, voltage stability, frequency stability and inter-area oscillation have become greater concerns than before. Therefore, it is necessary to review the specific definition and classification of power system stability.

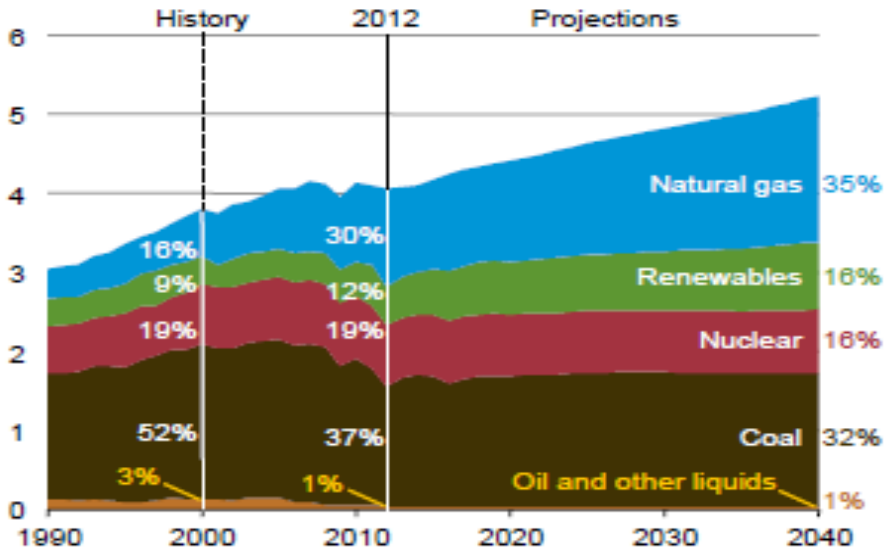

Figure 1.1 Electricity generation by fuel, 1990-2040 (trillion kilowatt hours).

Based on the literature [3-4], the precise definitions of stability are shown as follows. "Power system stability is the ability of an electric power system, for a given initial operating condition, to regain a state of operating equilibrium after being subjected to a physical disturbance, with most system variables bounded so that practically the entire system remains intact".

A typical power system is a highly nonlinear system. Operation conditions such as loads, generator outputs, key operating parameters, etc. are continually changing. Many small and large disturbances may occur in the system from time to time. An unstable system condition will lead to outages and shutdown of the power system. Therefore, power systems must remain stable under load changes and other small disturbances. Also, power

systems must survive numerous disturbances of a severe nature, such as a short circuit on a transmission line or the loss of a large generator [3-4].

Based on the physical nature of the resulting mode of instability, the size of the disturbance, processes, and the time span, power system stability can be classified as rotor angle stability, voltage stability, and frequency stability. The detail classifications are shown in Figure 1.2 [3-4].

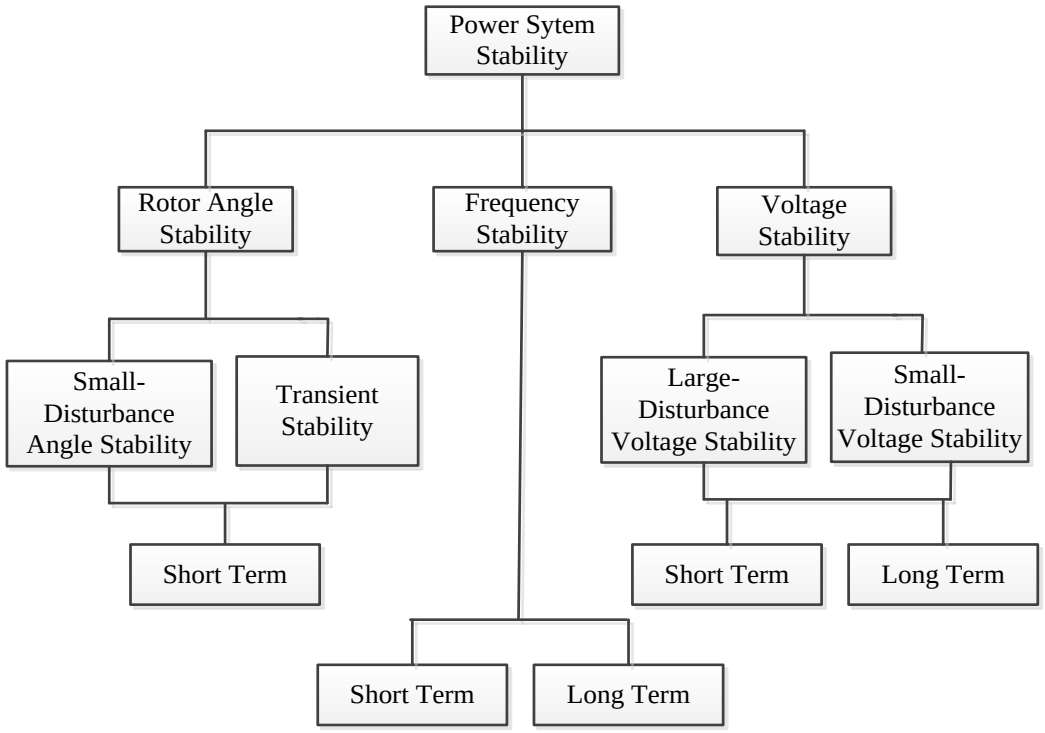

Figure 1.2 Classification of power system stability.

This work focuses on the voltage and frequency regulations. Therefore, only voltage stability and frequency stability will be discussed here.

1.1.2 Voltage Stability

Voltage stability is the ability of a power system to remain steady voltages at all buses in the system when it is subject to a disturbance from a given initial operating condition. The capability to maintain the equilibrium between the load demand and supply in power systems will determine the voltage stability. Voltage instability will result in the loss of load in some areas, tripping of transmission lines and other elements by the protective systems, and even a large-scale cascading blackout. The Voltage stability can be divided into the following two categories [3-4]:

(1) Large-disturbance voltage stability: This is the ability of power systems to maintain steady voltages when a severe disturbance such as system faults, loss of the generations, or circuit contingencies occurs in the system. Large-disturbance voltage stability is determined by the system and load characteristics, as well as the corresponding controls and protections. The study period of large disturbance voltage stability may extend from a few seconds to several hours.

(2) Small-disturbance voltage stability: This is the ability of power systems to maintain steady voltages when a small disturbance such as incremental change in system load occurs in the system. Small-disturbance voltage stability is affected by the characteristics of loads and controls at a given instant of time.

As discussed above, the time frame of interest for voltage stability problems may vary from a few seconds to several hours. Therefore, voltage stability may be either a short-term or a long-term phenomenon as shown in Figure 1.2.

1.1.3 Frequency Stability

Frequency stability is the ability of a power system to maintain a steady frequency when there is a significant imbalance between generation and load. Frequency stability depends on the ability to maintain equilibrium between system generation and load, with minimum unintentional loss of load.

Frequency deviations are caused by a mismatch between power supply and demand in the power system. If the power system supply is insufficient to meet the demand, the power system frequency will decrease; if the power system supply exceeds the demand, the system frequency will increase. Small power mismatches will result in small frequency deviations, which can be easily handled. However, large frequency deviations may lead to equipment damage and even blackouts. Frequency instability will result in frequency swings with generating units and loads tripping. During frequency excursions, the characteristic times of the processes and devices that are activated will range from fraction of seconds to several minutes. Therefore, as identified in Figure 1.2, frequency stability can be a short-term or a long-term phenomenon [5].

1.2 Power system voltage and frequency regulation

A power system is a large and complex interconnected network which consists of thousands of buses and hundreds of generators or even larger. With the increasing need for electrical energy, new installations of power generating stations and transmission lines are required, and the existing infrastructure operations are extended close to their limits. The installation of new lines and generations imposes many environmental and economic constraints. It was found that voltage and frequency instability are the main reasons for the recent North American blackout in August 2003 [7]. Moreover, renewable energy sources such as wind energy and photovoltaic (PV) sources have been widely installed in power systems recently, which make power systems under much more pressure than in the past regarding stability concerns. The general concept of voltage and frequency regulation will be discussed in this section.

1.2.1 Power system voltage regulation

If the power voltage becomes unstable, the system voltage will decrease to unacceptable low level and become impossible to recover. Then, the interruption of the power supply will occur in power systems. Therefore, voltage regulation or reactive compensation is an important subject in a power system. Also, it is the utilities' responsibility to keep the customer voltage within specified tolerances [6]. The only way to regulate system voltage is to reduce the reactive power load or install the reactive

generation devices at the weak voltage points in the system to increase the voltage at these weak points [7].

The recent development and use of Flexible Alternating Current Transmission Systems (FACTS) in power systems has led to many applications such as Thyristor Controlled Series Compensator (TCSC), Static Synchronous Series Compensator (SSSC), Static VAR Compensator (SVC), and Static Synchronous Compensator (STATCOM) [7]. These devices are not only able improve the voltage stability and provide flexible operation capabilities. However, with the growth of industry and the economy, the demands of lower power losses, faster response to system parameter change, and higher stability margin have become increasingly important. In particular, STATCOMs are one of the most popular devices for voltage regulation because of their constant current characteristics when the voltage is low/high over the limits.

STATCOM is a power electronic based synchronous voltage generator that generates a three-phase voltage from a dc capacitor. By controlling the magnitude of the STATCOM voltage and the reactive power exchanges between the STATCOM and the transmission line, the amount of shunt compensation in the power system can be controlled [8-9]. Therefore, the system voltage will be kept in the allowable range. In this work, the control of STATCOM will be studied.

1.2.2 Power system Frequency Regulation

The imbalance between the generation and the load will degrade a power system performance and sometimes will make the power system unstable. The power system frequency is sensitive to the power system loads and losses [10, 11]. In an interconnected power system, area load changes and abnormal disturbances will lead to mismatches in frequency and scheduled power interchanges between areas. These mismatches can be corrected by Load Frequency Control (LFC) [10]. This important component in power system operation and control is designed to minimize the deviations in frequency and tie-line power. It also can reduce steady-state errors to zero when there is a disturbance in power systems. Thus, LFC is essential for supplying sufficient and reliable electric power [12, 13].

In a power system, LFC can be divided into three levels [14, 15]:

(1) Primary control is a local automatic control that adjusts the active power generation of the generators and the consumption of controllable loads to restore the balance between the load and the generation to eliminate frequency variations. Primary control is indispensable for the stability of power systems, and is performed by the speed governors of the dedicated power generation units. With primary control, if a variation in power system frequency is greater than the dead band of the speed governor, a change in unit's generation will occur. At this time, generators are required to

participate in the control by setting the droop according to specifications by the TSO (Transmission System Operator).

(2) Secondary control is a centralized automatic control that adjusts the active power production of the generators to restore the frequency and the interchanges with other systems to their target values. In other words, if primary control cannot stop frequency excursions, secondary control will bring the frequency back to its target value, usually set as 60Hz in the United States. As opposed to the primary frequency control, the secondary frequency control is dispensable. Frequency control is thus not implemented in some power systems where the frequency is regulated using only automatic primary and manual tertiary control. However, the secondary frequency control is used in all large interconnected systems because manual control does not remove overloads on the tie lines quickly enough. Secondary control is also called load-frequency control (LFC), while the term automatic generation control (AGC) is preferred in North America. Transient time for secondary control is in the order of minutes.

(3) Tertiary control is to manual changes in the dispatch and commitment of generators. Tertiary control is used to restore the primary and secondary frequency control reserves, to manage congestions in the transmission network, and to bring the frequency and the interchanges back to their target value when the secondary control is

unable to perform this last task.

In this work, the control of AGC will be studied.

1.3 Contribution of this Work

In a power system, Proportional-integral (PI) controllers have been designed for STATCOM to obtain satisfactory dynamic responses [16]. In traditional PI control methods, the control gains in these controllers are tuned for a case-by-case study or trial-and-error approach. It is a time-consuming job for utility engineers to perform trial-and-error studies to find suitable parameters. Further, conventional PI controllers with fixed control gains are designed for one specific operating condition. A fixed controller, optimal in one specific operating condition may not be suitable in another operation condition and large oscillations may occur in the power system.

The purpose of this work is to propose a control method that can ensure a quick and consistent desired response when the system operation condition varies. In other words, we want to avoid negative impacts, such as slower response, overshoot, or instability to the system performance when external conditions change.

Based on this fundamental goal, an adaptive PI control of STATCOM for voltage regulation is presented. By this adaptive PI control method, the PI control parameters can be self-adjusted automatically and dynamically under different disturbances in a power system. When a disturbance occurs in the system, the PI control parameters for STATCOM

can be computed automatically in every sampling time period and can be adjusted in real time to track the reference voltage. Different from other control methods, this method will not be affected by the initial gain settings, changes of system conditions, and the limits of human experience and judgment. This will make the STATCOM a "plug-and-play" device. In addition, this research work demonstrates a fast, dynamic performance of STATCOM in various operating conditions.

Next, a flatness-based adaptive control method (FBAC) is also proposed and applied to STATCOM for voltage control in this work. By flatness-based control (FBC), the trajectories of all system variables can be directly estimated by flat output and its derivatives without solving differential equations. By adaptive control, the control gains can be dynamically tuned to satisfy the time-varying operation condition requirement. Different from other FBC methods, the proposed control method is robust to various system operating conditions and will not be affected by the limits of human experience and judgment. Even if the system operation condition has a drastic change, the FBAC method can consistently achieve a desired performance of STATCOM.

Finally, the frequency regulation is also discussed in this work. A number of control methods have been discussed in the literature to design control gains for proportional-integral (PI) controllers in automatic generation control (AGC) and to obtain a good frequency response performance. However, the existing methods are either time

consuming or easily affected by the designer's experience. Further, the control gains obtained by existing control methods are usually fixed and designed for specific scenarios in the studied power system. The desired response may not be obtained when variable wind power is integrated into power systems. To address these challenges, an adaptive gain-tuning control (AGTC) for AGC with effects of wind resources is presented in this work. By this control method, the PI control parameters can be automatically and dynamically calculated during differing disturbances in a power system. In the proposed method, the initial gains will be calculated first. Then, the wind energy with actual wind speed will be integrated into power systems. The PI control parameters for AGC can be computed automatically and can be adjusted in real time based on the area control error (ACE) signal to regulate the system frequency. The proposed method will not be affected by changes of the system conditions and human experience and judgment.

1.4 Organizations of the Dissertation

Chapter 2 provides a detailed review of the literature regarding STATCOM model, flatness-based control, and generic adaptive control.

Chapter 3 addresses the challenge of the traditional PI control methods to obtain the optimal response with varying power system operation conditions. Also, this chapter proposes a new control model based on adaptive PI control, which can self-adjust the control gains during disturbances such that the performance always matches a desired

response, regardless of changes in the operating condition. Finally, the conventional STATCOM control with tuned, fixed PI gains will be compared with the proposed method in simulation part.

Chapter 4 introduces a new method, called the flatness-based adaptive control (FBAC), for STATCOM voltage regulation. By this method, the nonlinear STATCOM variables can be easily and exactly controlled by controlling flat output without solving differential equations. Further, the control gains can dynamically self-adjust during the voltage regulation after a disturbance. In the simulation part, the conventional PI control with tuned, fixed PI gains, the flatness based control (FBC) and the FBAC will be compared.

Chapter 5 introduced an adaptive gain-tuning control (AGTC) for AGC with effects of wind resources. In the proposed method, the initial gains will be calculated first. Then, the wind energy sources with actual wind speeds are integrated in power systems. The PI control parameters for AGC can be computed automatically and adjusted in real time based on the area control error (ACE) signal to regulate the system frequency. The proposed method is tested in an IEEE 39 bus system with wind resources and compared with conventional control approach with well-tuned gains in the simulation.

In Chapter 6, the conclusion from the entire dissertation work is given, and possible future works are also discussed.

CHAPTER 2

LITERATURE REVIEW

2.1 Chapter Introduction

This chapter briefly reviews the past and on-going research findings relevant to the control of Static Synchronous Compensator (STATCOM) and automatic generation control (AGC).

2.2 Voltage Control of STATCOM Review

Voltage regulation is a critical consideration for improving the security and reliability of power systems. The Static Compensator (STATCOM), a popular device for reactive power control based on gate turn-off (GTO) thyristors, has gained much interest in the last decade for improving power system stability [17].

In the past, various control methods have been proposed for STATCOM control. For instance, nonlinear optimal control to STATCOM is introduced in [18-20]. A synchronous frame voltage regulator is presented in [21] to control system voltage by using separate regulation loops for positive and negative sequence components of the voltage. PI structures with feed forward are proposed in [22] to improve STATCOM performance. A STATCOM damping controller is introduced in [23-24] to offset the negative damping effect and to enhance system oscillation stability. A modified non-linear damping controller is presented in [25] to provide an improved transient performance over the whole

operating range. These previous works mainly focus on the control design rather than exploring how to set PI control gains.

In many STATCOM models, the control logic is implemented with the Proportional-integral (PI) controllers. The control parameters or gains play a key factor in STATCOM performance. Presently, few studies have focused on the control parameter settings. In the previous research works [26-28], the PI controller gains were designed in a case-by-case study or trial-and-error approach with tradeoffs in performance and efficiency. Generally speaking, it is not feasible for utility engineers to perform trial-and-error studies to find suitable parameters when a new STATCOM is connected to a system. Further, even if the control gains have been tuned to fit the projected scenarios, performance may be disappointing when a change of the system conditions occurs, such as, when a line is upgraded or retires from service [29-30]. The situation can be even worse if such transmission topology change is due to a contingency. Thus, the STATCOM control system may not perform well when critically needed.

A few, but limited previous works in the literature discuss the STATCOM PI controller gains in order to improve voltage stability and to avoid time-consuming tuning. For instance, in [31-33], linear optimal controls based on the linear quadratic regular (LQR) control are proposed. In [35-36], a fuzzy PI control method is proposed to tune PI controller gains. In [40-42], a flatness-based control (FBC) is proposed and applied in the

voltage source converter. In [29-30], an autonomous and adaptive voltage control for distributed energy resources (DERs) is proposed. In subsections 2.2.1 to 2.2.4, the control methods in existing literature for control gain tuning will be discussed in detail.

2.2.1 Linear quadratic regular (LQR) control

In [31-33], linear optimal controls based on the linear quadratic regular (LQR) control are proposed. LQR is also a pole placement method. In this method, the poles of the system are placed indirectly by minimizing a given performance index *J*:

$$J = \int_0^{\infty} (x^T Q x + u^T R u) dt \tag{2.1}$$

where *x* is the state variable, *u* is the vector of input variables, *Q* and *R* are the weighting matrices, usually *Q* and *R* are positive semi-definite which are chosen by the designer. By optimizing the given performance index *J*, the feed-back gain matrix *K* can be obtained. In [31], the matrix *Q* is chosen to be a diagonal matrix, thus the elements act as a "weighting" of the STATCOM states in the performance index. The matrix *R* is also chosen to be a diagonal matrix. In the matrices *Q* and *R*, the elements must be chosen carefully. Very small values may result in excessive control force demand. However, very large values may result in sluggish system performance. The best range of values in *Q* and *R* varies depending on the system under consideration and the operating point. Therefore, the effectiveness of the LQR depends on the choice of the weighting matrices *Q* and *R*, and the optimal parameters may depend on the designer's experience.

2.2.2 Fuzzy PI control method

In [35-36], a fuzzy PI control method is proposed to tune PI controller gains. The control block is shown in Figure 2.1.

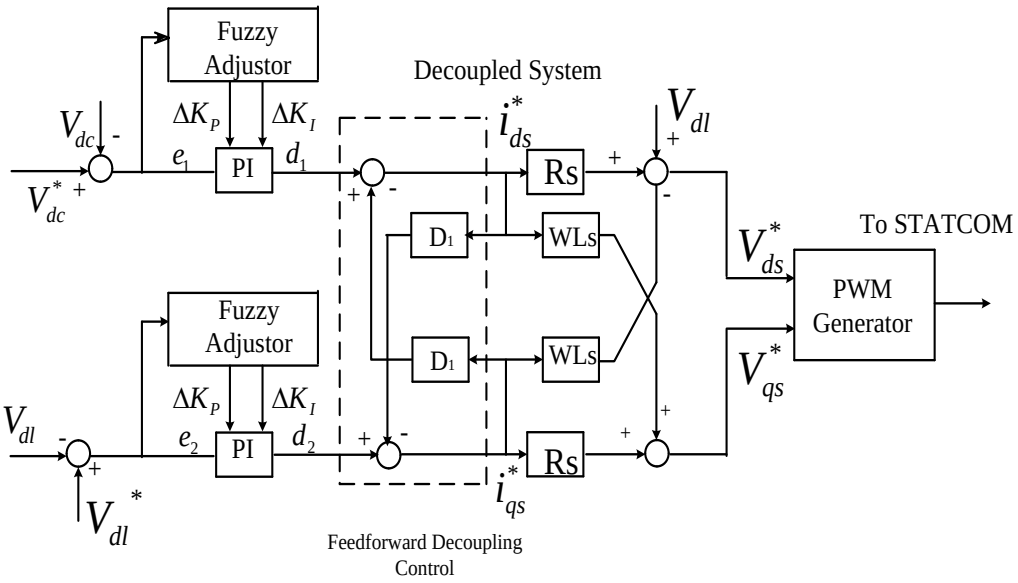

Figure 2.1 Direct-Output-Voltage with Fuzzy Control.

In the figure, the fuzzy adjustor is used to adjust the parameters of proportional gain K_P and integral gain K_I based on the error e and the change of error Δe. The control gains are determined by:

$$K_P = K_P^* + \Delta K_P \tag{2.2}$$

$$K_I = K_I^* + \Delta K_I \tag{2.3}$$

where K_P^* and K_I^* are the reference values of fuzzy-PI-based controllers. In [35-36], K_P^*

and K_I^* are calculated offline based on the Ziegler Nichols method.

By fuzzy control, numeric values of error e and the change of error Δe need to be translated into a linguistic value with a membership grade. The membership function is shown in Figure 2.2. In the figure, the following seven fuzzy sets are chosen: negative big (NB), negative medium (NM), negative small (NS), zero, positive small (PS), positive medium (PM), and positive big (PB).

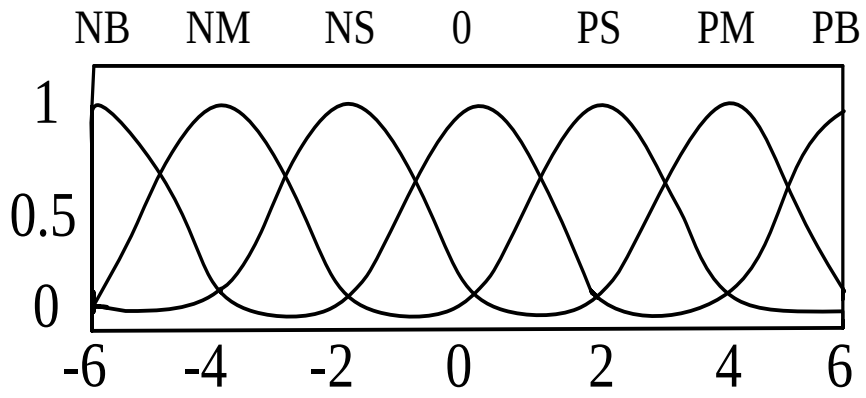

Figure 2.2 Membership functions of fuzzy variables.

The design process of fuzzy control rules involves defining the rules that relate the input variables to the output model properties. The fuzzy control rules usually are designed by the designer. In the [36], ΔK_P and ΔK_I are determined by the following rules:

1) If |e| is a large value, a large ΔK_P will be chosen, and vice versa.

2) If $e^*\Delta e>0$, a large ΔK_P will be selected, and vice versa.

3) If |e| and |Δe| are large values, ΔK_I is set to zero, which can avoid control saturation.

4) If |e| is small, ΔK_I is effective, and a large value is chosen for ΔK_I if |e| is small, which is good to decrease the steady-state error.

In the fuzzy control, the controller rule is mainly obtained from designers' intuition and experience. Therefore, the fuzzy control method essentially gives "fuzzy" recommendation and it is still up to the designer to choose the actual, deterministic gains.

2.2.3 Flatness based control

A flatness-based control (FBC), is proposed and applied in the voltage source converter [40-42]. Flatness is a mathematical property of a system described by a set of differential equations. With FBC, a nonlinear flat system is equivalent to a linear controllable system, and the trajectories of all system variables can be directly estimated by flat output and its derivatives [43-45]. Flat systems are a subset of nonlinear systems; in other words, some nonlinear systems may demonstrate the characteristic of flatness. The flatness feature can be utilized for motion planning, trajectory generation, and stabilization. Theoretically, a flat system can be feedback linearized, which is, however, not a better choice than the flat control approach. Further, flatness is a feature independent of coordinate choice which is critical to the linearization in nonlinear control. That is, choosing a different coordinate system may not convert the nonlinear system to a linear one. However, coordinate choice is irrelevant in flatness-based control [46-47].

Consider a general nonlinear system of the form:

$$\dot{x} = f(x) + g(x)u \tag{2.4}$$

$$x = [x_1, x_2, \dots x_n]^T \quad x \epsilon R^n \tag{2.5}$$

$$u = [u_1, u_2, \dots u_m]^T \quad u \epsilon R^m \tag{2.6}$$

where $(n, m) \in N$. If the state variable x can be parameterized by output y and its derivatives, the system is said to be differentially flat and admits the flat output $y=[y_1, y_2, \dots, y_m]^T$ [43-45]. Then, the state variables and control variables can be written as follows:

$$x = \phi\left(y, \dot{y}, \dots, y^{(\beta)}\right) \tag{2.7}$$

$$u = \phi\left(y, \dot{y}, \dots, y^{(\beta+1)}\right) \tag{2.8}$$

where β is the finite numbers of derivative. By this process, a nonlinear flat system can be equivalent to a linear controllable system as described in references [43-45], the control block shown in Figure 2.3.

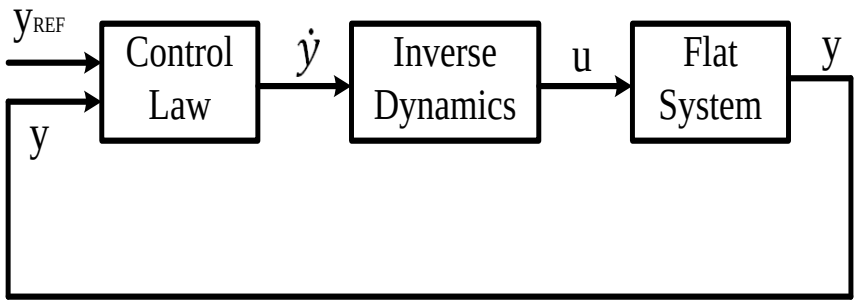

Figure 2.3 Flatness based control block.

In the FBC [40-42], the control laws are normally designed by the pole-placement method. By this method, the final results will also be affected by the designer's experiences as discussed before. Further, even if the control gains have been tuned to fit the projected scenarios, it may not perform as initially expected when a considerable change of the system condition occurs such as when a transmission line is upgraded or retires from service. The situation can be even worse if such transmission topology change is due to a contingency. Thus, the STATCOM control system may not perform well when urgently needed. Therefore, this issue leads to an exploration for an improved flatness based control.

2.2.4 Adaptive control by previous work

In [29-30], adaptive voltage regulation for distributed energy resources (DERs) is proposed and an adaptive voltage regulation method is developed with a PI feedback controller. Based on these previous researches, if the control gains K_P and K_I are not chosen appropriately, the system response may be poor and even cause instability. So it is important to design the control gains. In [29-30], an adaptive PI design is proposed such that it can dynamically adjust the PI controller in real-time based on the system behavior and configuration. The proposed adaptive PI control method includes three procedures:

1) Determine the DC source voltage of the DE.
2) Set the initial controller values.

3) Adjust the controller parameters according to the real-time system conditions.

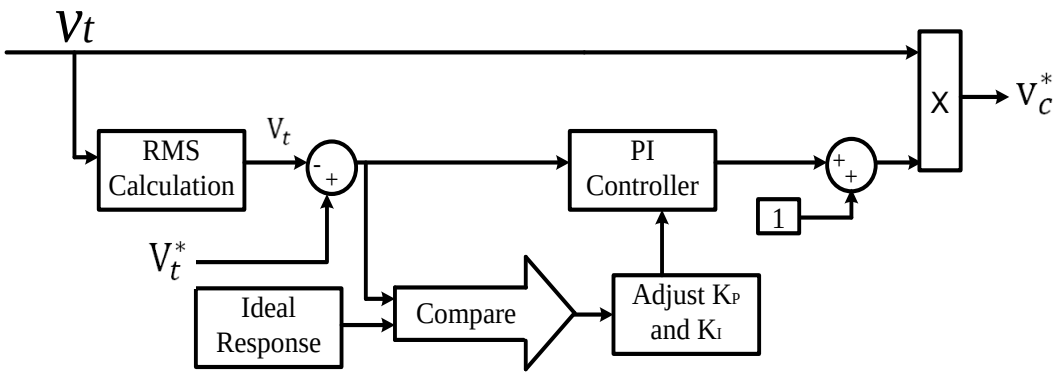

Figure 2.4 Adaptive control of the voltage regulation.

The control diagram for DERs is shown in Figure 2.4. The point of common coupling (PCC) voltage v_t (or terminal voltage), is measured and its RMS value V_t is calculated. The V_t is then compared to the voltage reference V_t^*. The error between the actual voltage V_t and reference voltage V_t^* is fed back to adjust the reference compensator output voltage V_c^*, which is the reference for generating pulse-width modulation (PWM) signals to drive the inverter. The compensator output voltage V_c^* is controlled to regulate V_t to the reference V_t^*. The expression for V_c^* can be obtained by:

$$V_c^* = v_t(t)\left[1 + K_P\left(V_t^*(t) - V_t(t)\right) + K_I \int_0^t \left(V_t^*(t) - V_t(t)\right)dt\right] \quad (2.9)$$

By the proposed control method, the initial value of control gains K_P, can be empirically set to half of the right-hand side (RHS) value defined by:

$$K_p \leq \frac{\frac{\frac{1}{2}V_{dc}}{V_t^{0,p}} - 1}{\Delta V_t^0} \tag{2.10}$$

where $\Delta V_t^0 = V_t^*(t) - V_t^0(t)$ is the initial RMS voltage deviation at time 0+.

By the adaptive control, the actual voltage deviation which is the voltage error between the measured voltage and the reference voltage will be compared with the desired voltage deviation, which is the voltage error between the defined exponential voltage curve and the reference voltage. The PI control gains will be adjusted based on the scaling factor r_v=actual voltage deviation/ideal voltage deviation. This adaptive control approach will be expanded to STATCOM control in this work while eliminating the initial gain settings which is somewhat empirically determined.

2.2.5 Summary

Based on the above discussion, the gains in LQR control depend on the designer's choice of a weighting matrix. This makes the optimal parameters depend on the designer's experience. The fuzzy control method essentially gives "fuzzy" recommendation and it is still up to the designer to choose the actual, deterministic gains. The FBC also uses the pole placement method to determine the control gains. Therefore, again, the designer's experience may affect the final results. Different from these previous works, this work proposes a control method that can ensure a quick and consistent desired response when the system operation condition varies. In other words, the change of the external condition

will not have a negative impact, such as slower response, overshoot, or instability on the performance.

2.3 Frequency Control of AGC Review

The power system frequency is sensitive to power system loads and losses [10, 11]. In an interconnected power system, area load changes and abnormal disturbances will lead to mismatches in frequency and scheduled power interchanges between areas. All generators are equipped with speed governor systems, but during sudden and big load change, zero frequency deviation may not be obtained. In this case, the mismatches can be corrected by Load Frequency Control (LFC) or automatic generation control (AGC) [10]. AGC, an important component in power system operation and control, is designed to minimize the deviations in frequency and tie-line power and reduce steady-state errors to zero when there is a disturbance in power systems. Thus, its implementation is essential for supplying sufficient and reliable electric power [12, 13].

The commonly used technique for LFC [12-13] is based on the Area Control Error (ACE) which is a linear combination of tie line error and frequency deviations. The main objectives of the LFC are to minimize the transient errors of the frequency and tie-line power and to ensure zero steady-state errors of these quantities. Droop control strategies have been proposed for traditional AGC [10-11]. Existing droop controllers are designed for small load changes. To improve droop controllers, other classical control methods,

such as proportional-integral(PI), integral-derivative (ID), proportional-integral-derivative (PID) and integral-double derivative (IDD) controllers, are investigated in [48]. The flatness-based controls for automatic generation control (AGC) of a multi-machine system are proposed in [49-50]. However, the control gains in these controllers are designed by trial and error method which can be time consuming. Moreover, the fixed control gains used in these controllers are designed for a specific operation condition, which cannot guarantee the optimal control response in varying power system operation conditions.

In order to obtain a better frequency response, the pole placement method is proposed in literatures [13, 67]. Since the gains by this method depend on the designer's choice of the pole, the optimal parameters may depend on the designer's experience. Therefore, the designer's experience may affect the final results. Intelligent controllers are proposed to AGC to obtain fast and good dynamic response for load frequency control. Many intelligent techniques such as differential evolution algorithm, particle swarm optimizations, bacteria foraging algorithm, etc. are being used extensively and in interconnected power systems [54-64, 68]. The detail of selected previous control methods will be discussed in subsections 2.3.1 to 2.3.4.

2.3.1 Differential Evolution

In [54], the application of differential evolution (DE) algorithm in load frequency control for controller parameters tuning is proposed. The DE is a population-based

stochastic optimization algorithm. DE works with two populations such as old generation and new generation of the same population. The size of the population is adjusted by the parameter N_P. The population consists of real valued vectors with dimension D which is equal to the number of control variables. The population is randomly initialized within the initial parameter bounds. The optimization process is conducted by three main steps: mutation, crossover, and selection. In each generation, individuals of the current population become target vectors. By adding the weighted difference between two randomly chosen vectors to a third vector, a mutant vector will be produced during the mutation operation. By mixing the parameters of the mutant vector with those of the target vector, a new vector, called trial vector, will be generated during the crossover operation. If the trial vector obtains a better fitness value than the target vector, then the trial vector replaces the target vector in the next generation. The flow chart of the differential evolution is shown in Figure 2.5.

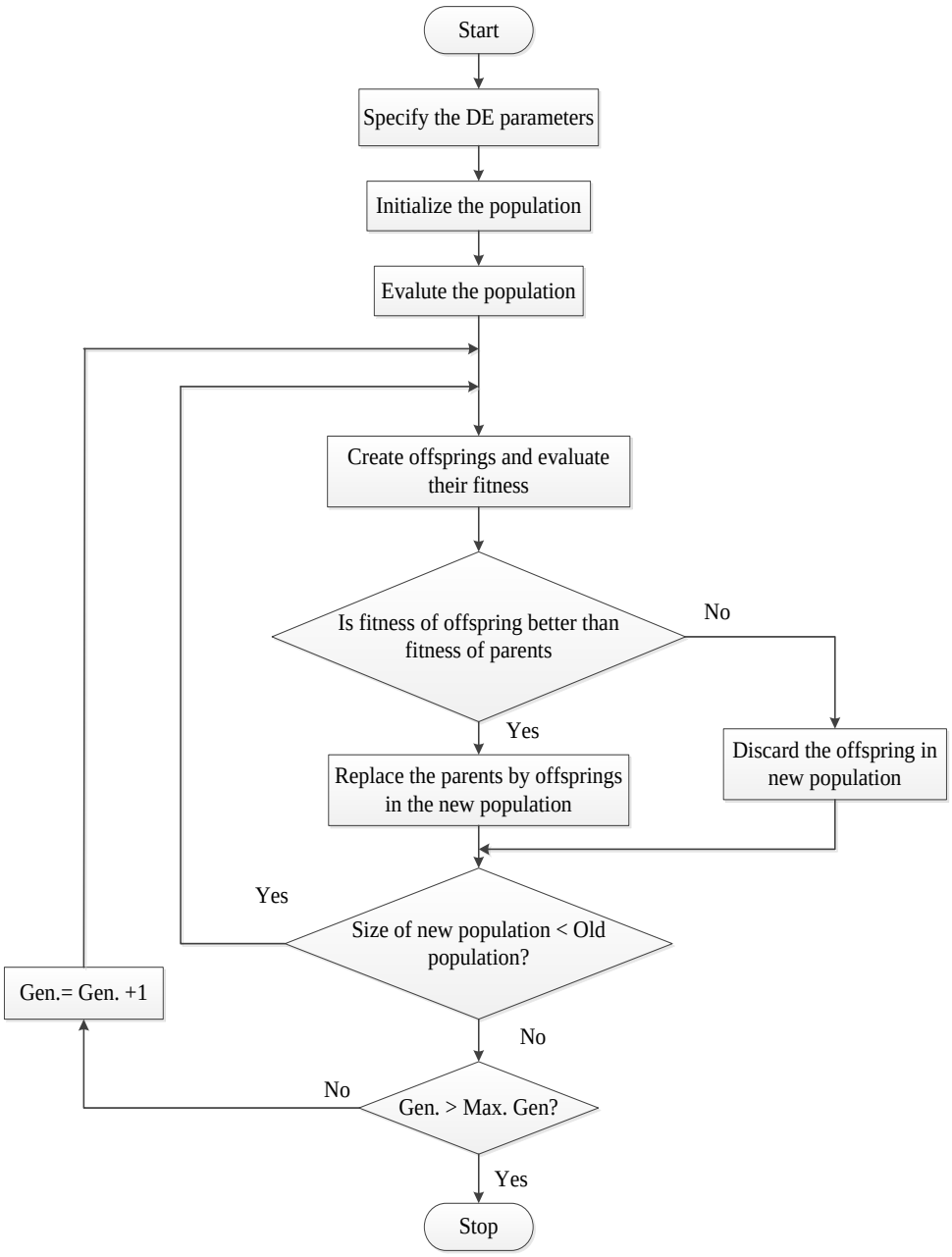

Figure 2.5 Flow chart of the differential evolution algorithm.

Implementation of DE requires the determination of some fundamental issues like: mutation strategy, DE step size function also called scaling factor (*F*), crossover

probability (*CR*), the number of population (N_P), initialization, the termination, and evaluation functions. The success of DE is dependent on setting the control parameters such as population size N_P, DE step size F and crossover probability of CR. Therefore, when applying DE, the strategy and control parameters should be carefully chosen for the successful implementation of the algorithm. Usually, the control parameters of DE algorithm are tuned by carrying out multiple runs of algorithm for each control parameter variation which is time consuming.

2.3.2 Particle swarm optimization

In [62], a new gain scheduling PI control strategy for AGC based on particle swarm optimization (PSO) is proposed. The PSO is a population based optimization algorithm which can obtain high quality solutions within shorter calculation time and stable convergence characteristics. PSO uses particles which represent potential solutions of the problem. Each particle flies in search space at a certain velocity which can be adjusted in light of preceding flight experiences. The projected position of the i_{th} particle of the swarm x_i, and the velocity of this particle v_i at $(t+1)_{th}$ iteration are defined and updated as the following two equations:

$$v_i^{t+1} = v_i^t + c_1 r_1 (p_i^t - x_i^t) + c_2 r_2 (g_i^t - x_i^t) \tag{2.11}$$

$$x_i^{t+1} = x_i^t + v_i^{t+1} \tag{2.12}$$

where $i = 1 \sim n$ and n is the size of the swarm, c_1 and c_2 are positive constants, r_1 and r_2 are

random numbers which are uniformly distributed in [0, 1], t represents the iteration number, p_i represents the best previous position (the position giving the best fitness value) of the i_{th} particle, and g represents the best particle among all the particles in the swarm. At the end of the iterations, the best position of the swarm will be the solution of the problem. The flow chart of PSO applied in AGC control is shown in Figure 2.6.

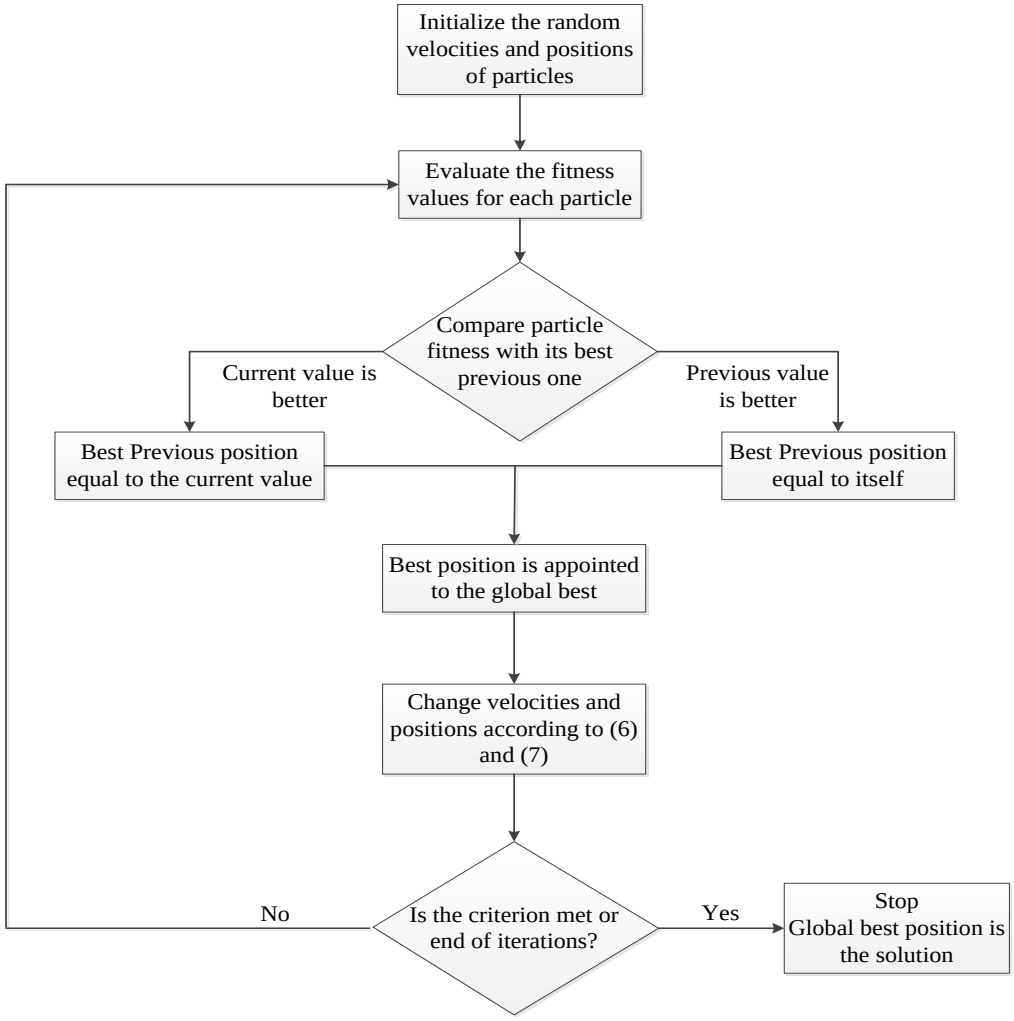

Figure 2.6 Flowchart of the standard PSO algorithm.

The objective for achieving optimal solutions of control inputs is taken as an optimization problem, and the proposed PSO algorithm is being used to tune the gains of the controllers and cost function weights w_1, w_2, and w_3. In the AGC system, in order to converge to optimal solution, two different cost functions in (2.13) and (2.14) are derived. Equation (2.13) is derived through the frequency deviations of the control areas and tie-line power changes. Equation (2.14) is derived based on the rates of changes in these deviations according to time.

$$J = \int_0^t t\left[\left(\omega_1 \frac{d\Delta f_1}{dt}\right)^2 + \left(\omega_2 \frac{d\Delta f_2}{dt}\right)^2 + \left(\omega_3 \frac{d\Delta P_{tie}}{dt}\right)^2\right] dt \quad (2.13)$$

$$J = \int_0^t t[(\omega_1 \Delta f_1)^2 + (\omega_2 \Delta f_2)^2 + (\omega_3 \Delta P_{tie})^2]\, dt \quad (2.14)$$

In the PSO algorithm, the continually varying power system operation condition has not been considered. Also, the control gains are designed to remain constant during the disturbance which prevents obtaining the desired response sometimes.

2.3.3 Bacteria forging algorithm

In [64], the bacterial foraging scheme (BF) is proposed to optimize several important parameters in automatic generation control (AGC). BF algorithm, a recent evolutionary computation technique, used for searching the total solution space, is more popular than GA. To overcome the possibility of being trapped in local minima, in GA only two operations (crossover and mutation) between the chromosomes are adopted. However, in BF, the foraging (methods of locating, handling, and ingesting food) behavior of E.coli

bacteria in the intestine is mimicked. BF algorithm can be divided into four sections, chemotaxis, swarming, reproduction, and elimination and dispersal. These operations among the bacteria are used for searching the total solution space. Thus the possibility of avoiding local minimum and achieving faster convergence is much higher than GA.

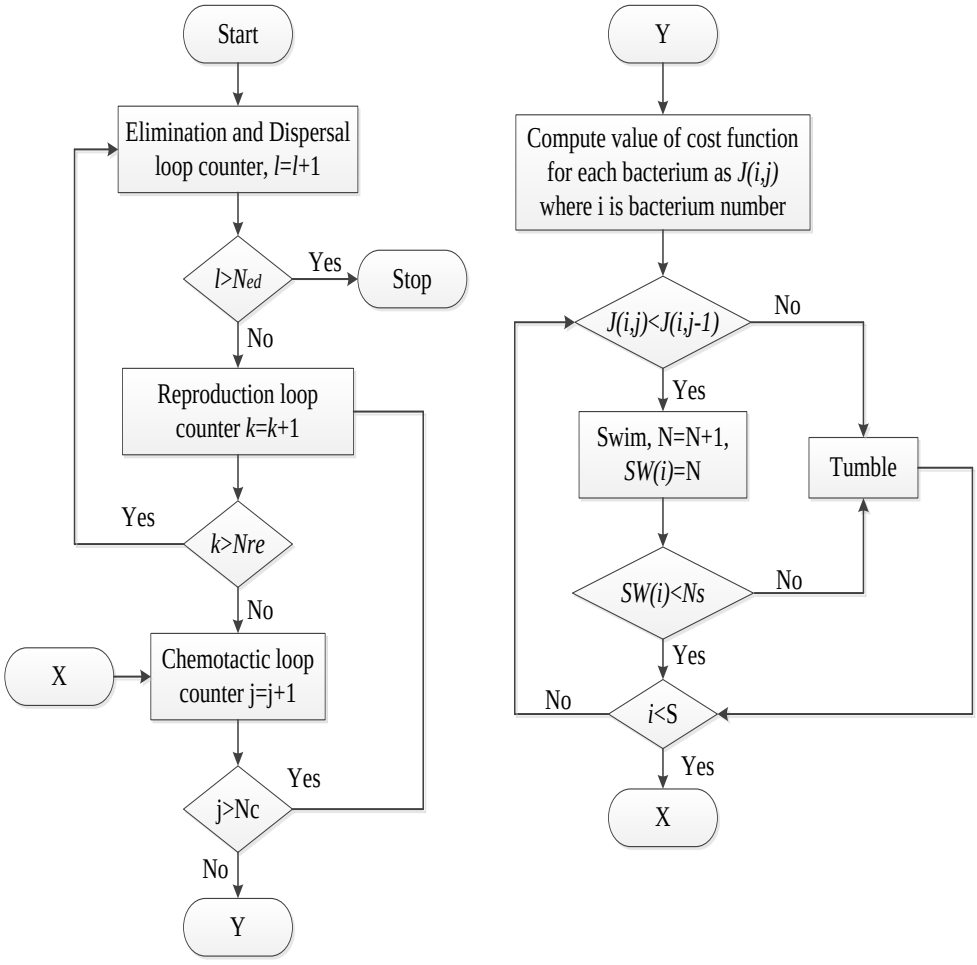

Figure 2.7 Flow chart for bacterial foraging algorithm.

In BF algorithm, each bacterium are assigned with random values (Δ) within the defined upper and lower limit between which the optimum value is likely to fall. In [64], each bacterium is allowed to take all possible values within the range. The objective function is defined by the following:

$$J = \int_0^T \left\{ (\Delta f_i)^2 + \left(\Delta P_{tiei-j}\right)^2 \right\} dt \tag{2.15}$$

where T is the simulation time, Δf_i is the incremental change in frequency of area i, and ΔP_{tiei-j} is the incremental change in tie power of tie i to j. The flow chart of BF is shown in Figure 2.7. In the figure, N_c is the number of iterations to be undertaken in a chemotactic loop. N_{re} is the maximum number of reproductions to be undertaken. N_{ed} is the maximum number of elimination and dispersal events to be imposed over bacteria. S is number of bacteria. In BF algorithm, the fixed control gains are used at the different system operation condition which cannot guarantee the optimal control response.

2.3.4 Decentralized Sliding Mode Load Frequency Control

In [68], a novel decentralized sliding mode control, based on PI and slide mode control is proposed to solve the LFC problem of multi-area interconnected power systems with matched and unmatched uncertainties. The sliding mode control (SMC) has been proven to be an effective robust control strategy for nonlinear systems and incompletely modeled systems. The SMC utilizes a discontinuous control to force the system state trajectories to some predefined sliding surfaces on which the system has desired

properties such as stability, disturbance rejection capability, and tracking ability. The traditional SMC design includes the two relatively independent parts of the sliding mode surface $\delta_i(t)$ for the desired performance and the controller law u_i to force the system trajectory to the surface and to maintain motion on it.

To improve the dynamic performance and robustness, the PI switching surface is selected as:

$$\sigma_i(t) = \mathrm{G}_i x_i(t) - \int_0^t G_i(A_i' - B_i' K_i)\, x_i(\tau) d\tau \qquad (2.16)$$

where G_i and K_i are constant matrices. Matrix G_i is selected to assure that matrix $G_i B_i'$ is nonsingular. Matrix K_i is designed through pole assignment such that the eigenvalues of matrix $(A_i' - B_i' K_i)$ are less than zero. When the dynamic trajectory reaches the sliding mode, the switching function satisfies the following conditions.

$$\sigma_i(t) = 0 \text{ and } \dot{\sigma}_i(t) = 0 \qquad (2.17)$$

In the SMC, the control gains are designed to remain the same during the disturbance, which sometimes prevents obtaining the desired response.

2.3.5 Summary

The discussions from 2.3.1 to 2.3.4 have not considered the continually varying power system operation condition. Moreover, the control gains in these previous AGC control methods are designed for different operation conditions, but during the disturbance, the control gains are kept the same. This makes the optimal response

unachievable when variable wind power is integrated into a power system. To address these challenges, an adaptive gain-tuning control (AGTC) for AGC with wind resources effects is presented in this work. By this control method, the PI control parameters can be automatically and dynamically calculated during different disturbances in a power system.

2.4 Scope of this Work

As discussed in 2.2, the traditional PI control methods for STATCOM use the time-consuming try and error methods to calculate the control gains. The fixed control gains may obtain the optimal response in a specific condition. However, when a considerable change of the system conditions occurs such as when a line is upgraded or retires from service, performance may be disappointing. To improve this, some new control methods such as pole placement and fuzzy control methods are proposed. These methods are affected by the designer's experience which makes obtaining the optimal response uncontrollable.

Therefore, an adaptive PI control of STATCOM for voltage regulation is presented in this work. By this adaptive PI control method, the PI control parameters can be self-adjusted automatically and dynamically under different disturbances in a power system. When a disturbance occurs in the system, the PI control parameters for STATCOM can be computed automatically in every sampling time period and can be adjusted in real

time to track the reference voltage. Different from other control methods, this method will not be affected by the initial gain settings, changes of system conditions, and the limits of human experience and judgment. This will make the STATCOM a "plug-and-play" device. In addition, this research work demonstrates a fast, dynamic performance of STATCOM in various operating conditions.

Next, a flatness-based adaptive control (FBAC) method is proposed and applied to STATCOM for voltage control in this work, since the existing flatness based control (FBC) may not satisfy the requirements of the varying power system operation conditions. By this method, the nonlinear STATCOM variables can be easily and exactly controlled by controlling flat output without solving differential equations. Further, the control gains can dynamically self-adjust during the voltage regulation after a disturbance. Thus, the performance from the FBAC will consistently match a desired response, regardless of the change of operating conditions.

Finally, as discussed in 2.3, automatic generation control (AGC) is very important to regulate power system frequency. A number of control methods have been discussed in order to design control gains for proportional-integral (PI) controllers in AGC and to obtain the desired frequency response performances. However, the existing methods are either time consuming or are affected by the designer's experience. Also, the control gains obtained by existing control methods are usually fixed and designed for specific scenarios

in the studied power system. The desired response may not be obtained when variable wind power is integrated into power systems. To address these challenges, an adaptive gain-tuning control (AGTC) for AGC is proposed in this paper. The wind speed recordings from an actual field data are used in the MATLAB simulation and wind power model is built. By the proposed control method, PI control gains can be dynamically self-adjusted to reach the desired performance. In addition, the proposed control provides better AGC response with less deviation of system frequency and tie line flow under variable wind power.

CHAPTER 3

ADAPTIVE PI CONTROL OF STATCOM

3.1 Chapter Introduction

This chapter presents an adaptive PI control of STATCOM for voltage regulation. By this adaptive PI control method, the PI control parameters can be self-adjusted automatically and dynamically under different disturbances in the power system.

3.2 STATCOM Model and Control

3.2.1 System Configuration

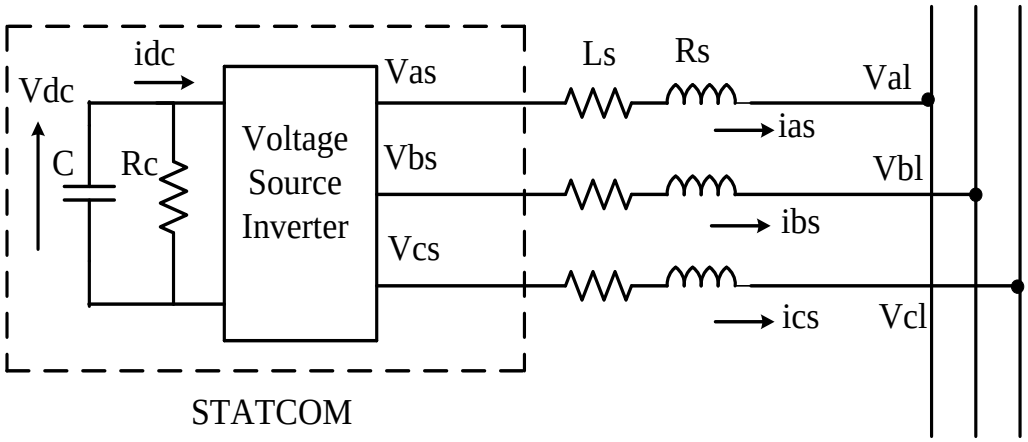

Figure 3.1 Equivalent circuit of STATCOM.

The equivalent circuit of the STATCOM is shown in Figure 3.1. In this power system, the resistance R_s in series with the voltage source inverter represents the sum of the transformer winding resistance losses and the inverter conduction losses. The inductance

L_s represents the leakage inductance of the transformer. The resistance R_c in shunt with the capacitor C represents the sum of the switching losses of the inverter and the power losses in the capacitor. In Figure 3.1, V_{as}, V_{bs}, and V_{cs} are the three-phase STATCOM output voltages; V_{al}, V_{bl}, and V_{cl} are the three phase bus voltages; i_{as}, i_{bs}, and i_{cs} are the three-phase STATCOM output currents [31].

3.2.2 STATCOM Dynamic Model

The three-phase mathematical expressions of the STATCOM can be written in the following form [31]:

$$L_s \frac{di_{as}}{dt} = -R_s i_{as} + V_{as} - V_{al} \tag{3.1}$$

$$L_s \frac{di_{bs}}{dt} = -R_s i_{bs} + V_{bs} - V_{bl} \tag{3.2}$$

$$L_s \frac{di_{cs}}{dt} = -R_s i_{cs} + V_{cs} - V_{cl} \tag{3.3}$$

$$\frac{d}{dt}\left(\frac{1}{2} C V_{dc}^2(t)\right) = -[V_{as} i_{as} + V_{bs} i_{bs} + V_{cs} i_{cs}] - \frac{V_{dc}^2(t)}{R_c} \tag{3.4}$$

In order to conveniently analyze the balanced three-phase system, the three-phase voltages and currents are converted to synchronous rotating frame by *abc*/*dq* transformation. By this rotation, the control problem is greatly simplified since the system variables become DC values under the balanced condition. Further, multiple control variables are decoupled, permitting the use of the classic control method. The transformation from phase variables to *d* and *q* coordinates is given as follows:

$$\begin{bmatrix} i_{ds} \\ i_{qs} \\ 0 \end{bmatrix} = [C] \begin{bmatrix} i_{as} \\ i_{bs} \\ i_{cs} \end{bmatrix} = \frac{2}{3} \begin{bmatrix} 1 & -\frac{1}{2} & -\frac{1}{2} \\ 0 & \frac{\sqrt{3}}{2} & -\frac{\sqrt{3}}{2} \\ \frac{1}{\sqrt{2}} & \frac{1}{\sqrt{2}} & \frac{1}{\sqrt{2}} \end{bmatrix} \begin{bmatrix} i_{as} \\ i_{bs} \\ i_{cs} \end{bmatrix} \tag{3.5}$$

$$\begin{bmatrix} V_{ds} \\ V_{qs} \\ 0 \end{bmatrix} = [C] \begin{bmatrix} V_{as} \\ V_{bs} \\ V_{cs} \end{bmatrix} = \frac{2}{3} \begin{bmatrix} 1 & -\frac{1}{2} & -\frac{1}{2} \\ 0 & \frac{\sqrt{3}}{2} & -\frac{\sqrt{3}}{2} \\ \frac{1}{\sqrt{2}} & \frac{1}{\sqrt{2}} & \frac{1}{\sqrt{2}} \end{bmatrix} \begin{bmatrix} V_{as} \\ V_{bs} \\ V_{cs} \end{bmatrix} \tag{3.6}$$

where i_{ds} and i_{qs} are the *d* and *q* currents corresponding to i_{as}, i_{bs}, and i_{cs}; V_{ds} and V_{qs} represent the *d* and *q* voltages corresponding to V_{as}, V_{bs}, and V_{cs}.

The output voltage of the STATCOM can be expressed as:

$$V_{ds} = KV_{dc} \cos(\alpha) \tag{3.7}$$

$$V_{qs} = KV_{dc} \sin(\alpha) \tag{3.8}$$

where *K* is a factor that relates the DC voltage to the peak phase-to-neutral voltage on the AC side; V_{dc} is the DC-side voltage; α is the phase angle which the STATCOM output voltage leads the bus voltage.

By using the *abc*/*dq* transformation, the equations from (3.1) to (3.4) can be rewritten as:

$$\frac{d}{dt} \begin{bmatrix} i_{ds} \\ i_{qs} \\ V_{dc} \end{bmatrix} = \begin{bmatrix} -\frac{R_s}{L_s} & \omega & \frac{K}{L_s} \cos\alpha \\ -\omega & -\frac{R_s}{L_s} & \frac{K}{L_s} \sin\alpha \\ -\frac{3K}{2C} \cos\alpha & -\frac{3K}{2C} \sin\alpha & -\frac{1}{R_c C} \end{bmatrix} \begin{bmatrix} i_{ds} \\ i_{qs} \\ V_{dc} \end{bmatrix} - \frac{1}{L_s} \begin{bmatrix} V_{dl} \\ V_{ql} \\ 0 \end{bmatrix} \tag{3.9}$$

where ω is the synchronously rotating angle speed of the voltage vector; V_{dl} and V_{ql}

represent the *d* and *q* axis voltage corresponding to V_{al}, V_{bl}, and V_{cl}. Since V_{ql} =0, based on the instantaneous active and reactive power definition, (3.10) and (3.11) can be obtained as follows [23-24]:

$$p_l = \frac{3}{2} V_{dl} i_{ds} \tag{3.10}$$

$$q_l = \frac{3}{2} V_{dl} i_{qs} \tag{3.11}$$

Based on the above equations, the traditional control strategy can be obtained, and the STATCOM control block diagram is shown in Figure 3.2 [26-27].

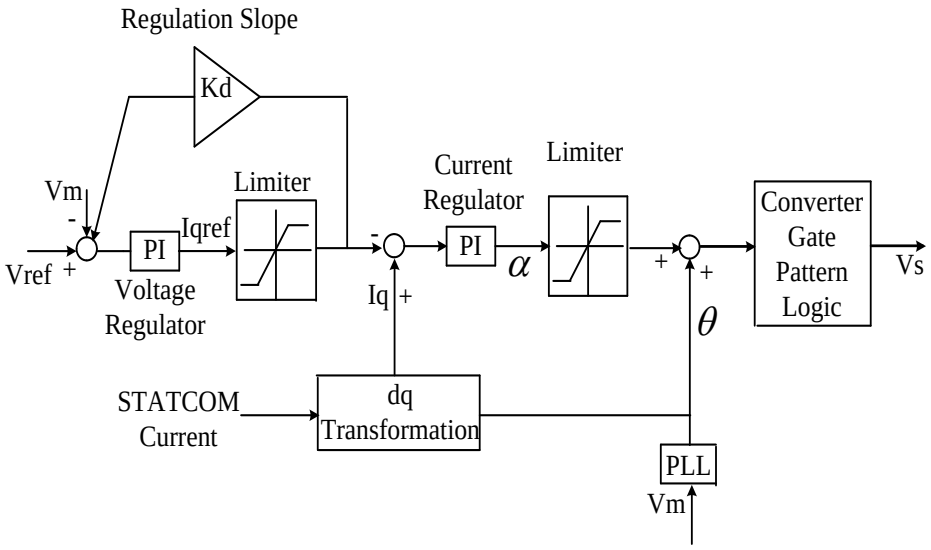

Figure 3.2 Traditional STATCOM PI control block diagram.

As shown in Figure 3.2, the phase locked loop (PLL) provides the basic synchronizing signal which is the reference angle to the measurement system. Measured bus line voltage

V_m is compared with the reference voltage V_{ref} and the voltage regulator provides the required reactive reference current I_{qref}. The droop factor, K_d, is defined as the allowable voltage error at the rated reactive current flow through the STATCOM. The STATCOM reactive current I_q is compared with I_{qref}, and the output of the current regulator is the angle phase shift of the inverter voltage w.r.t. the system voltage. The limiter is the limit imposed on the value of control with the consideration of the maximum reactive power capability of the STATCOM.

3.3 Adaptive PI Control for STATCOM

3.3.1 Concept of the proposed adaptive PI control method

The STATCOM with fixed PI control parameters may not reach the desired and acceptable response in a power system when the power system operating condition (e.g., loads or transmissions) changes. An adaptive PI control method is presented in this section in order to obtain the desired response and to avoid performing trial-and-error studies to find suitable parameters for PI controllers when a new STATCOM is installed in a power system. With this adaptive PI control method, the dynamical self-adjustment of PI control parameters can be realized.

An adaptive PI control block for STATCOM is shown in Figure 3.3. In Figure 3.3, the measured voltage $V_m(t)$ and the reference voltage $V_{ref}(t)$, the q-axis reference current I_{qref} and the q-axis current I_q are in per unit values. The proportional and integral parts of the voltage regulator gains are denoted by K_{p_V} and K_{i_V}, respectively. Similarly, the gains K_{p_I} and K_{i_I} represent the proportional and integral parts, respectively, of the current regulator. In this control system, the allowable voltage error K_d is set to 0. The K_{p_V}, K_{i_V}, K_{p_I} and K_{i_I} can be set to an arbitrary initial value such as simply 1.0. One exemplary desired curve is an exponential curve in terms of the voltage growth, shown in Figure 3.4, which is set as the reference voltage in the outer loop. Other curves may also be used than the depicted exponential curve so long as the measured voltage returns to the desired steady state voltage in the desired time duration.

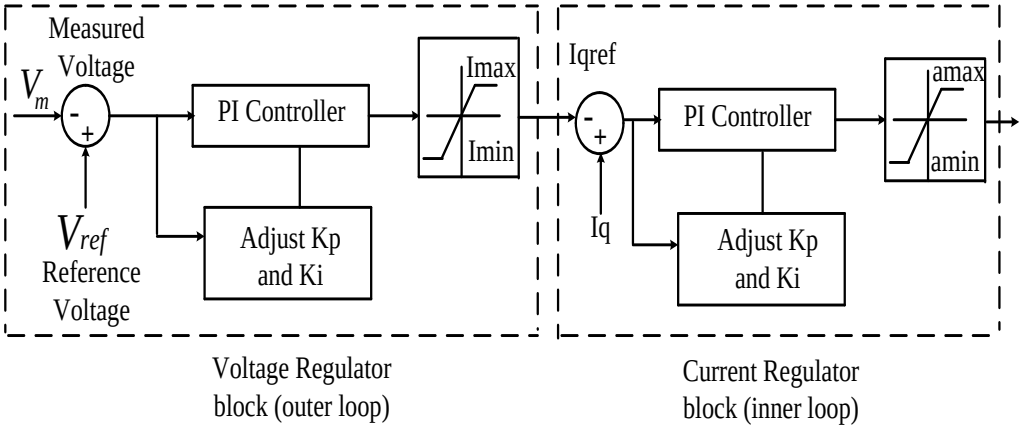

Figure 3.3 Adaptive PI control block for STATCOM.

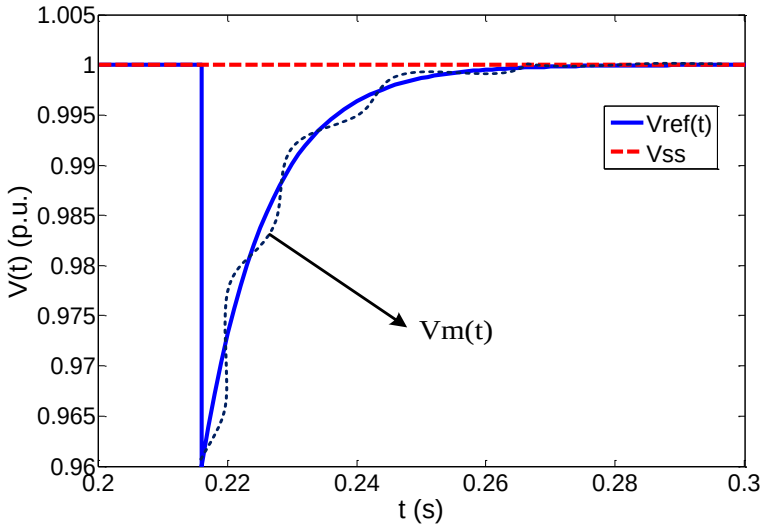

Figure 3.4 Reference voltage curve.

The process of adaptive voltage control method for STATCOM is described as follows:

(1) The bus voltage $V_m(t)$ is measured in real time.

(2) When the measured bus voltage over time $V_m(t) \neq V_{ss}$, the target steady-state voltage (which is set to 1.0 per unit (p.u.) in the discussion and examples), the measured voltage is compared with V_{ss}. Based on the desired reference voltage curve, K_{p_V} and K_{i_V} are dynamically adjusted in order to make the measured voltage match the desired reference voltage, and the q-axis reference current I_{qref} can be obtained.

(3) In the inner loop, I_{qref} is compared with the q-axis current I_q. Using the similar control method like the one for the outer loop, the parameters K_{p_I} and K_{i_I} can be adjusted based on the error. Then, a suitable angle can be found and eventually the DC voltage in

STATCOM can be modified such that STATCOM provides the exact amount of reactive power injected into the system to keep the bus voltage at the desired value.

It should be noted that the current I_{max} and I_{min} and the angle α_{max} and α_{min} are the limits imposed with the consideration of the maximum reactive power generation capability of the STATCOM controlled in this manner. If one of the maximum or minimum limits is reached, the maximum capability of the STATCOM to inject reactive power has been reached. Certainly, as long as the STATCOM sizing has been appropriately studied during planning stages for inserting the STATCOM into the power system, the STATCOM should not reach its limit unexpectedly.

3.3.2 Derivation of the key equations

Since the inner loop control is similar to the outer loop control, the mathematical method to automatically adjust PI controller gains in the outer loop is discussed in this section for illustrative purpose. Similar analysis can be applied to the inner loop.

Here the measured bus voltages of three phases are denoted by $V_{al}(t)$, $V_{bl}(t)$, and $V_{cl}(t)$, respectively. Then, $V_{dl}(t)$ and $V_{ql}(t)$ can be computed with *d-q* transformation.

$$\begin{bmatrix} V_{dl}(t) \\ V_{ql}(t) \\ 0 \end{bmatrix} = \frac{2}{3}\begin{bmatrix} 1 & -\frac{1}{2} & -\frac{1}{2} \\ 0 & \frac{\sqrt{3}}{2} & -\frac{\sqrt{3}}{2} \\ \frac{1}{\sqrt{2}} & \frac{1}{\sqrt{2}} & \frac{1}{\sqrt{2}} \end{bmatrix}\begin{bmatrix} V_{al}(t) \\ V_{bl}(t) \\ V_{cl}(t) \end{bmatrix} \tag{3.12}$$

Then, we have

$$V_m(t) = \sqrt{V_{dl}^2(t) + V_{ql}^2(t)} \tag{3.13}$$

Based on $V_m(t)$, the reference voltage $V_{ref}(t)$ is set as:

$$\mathrm{V}_{ref}(t) = V_{SS} - \left(V_{ss} - V_m(t)\right)e^{-\frac{t}{\tau}} \tag{3.14}$$

In (3.14), V_{ss} is the target steady-state voltage (which is set to 1.0 per unit (p.u.) in the discussion and examples); $V_m(t)$ is the measured voltage; τ=0.01s. The curve in Figure 3.4 is one of the examples for $V_{ref}(t)$.

If the system is operating in the normal condition, then $V_m(t)$=1 p.u., and thus, $V_{ref}(t)$=1 p.u. This means that K_{p_V} and K_{i_V} will not change and the STATCOM will not inject or absorb any reactive power to maintain the voltage meeting the reference voltage. However, once there is a voltage disturbance in the power system, based on $V_{ref}(t) = V_{SS} - \left(V_{ss} - V_m(t)\right)e^{-\frac{t}{\tau}}$, K_{p_V} and K_{i_V} will become adjustable and the STATCOM will provide reactive power to increase the voltage. Here, the error between $V_{ref}(t)$ and $V_m(t)$ is denoted by $\Delta V(t)$ when there is a disturbance in the power system. Based on the adaptive voltage control model, at any arbitrary time instant t, the following equation can be obtained:

$$\Delta\mathrm{V}(t)K_{p\_V}(t) + K_{i\_V}(t)\int_t^{t+T_s}\Delta\mathrm{V}(t)dt = I_{qref}(t+T_s) \tag{3.15}$$

where in this example, T_s is the sample time, which is set to 2.5×10^{-5} second.

In this system, the Discrete-Time Integrator block in place of the Integrator block is used to create a purely discrete system, and the Forward-Euler method is used in the

Discrete-Time Integrator block. Therefore, the resulting expression for the output of the Discrete-Time Integrator block at *t* is

$$y(t) = y(t - T_s) + K_{i\_V}(t - T_s) \times T_s \times \Delta V(t - T_s) \tag{3.16}$$

where $y(t) = K_{i\_V}(t) \int_t^{t+T_s} \Delta V(t)dt$; $y(t - T_s) = K_{i\_V}(t - T_s) \int_{t-T_s}^{t} \Delta V(t - T_s)dt$.

Considering $y(t - T_s) = I_{qref}(t)$, we can rewrite (3.15) as follows:

$$\Delta V(t)K_{p\_V}(t) + K_{i\_V}(t) \int_t^{t+T_s} \Delta V(t)dt - K_{i\_V}(t - T_s) \ldots$$

$$\int_{t-T_s}^{t} \Delta V(t - T_s)dt = I_{qref}(t + T_s) - I_{qref}(t) \tag{3.17}$$

Over a very short time duration, we can consider $K_{i\_V}(t) = K_{i\_V}(t - T_s)$. Hence, (3.17) can be rewritten as:

$$\Delta V(t)K_{p\_V}(t) + K_{i\_V}(t) \int_t^{t+T_s} A dt = I_{qref}(t + T_s) - I_{qref}(t) \tag{3.18}$$

where A=$\Delta V(t) - \Delta V(t - T_s)$.

Based on (3.16), if we can determine in ideal response the radio $\frac{I_{qref}(t+T_s) - I_{qref}(t)}{\Delta V(t)}$ and the ideal ratio $\frac{K_{i\_V}(t)}{K_{p\_V}(t)}$, the desired $K_{p\_V}(t)$ and $K_{i\_V}(t)$ can be solved.

Assuming at the ideal response, we have

$$I_{qref}(t + T_s) - I_{qref}(t) = R \times \Delta V(t) \tag{3.19}$$

Since the system is expected to be stable, without losing generality, we may assume that the bus voltage will come back to 1 per unit in 5τ, where 5τ is the delay defined by users as shown in Figure 3.4. Since $I_{qref}(t_0)$=0 based on (3.15) and (3.19), (3.15) can be rewritten as:

$$\Delta V(t_0)K_{p\_V}(t_0) + K_{i\_V}(t_0)\int_{t_0}^{t_0+5\tau}\Delta V(t)dt = R \times \Delta V(t_0) \quad (3.20)$$

where t_0 is the time that the system disturbance occurs.

Set $K_{i\_V}(t_0^-)$=0, then we have

$$K_{p\_V}(t_0) = R \quad (3.21)$$

Set $K_{p\_V}(t_0^-)$=0, then we have

$$K_{i\_V}(t_0) = \frac{\Delta V(t_0)\times R}{\int_{t_0}^{t_0+5\tau}\Delta V(t)dt} \quad (3.22)$$

Now the ratio $m_V = \frac{K_{i\_V}(t_0)}{K_{p\_V}(t_0)}$ can be considered as the ideal ratio of the values of $K_{p\_V}(t)$ and $K_{i\_V}(t)$ after disturbances.

Thus, (3.19) can be rewritten as

$$I_{qref}(t+5\tau) - I_{qref}(t) = k_V \times \Delta V(t_0) \quad (3.23)$$

Here k_V can be considered as the steady and ideal ratio $\frac{I_{qref}(t+T_s)-I_{qref}(t)}{\Delta V(t)}$.

Based on the system bus capacity and the STATCOM rating, ΔV_{max} can be obtained, which means any voltage change greater than ΔV_{max} cannot come back to 1 per unit. Since we have $-1 \le I_{qref}(t) \le 1$, we have the following equation:

$$\frac{\Delta V(t_0)}{\Delta V_{max}} = k_V \times \frac{\Delta V(t_0)K_{p\_V}(t_0)+K_{i\_V}(t_0)\int_{t_0}^{t_0+5\tau}\Delta V(t)dt}{R} \quad (3.24)$$

Based on (3.20), (3.23) and (3.24), k_v can be calculated by:

$$k_V = \frac{R\times\Delta V(t_0)}{\left(K_{p\_V}(t_0)\Delta V(t_0)+K_{i\_V}(t_0)\int_{t_0}^{t_0+5\tau}\Delta V(t)dt\right)\times\Delta V_{max}} \quad (3.25)$$

In order to exactly calculate the PI controller gains, based on (3.18), we can derive:

$$\Delta V(t)K_{p\_V}(t) + m_V K_{p\_V}(t)\int_t^{t+T_S} A dt = k_V \times \Delta V(t) \quad (3.26)$$

Therefore, $K_{p\_V}(t)$ and $K_{i\_V}(t)$ can be computed by the following equations:

$$K_{p\_V}(t) = \frac{k_V \times \Delta V(t)}{\left(\Delta V(t) + m_V \times \int_t^{t+T_S} A dt\right)} \quad (3.27)$$

$$K_{i\_V}(t) = m_V \times K_{p\_V}(t) \quad (3.28)$$

Therefore, based on (3.27) and (3.28), $K_{p\_V}(t)$ and $K_{i\_V}(t)$ can be adjusted dynamically.

Using similar process, the following expressions for current regulator PI gains can be obtained:

$$K_{p\_I}(t) = \frac{k_I \times \Delta I_q(t)}{\left(\Delta I_q(t) + m_I \times \int_t^{t+T_S} B dt\right)} \quad (3.29)$$

$$K_{i\_I}(t) = m_I \times K_{p\_I}(t) \quad (3.30)$$

where $\Delta I_q(t)$ is the error between I_{qref} and I_q; k_I is the steady and ideal ratio $\frac{\alpha(t+T_S)-\alpha(t)}{\Delta I_q(t)}$ and $\alpha(t)$ is the angle that phase shift of the inverter voltage with respect to the system voltage at time t; m_I is the ideal ratio of the values of $K_{p\_I}(t)$ and $K_{i\_I}(t)$ after disturbances; and B is equal to $\Delta I_q(t) - \Delta I_q(t-T_S)$.

Note that the derivation from Equations (3.14) to (3.30) is fully reversible so it ensures that the measured voltage curve can follow the desired ideal response, as defined in Eq. (3.14).

3.3.3 Flow charts of the adaptive PI control procedure

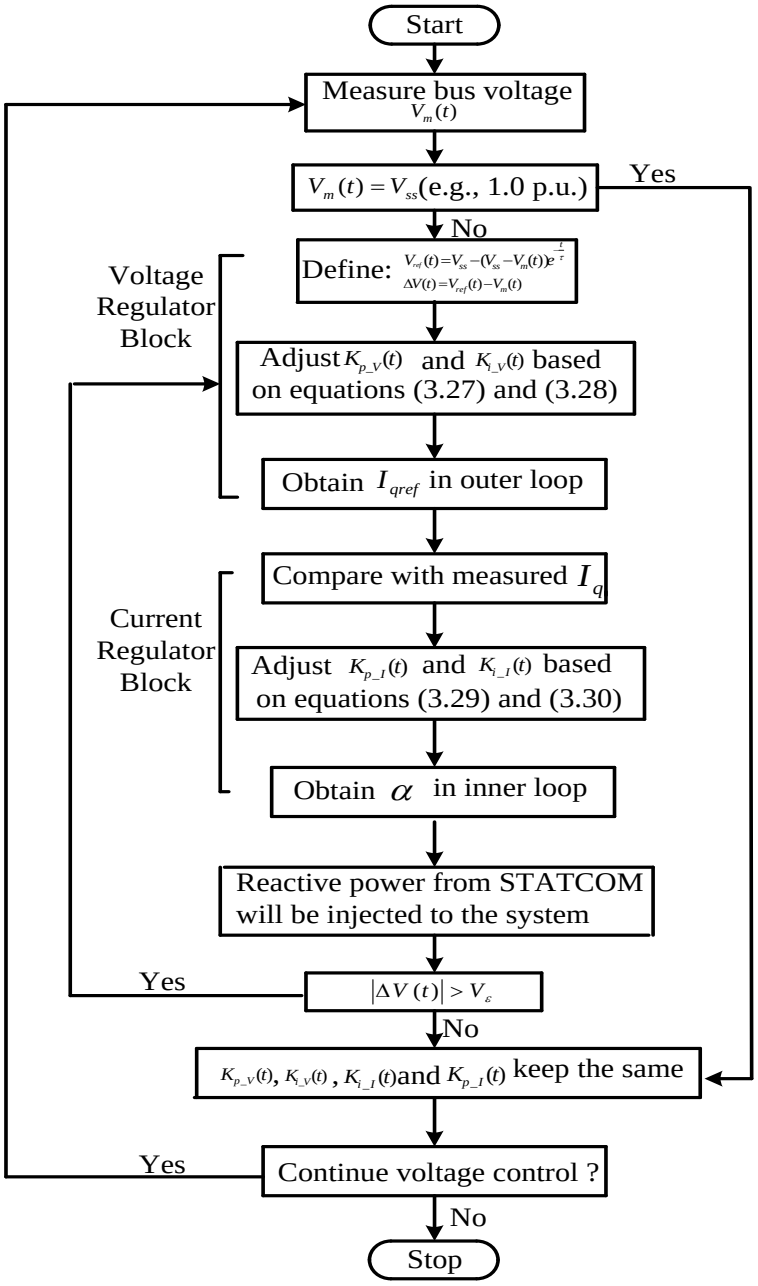

Figure 3.5 Adaptive PI control algorithm flow chart.

Figure 3.5 is an exemplary flowchart of the proposed adaptive PI control for STATCOM for the block diagram of Figure 3.3.

The adaptive PI control process begins at Start. The bus voltage over time $V_m(t)$ is sampled according to a desired sampling rate. Then, $V_m(t)$ is compared with V_{ss}, the desired steady-state voltage. If $V_m(t)=V_{ss}$, then, there is no reason to change any of the identified parameters: $K_{p\_V}(t)$, $K_{i\_V}(t)$, $K_{i\_I}(t)$ and $K_{p\_I}(t)$. The power system is running smoothly. On the other hand, if $V_m(t) \neq V_{ss}$, then adaptive PI control begins.

The measured voltage is compared with $V_{ref}(t)$, the reference voltage defined in (3.14). Then, $K_{p\_V}(t)$ and $K_{i\_V}(t)$ are adjusted in the voltage regulator block (outer loop) based on Eqs. (3.27) and (3.28), which leads to an updated I_{qref} via a current limiter as shown in Figure 3.3.

Then, the I_{qref} is compared with the measured q-current, I_q. The control gains $K_{p\_I}(t)$ and $K_{i\_I}(t)$ are adjusted based on Eqs. (3.29) and (3.30). Then, the phase angle α is determined and passed through a limiter for output, which essentially decides the reactive power output from the STATCOM.

Next, if $|\Delta V(t)|$ is not within a tolerance threshold, V_ε, which is a very small value such as 0.001 p.u., the voltage regulator block and current regulator blocks are reentered until the change is less than the given threshold V_ε. Thus, the values for $K_{p\_V}(t)$, $K_{i\_V}(t)$, $K_{i\_I}(t)$ and $K_{p\_I}(t)$ are maintained.

If it is needed to continuously perform the voltage control process which is usually the case, then the process returns to measured bus voltage. Otherwise, the voltage control process stops, i.e., the STATCOM control is deactivated.

3.4 Simulation Results

3.4.1 System Data

In the system simulation diagram shown in Figure 3.6, a +/-100 MVAR STATCOM is implemented with a 48-pulse VSC and connected to a 500kV bus. This is the standard sample STATCOM system in MATLAB/Simulink library, and all machines used in the simulation are dynamical models [26-28]. Here, the attention is focused on the STATCOM control performance in bus voltage regulation mode. In the original model, the compensating reactive power injection and the regulation speed are mainly affected by PI controller parameters in the voltage regulator and the current regulator. The original control will be compared with the proposed adaptive PI control model.

Assume the steady-state voltage, V_{ss}=1.0 per unit. In subsection 3.4.2, 3.4.3 and 3.4.6, a disturbance is assumed to cause a voltage drop at 0.2 sec from 1.0 to 0.989 per unit at the source (substation A). Here, the 0.989 p.u. voltage at the substation is the lowest voltage that the STATCOM system can support due to its capacity limit. The third simulation study in subsection 3.4.4 assumes a voltage drop from 1.0 to 0.991 under a changed load. The

fourth simulation study in subsection 3.4.5 assumes a disturbance at 0.2 sec causing a voltage rise from 1.0 to 1.01 per unit at the substation under a modified transmission network. When there is a severe voltage sag (i.e. to 60% of the rated voltage), the voltage will be corrected to the maximum of STATCOM's capability (i.e., injecting the highest reactive current). When the fault clears, the voltage should get back to 1.0 per unit or very close. This case is studied in substation 3.4.7. In all simulation studies, the STATCOM immediately operates after the disturbance with the expectation of bringing the voltage back to 1.0 p.u.

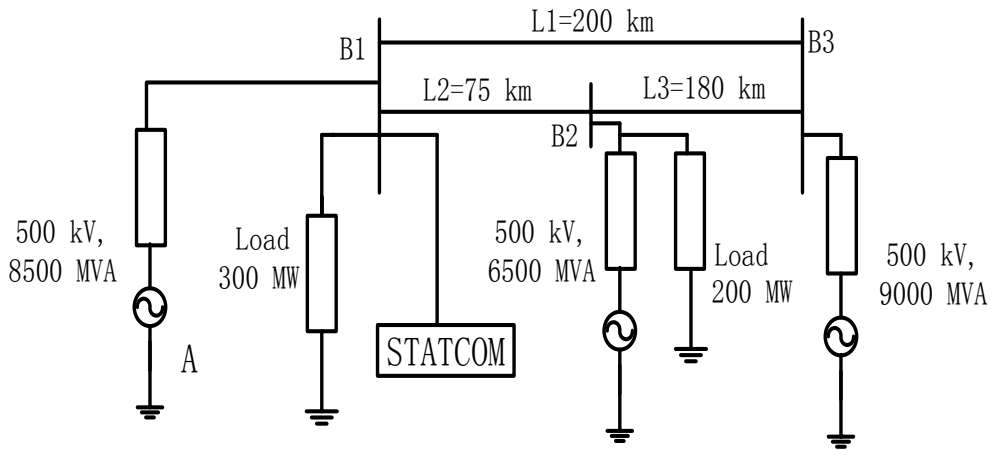

Figure 3.6 The studied system.

3.4.2 Response of the original model

In the original model, K_{p_V}=12, K_{i_V}=3000, K_{p_I}=5, K_{i_I}=40. Here, we keep all the parameters unchanged. The initial voltage source, shown in Figure 3.6, is 1.0 p.u., with the

voltage base being 500kV. In this case, if we set R=1, based on (3.21) and (3.22), then we have the initial m_v calculated as:

$$m_V = \frac{K_{i\_V}(t_0)}{K_{p\_V}(t_0)} = 770.8780$$

Based on (3.25), k_V =84.7425 can be obtained. Then, based on (3.27) to (3.30), we have

$$K_{p\_V}(t) = \frac{84.7425 \times \Delta V(t)}{\left(\Delta V(t) + 770.8780 \times \int_t^{t+T_s} A dt\right)} \tag{3.31}$$

$$K_{i\_V}(t) = 770.8480 \times K_{p\_V}(t) \tag{3.32}$$

$$K_{p\_I}(t) = \frac{57.3260 \times \Delta I_q(t)}{\left(\Delta I_q(t) + 2.3775 \times \int_t^{t+T_s} B dt\right)} \tag{3.33}$$

$$K_{i\_I}(t) = 2.3775 \times K_{p\_I}(t) \tag{3.34}$$

Based on (3.31) to (3.34), the adaptive PI control system can be designed. m_V and k_V will be changed according to the different disturbances. The steps listed above show how to obtain the control gains in the above case. The PI control gains of the proposed control are also shown in Figures 3.7 and 3.8. In order to avoid unnecessary overshooting, the threshold for K_{i_V} and K_{i_I} is 10000. The threshold for K_{p_V} and K_{p_I} is 400. The sample time in this simulation model is 25μs. Since during some sample times the control gains change quickly to track the desired response, which causes the spikes in the 0.2 sec to 0.6 sec time range. The spikes actually show the change of control gains in very short time (see Figure 3.8). The results of the original control method and the adaptive PI control method are shown in Figure 3.9, 3.10 and 3.11 respectively. Observations are summarized in Table 3.1.

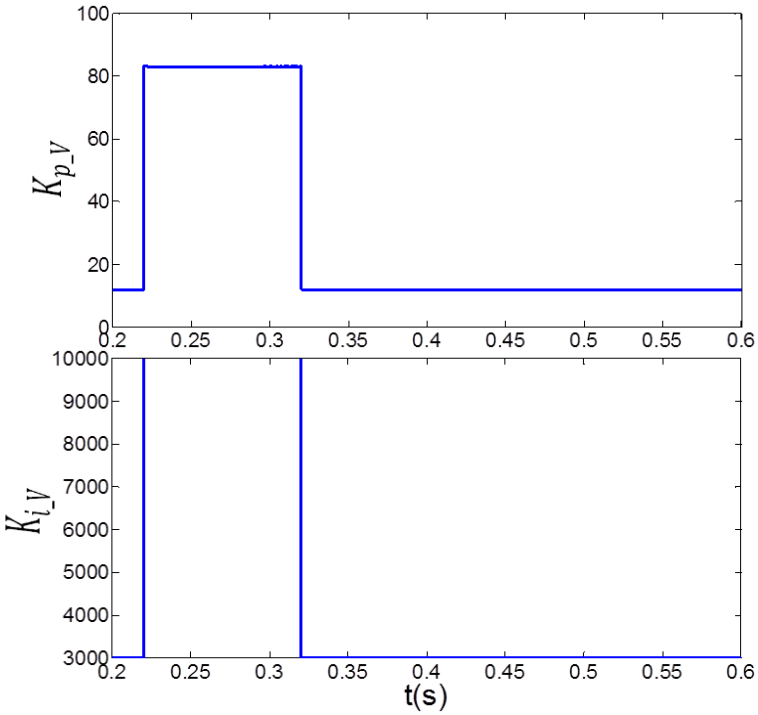

Figure 3.7 PI control gains of voltage regulator using the same network and loads.

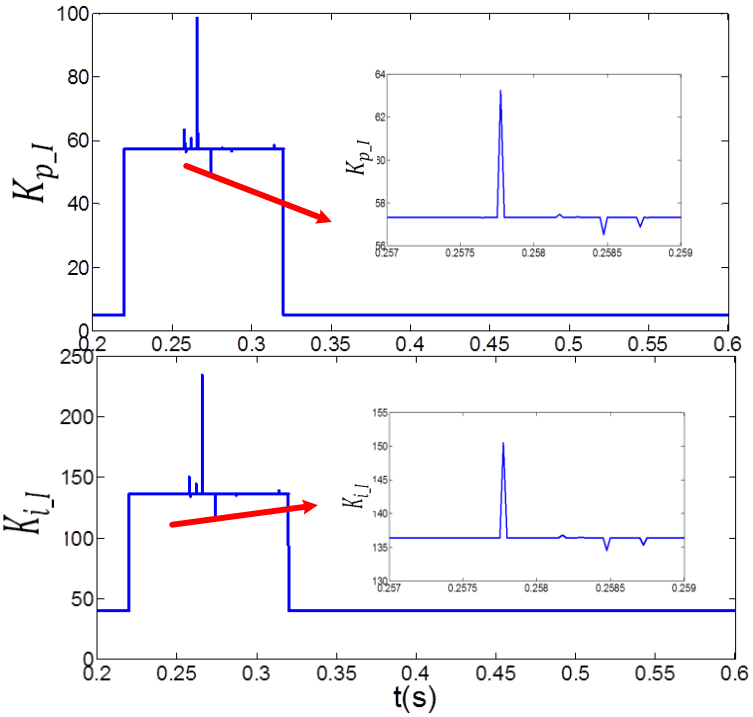

Figure 3.8 PI control gains of current regulator using the same network and loads.

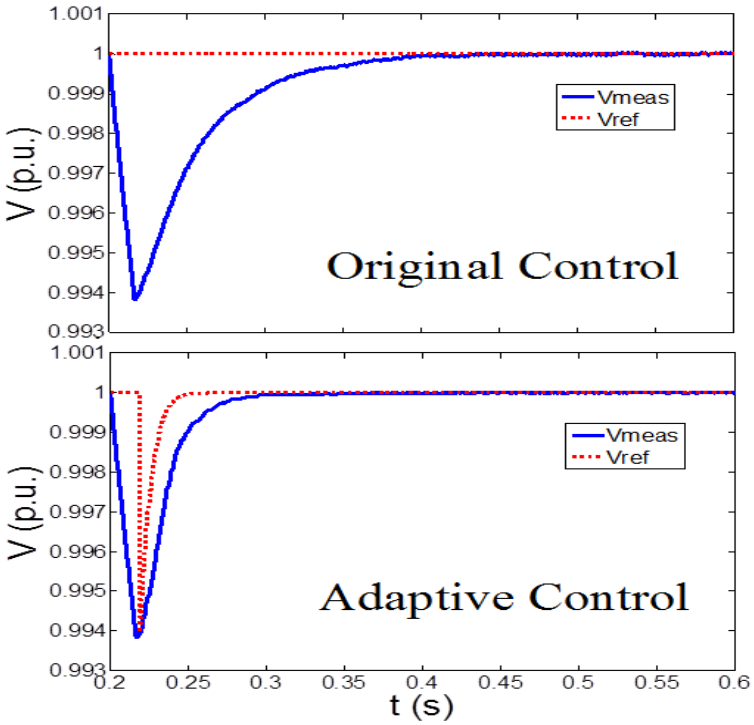

Figure 3.9 Results of the voltages using the same network and loads.

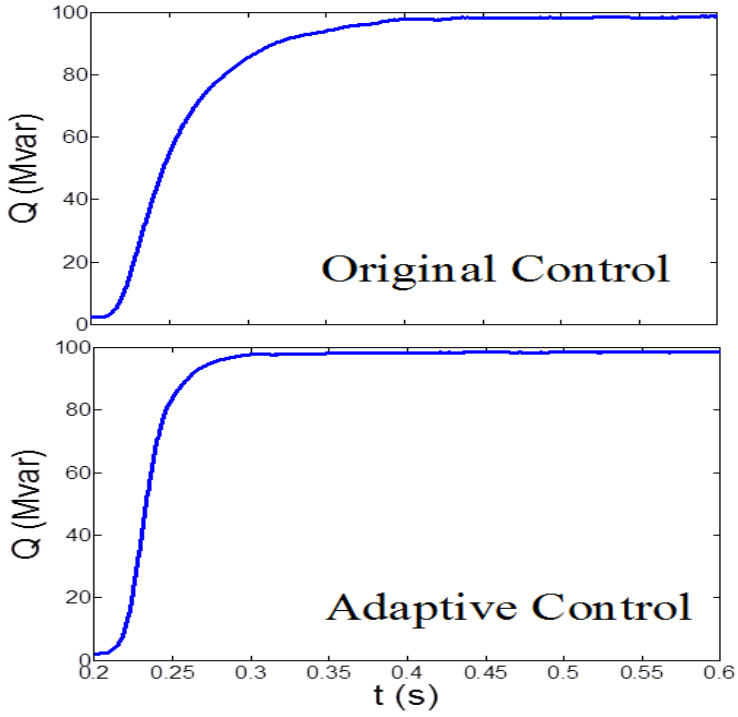

Figure 3.10 Results of the output reactive power using the same network and loads.

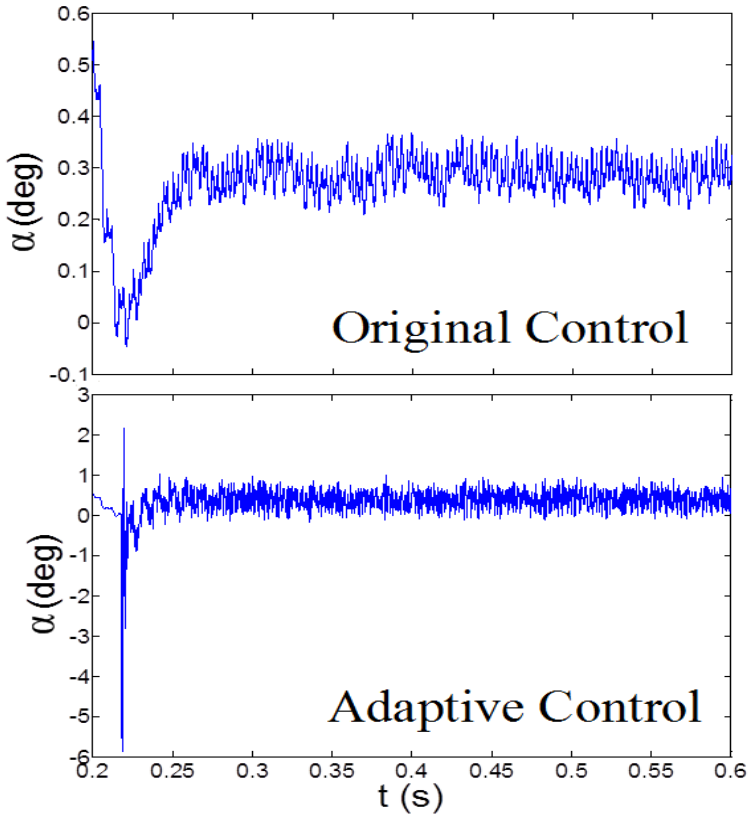

Figure 3.11 Results of α using the same network and loads.

Table 3.1 Performance comparison for the original system parameters

	Original Ctrl.	Adaptive Ctrl.
Lowest Voltage after disturbance	0.9938 p.u.	0.9938 p.u.
Time (sec) when V=1.0	0.4095 sec	0.2983 sec
Δt to reach V=1.0	0.2095 sec	0.0983 sec
Var Amount at steady state	97.76 MVar	97.65 MVar
Time to reach steady state Var	0.4095 sec	0.2983 sec

From the results, it is obvious that the adaptive PI control can achieve quicker response than the original control. The needed reactive power amount is the same while the adaptive PI approach runs faster, as the voltage does.

Set $\omega t = \alpha + \theta$, where α is the output angle of the current regulator, θ is the reference angle to the measurement system. In the STATCOM, it is ωt that decides the control signal. Since θ is a very large value (varying between 0 to 2π), the ripples of α in the scale shown in Figure 3.11 will not affect the final simulation results.

Note, there is a very slight difference of 0.12 MVar in Var amount at steady state in Table 3.1, which should be caused by computational round-off error. The reason is that the sensitivity of dVAR/dV is around 100MVar/0.011 p.u. of voltage. For simplicity, we may assume the ΔVar/ΔV sensitivity is a linear function. Thus, when the voltage error is 0.00001 p.u., ΔVar is 0.0909 MVar which is in the same range as the 0.12 MVar mismatch. Thus, it is reasonable to conclude that the slight Var difference in Table 3.1 is due to round-off error in the dynamic simulation which always gives tiny ripples beyond 5^{th} digits even in the final steady state.

3.4.3 Change of *Kp* and *Ki*

In this scenario, the other system parameters remain unchanged while the PI controller gains for the original control are changed to: K_{p_V}=1, K_{i_V}=1, K_{p_I}=1, K_{i_I}=1.

The dynamic control gains, which are independent of the initial values before the

disturbance but depending on the post-fault conditions, are given as:

$$K_{p\_V}(t) = \frac{80.1632 \times \Delta V(t)}{\left(\Delta V(t) + 732.3115 \times \int_t^{t+T_S} A dt\right)} \tag{3.35}$$

$$K_{i\_V}(t) = 732.3115 \times K_{p\_V}(t) \tag{3.36}$$

$$K_{p\_I}(t) = \frac{47.4959 \times \Delta I_q(t)}{\left(\Delta I_q(t) + 1.8232 \times \int_t^{t+T_S} B dt\right)} \tag{3.37}$$

$$K_{i\_I}(t) = 1.8232 \times K_{p\_I}(t) \tag{3.38}$$

Based on (3.35) to (3.38), the adaptive PI control model can be designed. The PI control gains of the proposed control are also shown in Figure 3.12 and Figure 3.13. The results of original and the adaptive PI control methods are shown in Figure 3.14, Figure 3.15 and Figure 3.16 respectively.

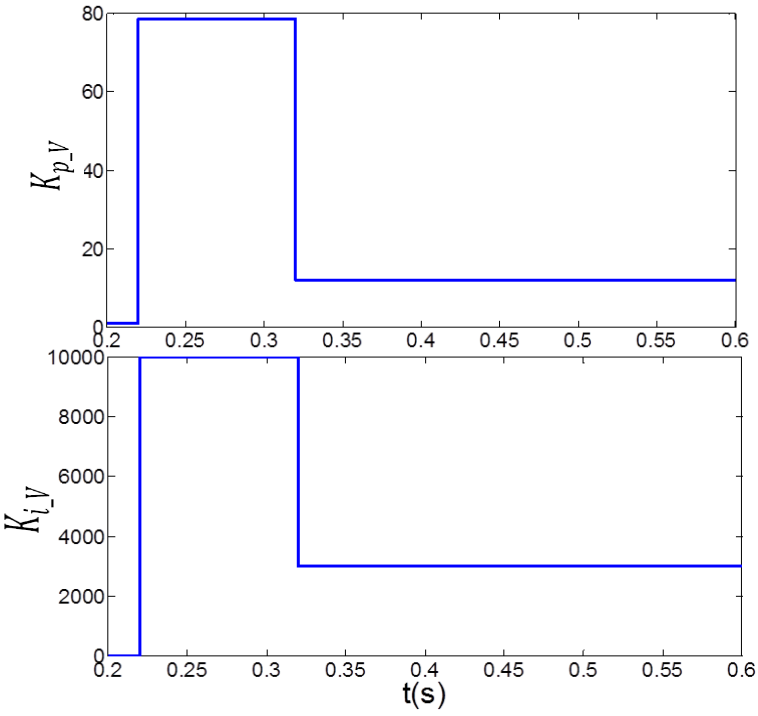

Figure 3.12 PI control gains of voltage regulator with changed K_p and K_i.

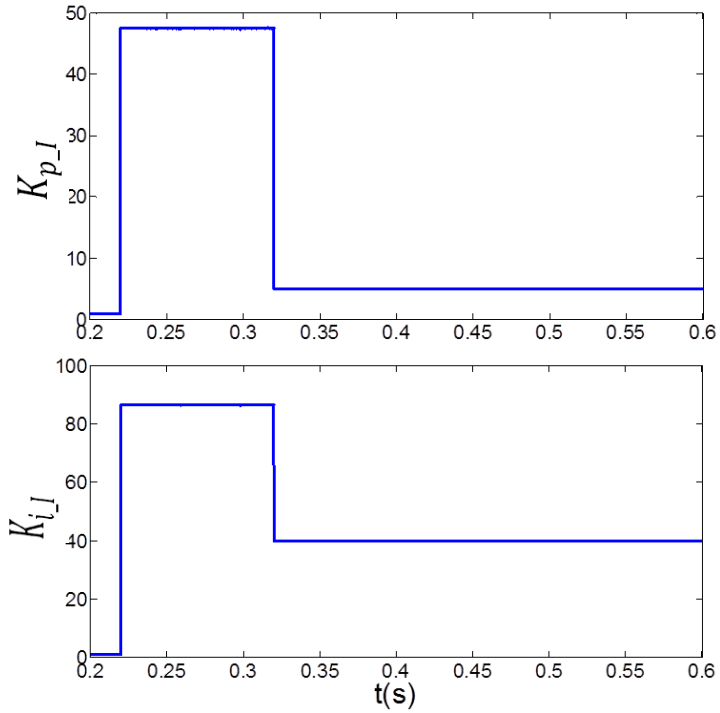

Figure 3.13 PI control gains of current regulator with changed K_p and K_i.

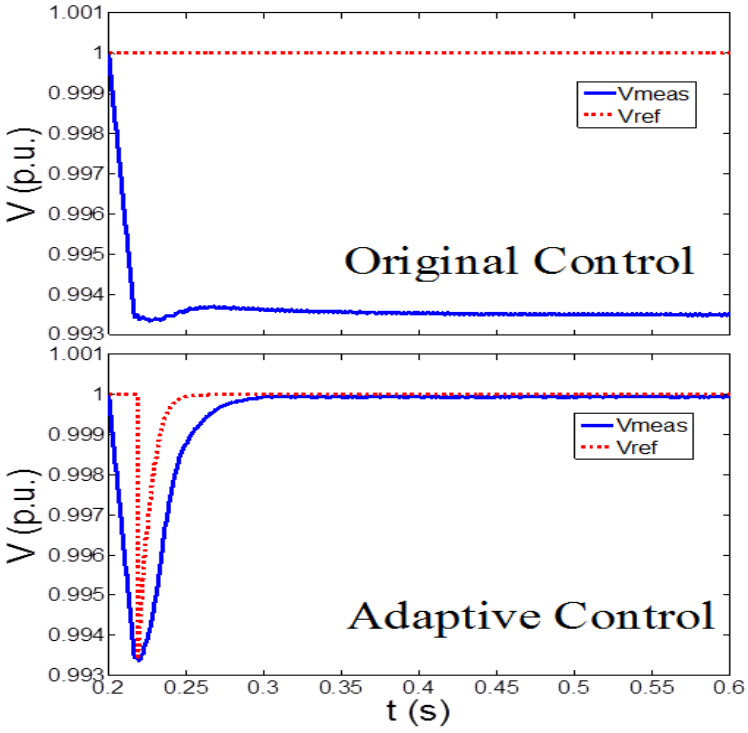

Figure 3.14 Voltages with changed K_p and K_i in the original control.

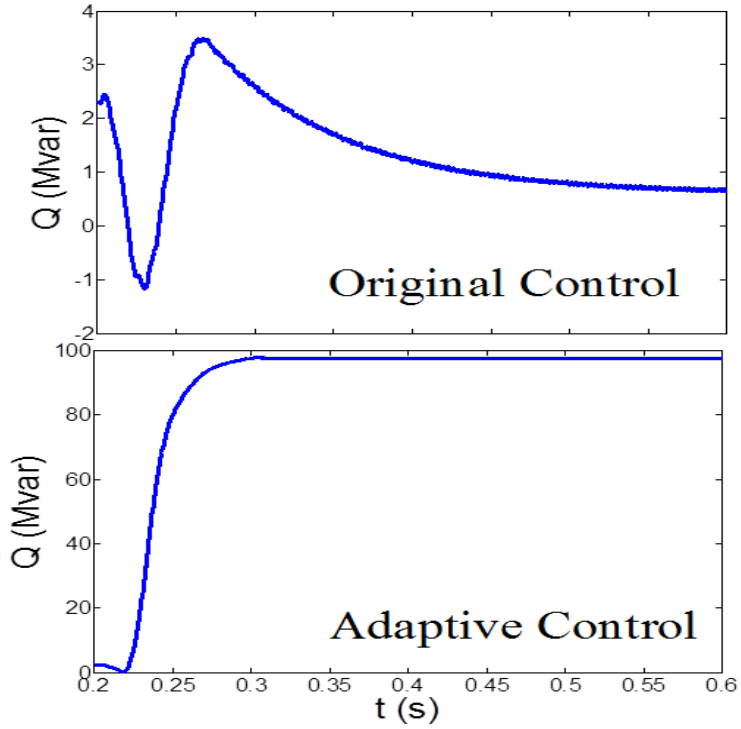

Figure 3.15 Output reactive power with changed K_p and K_i in the original control.

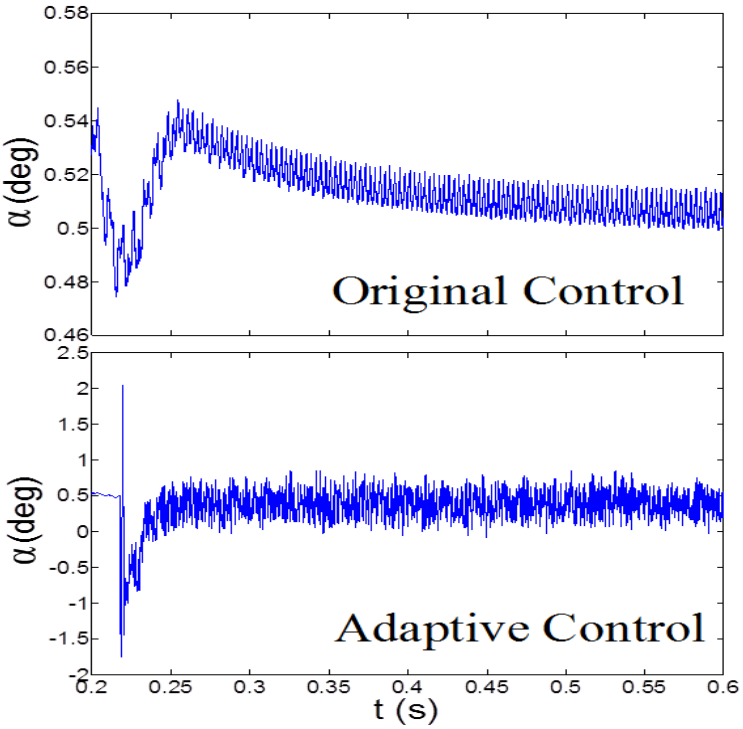

Figure 3.16 Results of α with changed K_p and K_i in the original control.

From Figure 3.14, it can be observed that when K_p and K_i are changed to different values, the original control model cannot make the bus voltage get back to 1.0 p.u. and the STATCOM has a poor response. The reactive power cannot be increased to a level to meet the need. However, by the adaptive PI control, the STATCOM can response to disturbance perfectly as desired, and the voltage can get back to 1.0 p.u. quickly within 0.1 sec. Figure 3.15 also shows that the reactive power injection cannot be continuously increased in the original control to support voltage, while the adaptive PI control performs as desired.

3.4.4 Change of Load

In this case, the original PI controller gains are kept, which means K_{p_V}=12, K_{i_V}=3000, K_{p_I}=5 and K_{i_I}=40. However, the load at Bus B1 is changed from 300MW to 400MW.

In this case, we have the dynamic control gains given by:

$$K_{p\_V}(t) = \frac{93.3890 \times \Delta \mathrm{V}(t)}{\left(\Delta \mathrm{V}(t) + 187.5579 \times \int_t^{t+T_S} \mathrm{A} dt\right)} \tag{3.39}$$

$$K_{i\_V}(t) = 187.5579 \times K_{p\_V}(t) \tag{3.40}$$

$$K_{p\_I}(t) = \frac{8.1731 \times \Delta \mathrm{I}_q(t)}{\left(\Delta \mathrm{I}_q(t) + 13.1652 \times \int_t^{t+T_S} \mathrm{B} dt\right)} \tag{3.41}$$

$$K_{i\_I}(t) = 13.1652 \times K_{p\_I}(t) \tag{3.42}$$

Based on (3.39) to (3.42), the adaptive PI control model can be designed for automatic reaction to change in loads. The PI control gains of the proposed control are also shown in Figures 3.17 and 3.18. The results from the original and the adaptive PI control methods are shown in Figures 3.19, 3,20 and 3.21. Table 3.2 shows a few key observations of the performance.

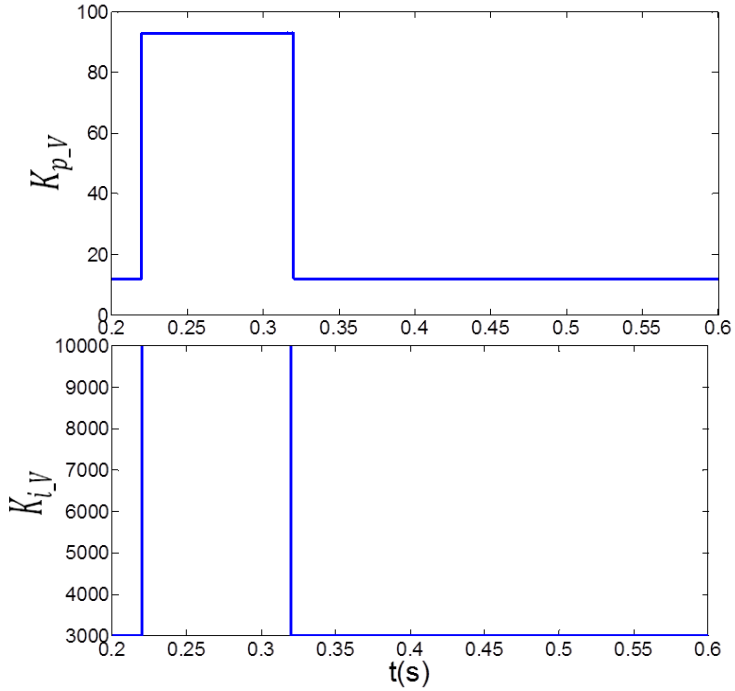

Figure 3.17 PI control gains of voltage regulator with change of load.

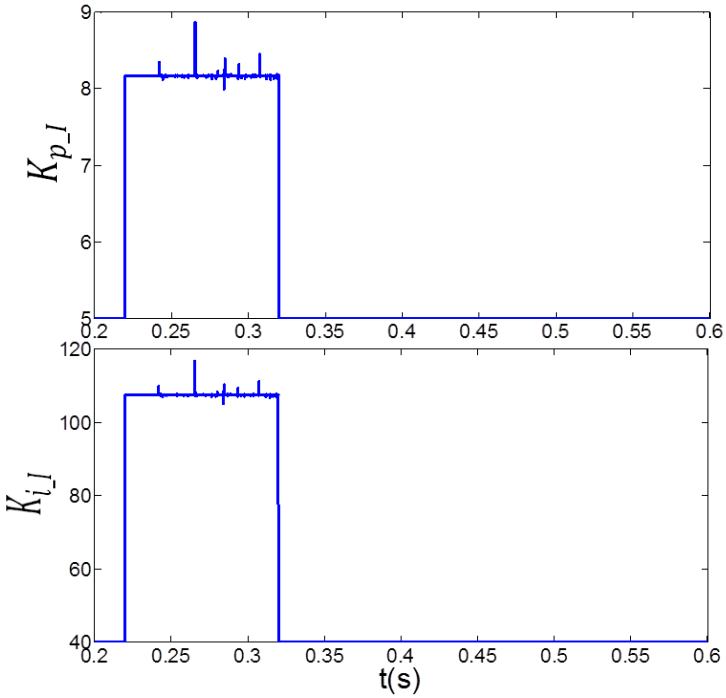

Figure 3.18 PI control gains of current regulator with change of load.

Table 3.2 Performance comparison with a change of load.

	Original Ctrl.	Adaptive Ctrl.
Lowest Voltage after disturbance	0.9949 p.u.	0.9949 p.u.
Time (sec) when V=1.0	0.4338 sec	0.3125 sec
Δt to reach V=1.0	0.2338 sec	0.1125 sec
Var Amount at steady state	93.08 MVar	92.72 MVar
Time to reach steady state Var	0.4338 sec	0.3125 sec

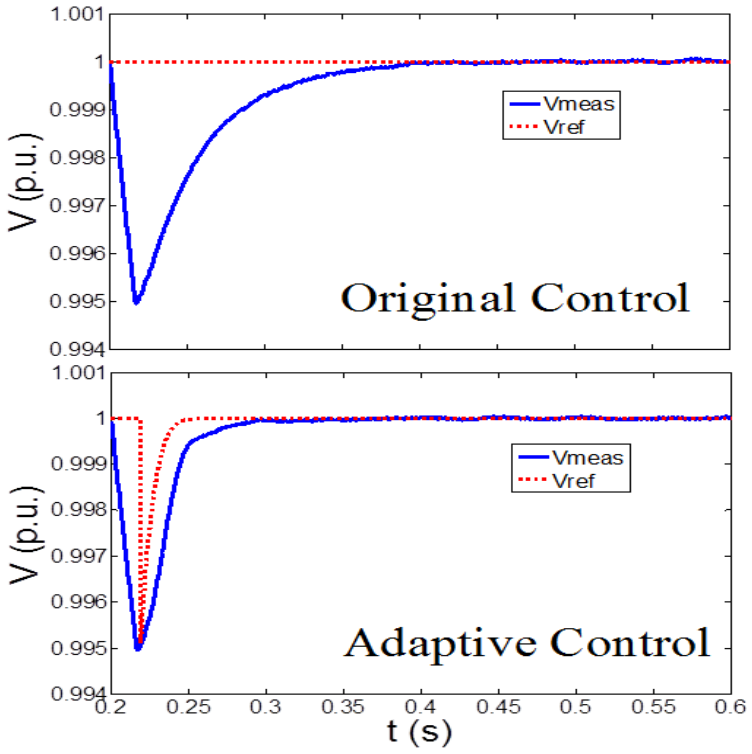

Figure 3.19 Results of measured voltage with change of load.

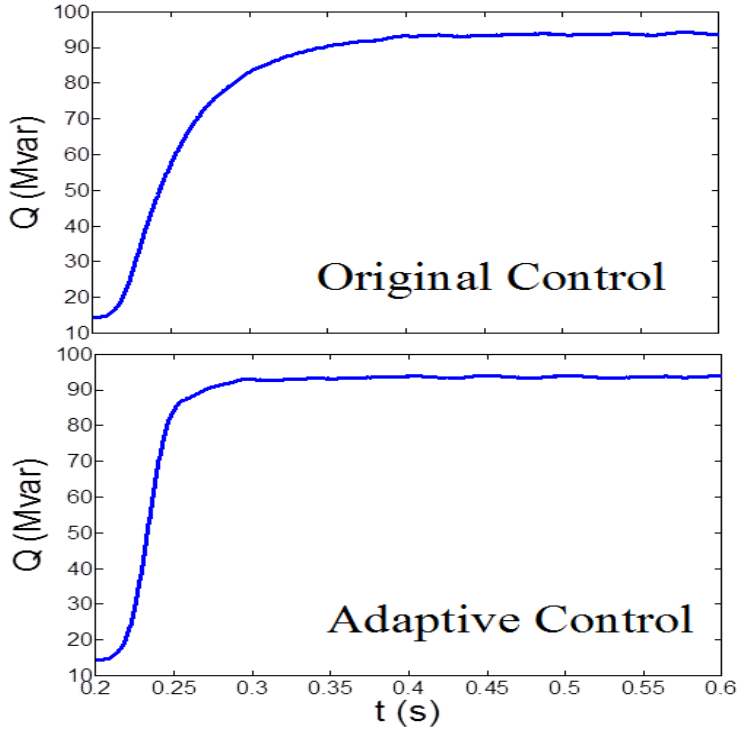

Figure 3.20 Results of output reactive power with change of load.

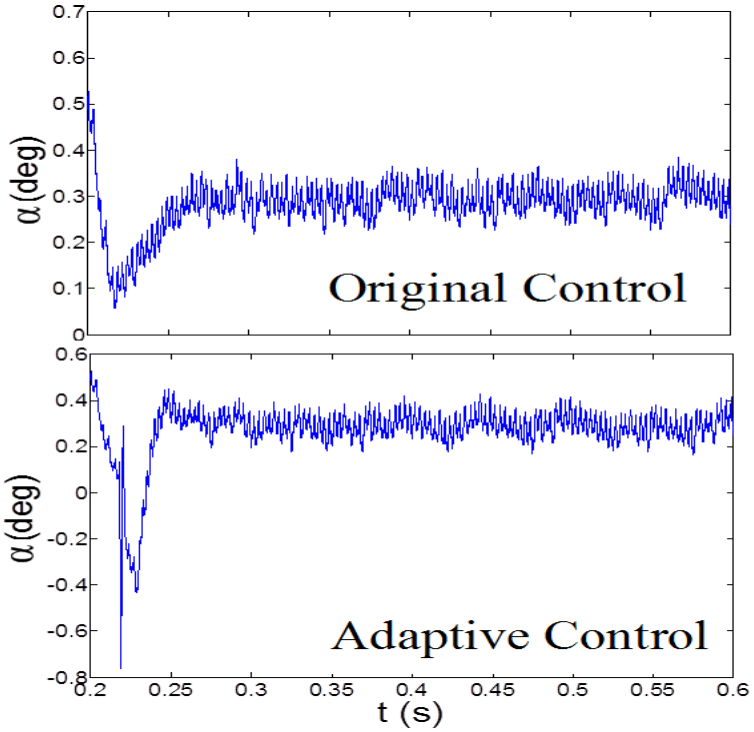

Figure 3.21 Results of α with change of load.

From the data shown in Table 3.2 as well as Figure 3.19 and Figure 3.20, it is obvious that the adaptive PI control can achieve quicker response than the original one.

3.4.5 Change of Transmission Network

In this case, the PI controller gains remain unchanged, as in the original model. However, line 1 is switched off at 0.2 sec to represent a different network which may corresponds to scheduled transmission maintenance. Here, we have

$$K_{p\_V}(t) = \frac{18.3245 \times \Delta V(t)}{\left(\Delta V(t) + 286.9512 \times \int_t^{t+T_s} A dt\right)} \tag{3.43}$$

$$K_{i\_V}(t) = 286.9512 \times K_{p\_V}(t) \tag{3.44}$$

$$K_{p\_I}(t) = \frac{41.4360 \times \Delta I_q(t)}{\left(\Delta I_q(t) + 412.0153 \times \int_t^{t+T_s} B dt\right)} \tag{3.45}$$

$$K_{i\_I}(t) = 412.0153 \times K_{p\_I}(t) \tag{3.46}$$

Based on (3.43) to (3.46), the adaptive PI control model can be designed to automatically react to changes in the transmission network. The PI control gains of the proposed control are also shown in Figure 3.22 and Figure 3.23. The results from the original and the adaptive PI control methods are shown in Figure 3.24, Figure 3.25 and Figure 3.26. Key observations are summarized in Table 3.3.

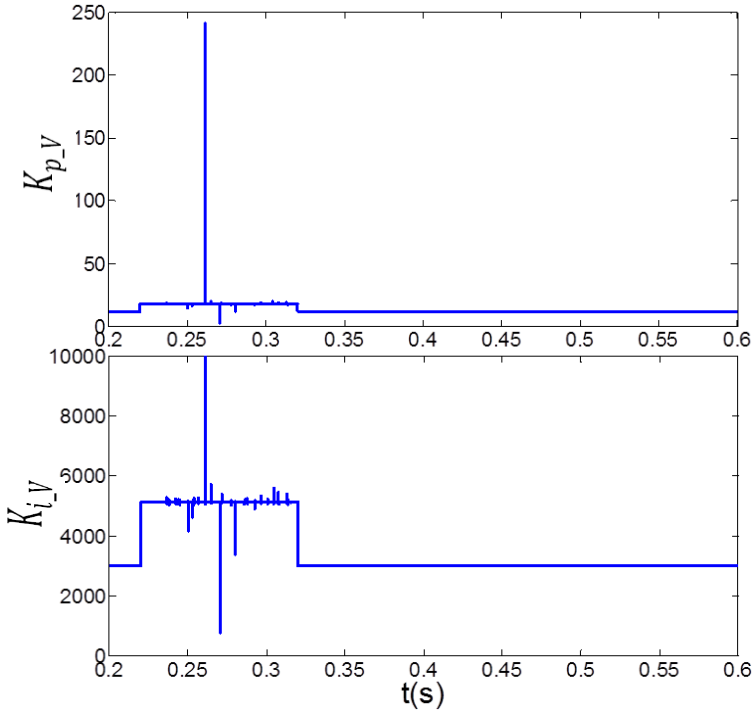

Figure 3.22 PI control gains of voltage regulator with change of transmission network.

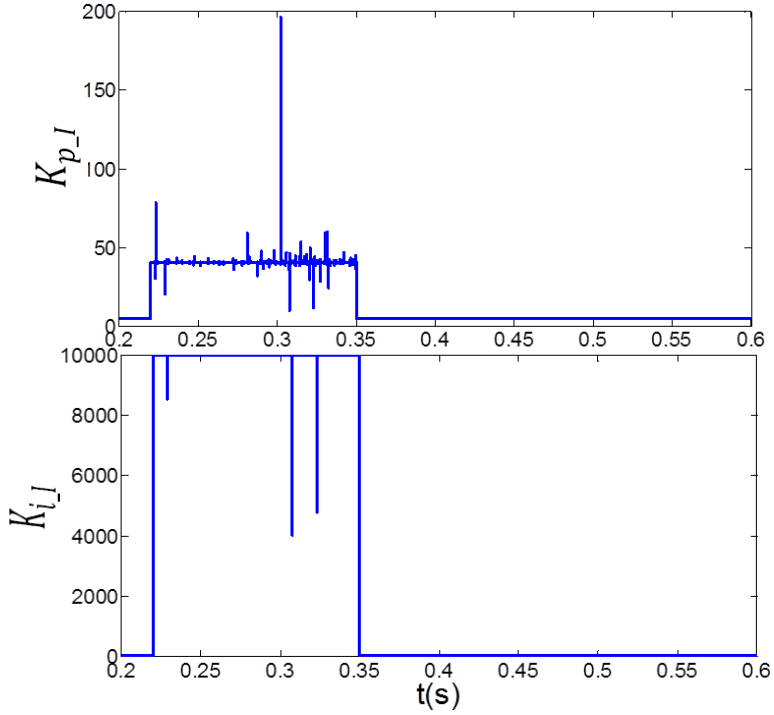

Figure 3.23 PI control gains of current regulator with change of transmission network.

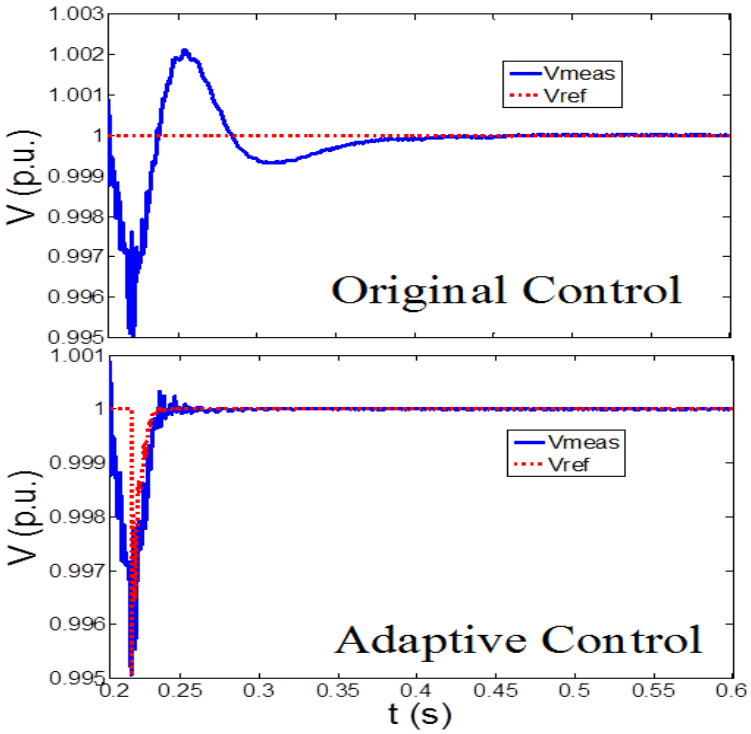

Figure 3.24 Results of measured voltage with change of transmission network.

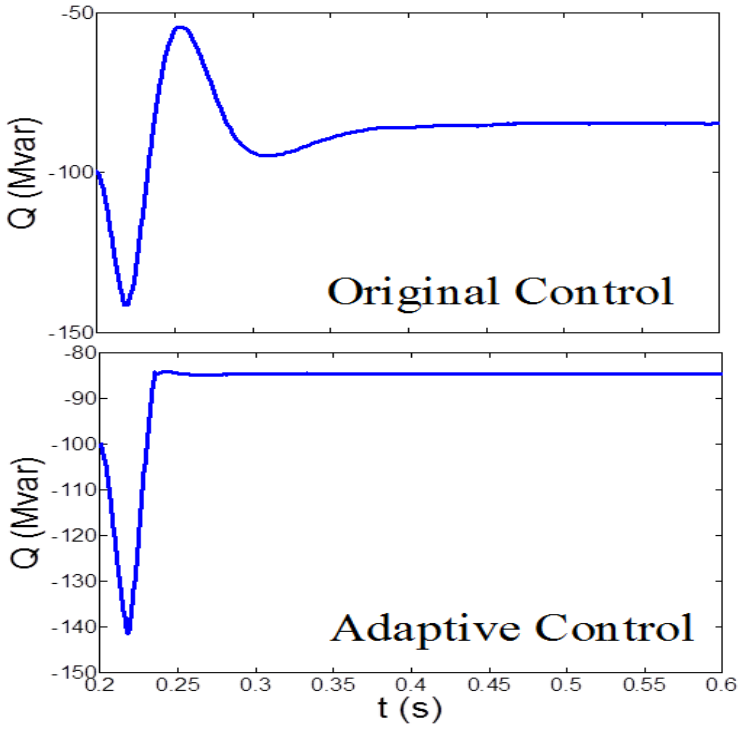

Figure 3.25 Results of output reactive power with change of transmission network.

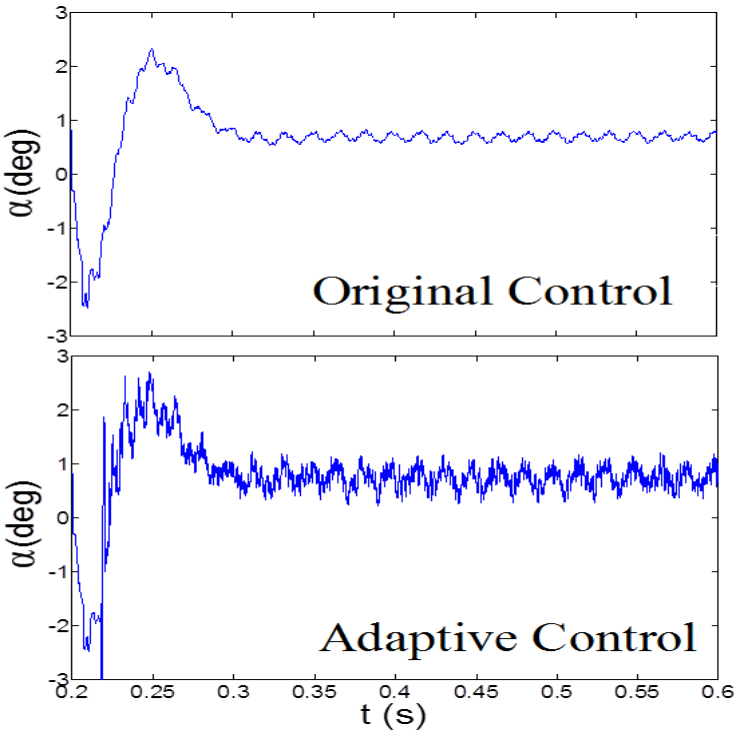

Figure 3.26 Results of α with change of transmission network.

Table 3.3 Performance comparison with changed transmission

	Original Ctrl.	Adaptive Ctrl.
Lowest Voltage after disturbance	0.9954 p.u.	0.9954 p.u.
Time (sec) when V=1.0	0.4248 sec	0.2744 sec
Δt to reach V=1.0	0.2248 sec	0.0744 sec
Var Amount at steady state	-84.92 MVar	-85.02 MVar
Time to reach steady state Var	0.4248 sec	0.2744 sec

Note the STATCOM absorbs VAR from the system in this case. Here, the disturbance is assumed to give a voltage rise at the source (substation) from 1.0 to 1.01 p.u.. Meanwhile, the system has a transmission line removed which tends to lower the voltages. The overall impact leads to a voltage rise to higher than 1.0 at the controlled bus in the steady state if the STATCOM is not activated. Thus, the STATCOM needs to absorb VAR in the final steady-state to reach 1.0 p.u. voltage at the controlled bus. Also, note that the initial transients immediately after 0.2 sec lead to an over-absorption by the STATCOM, while the adaptive PI control gives a much smoother and quicker response, as shown in Figure 3.24 and Figure 3.25.

3.4.6 Two consecutive disturbances

In this case, a disturbance at 0.2 sec causing a voltage decrease from 1.0 to 0.989 p.u. occurs at the substation. After that, line 1 is switched off at 0.25 sec. The PI control gains of the proposed control are also shown in Figure 3.27 and Figure 3.28.

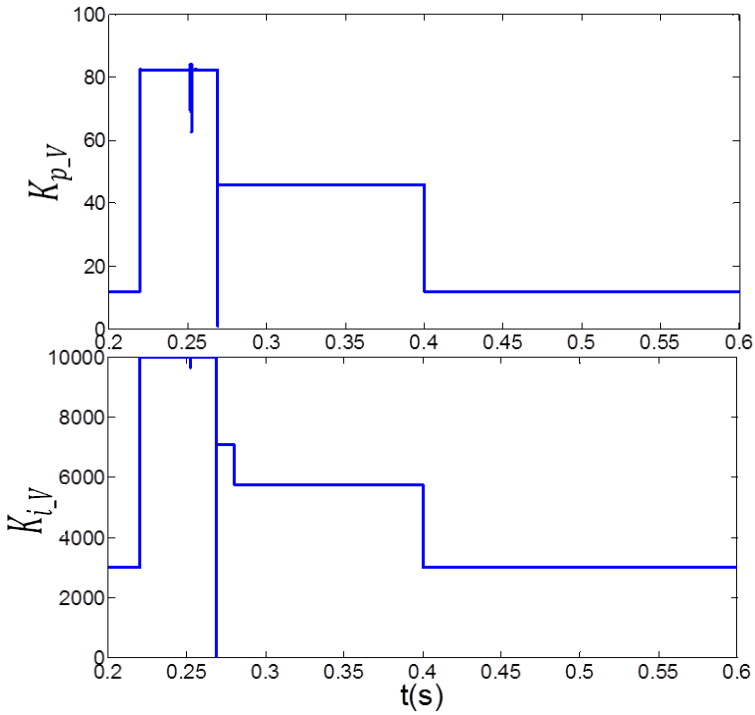

Figure 3.27 PI control gains of voltage regulator in two consecutive disturbances.

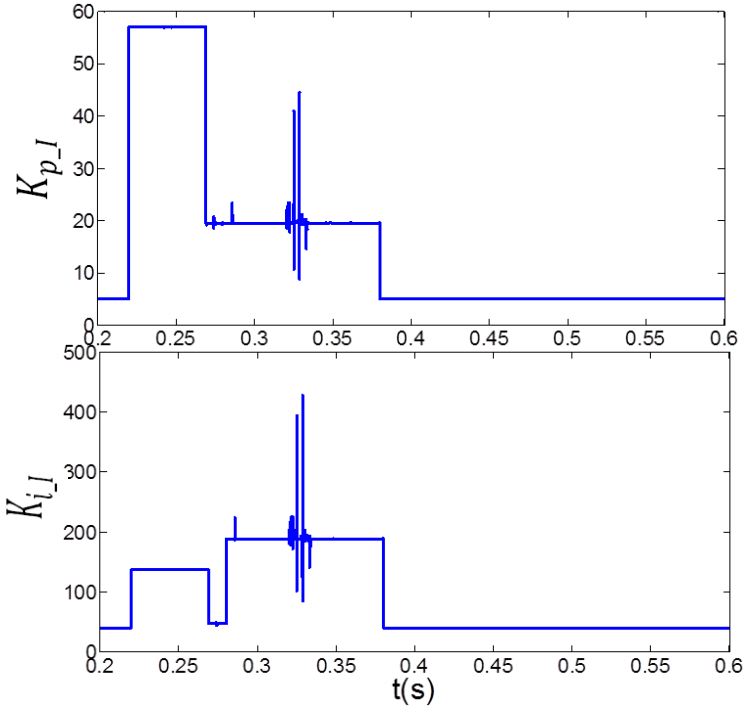

Figure 3.28 PI control gains of current regulator in two consecutive disturbances.

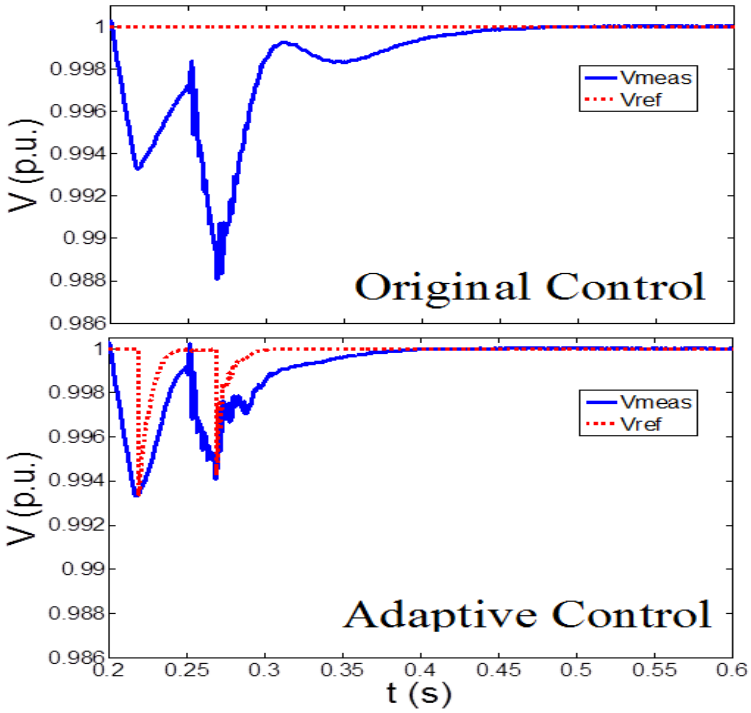

Figure 3.29 Results of measured voltage in two consecutive disturbances.

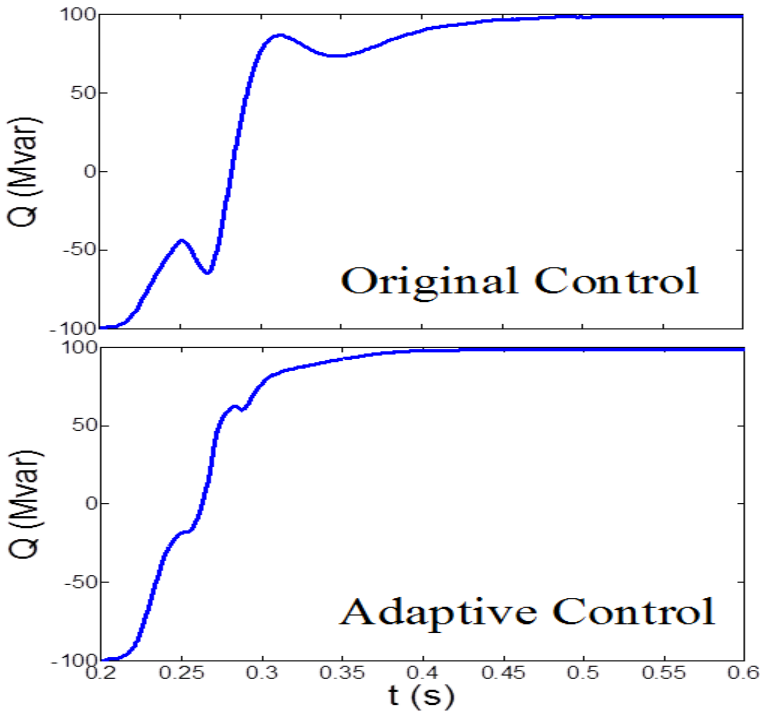

Figure 3.30 Results of output reactive power in two consecutive disturbances.

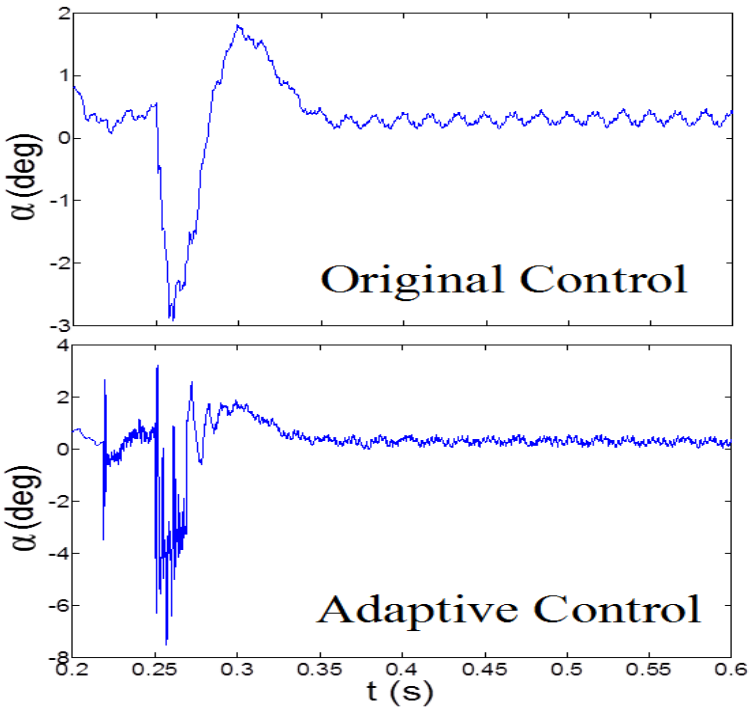

Figure 3.31 Results of α in two consecutive disturbances.

The results from the original and the adaptive PI control methods are shown in Figure 3.29, Figure 3.30 and Figure 3.31. From the results, it is apparent that the adaptive PI control can achieve a much quicker response than the original one, which makes the system voltage drop much less than the original control during second disturbance. Note, in Figure 3.29, the largest voltage drop during the second disturbance event (starting at 0.25 sec) with the original control is 0.012 p.u., while it is 0.006 p.u. with the proposed adaptive control. Therefore, the system is more robust in responding consecutive disturbances with adaptive PI control.

3.4.7 A Severe Disturbance

In this case, a severe disturbance at 0.2 sec causing a voltage decrease from 1.0 to 0.6 p.u. occurs at the substation. After that, the disturbance is cleared at 0.25 sec. The PI control gains of the proposed control are also shown in Figure 3.32 and Figure 3.33. The results from the original and the adaptive PI control methods are shown in Figure 3.34, Figure 3.35 and Figure 3.36.

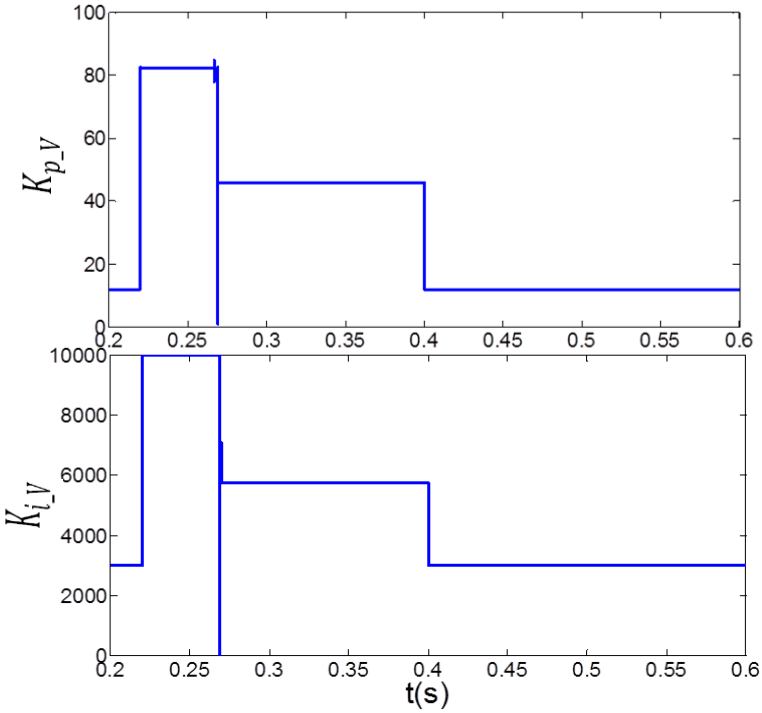

Figure 3.32 PI control gains of voltage regulator in a severe disturbance.

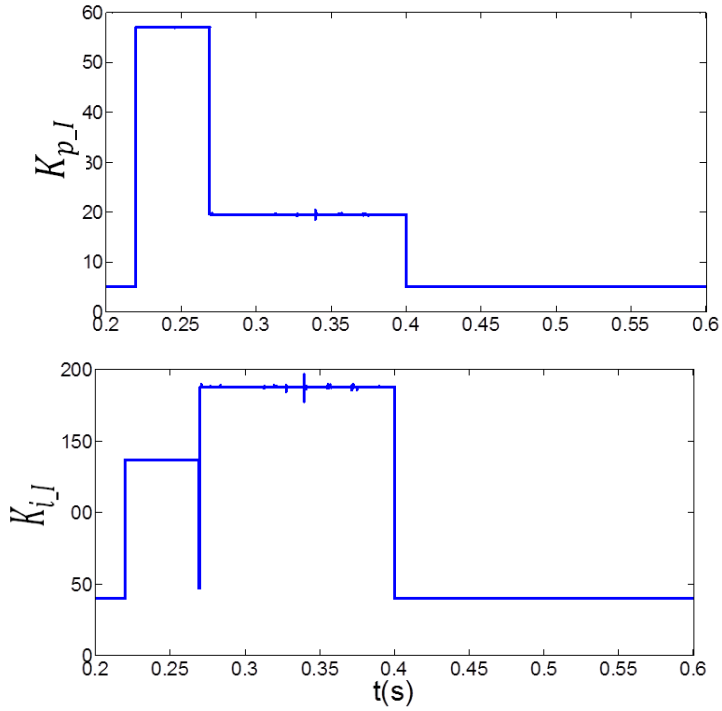

Figure 3.33 PI control gains of current regulator in a severe disturbance.

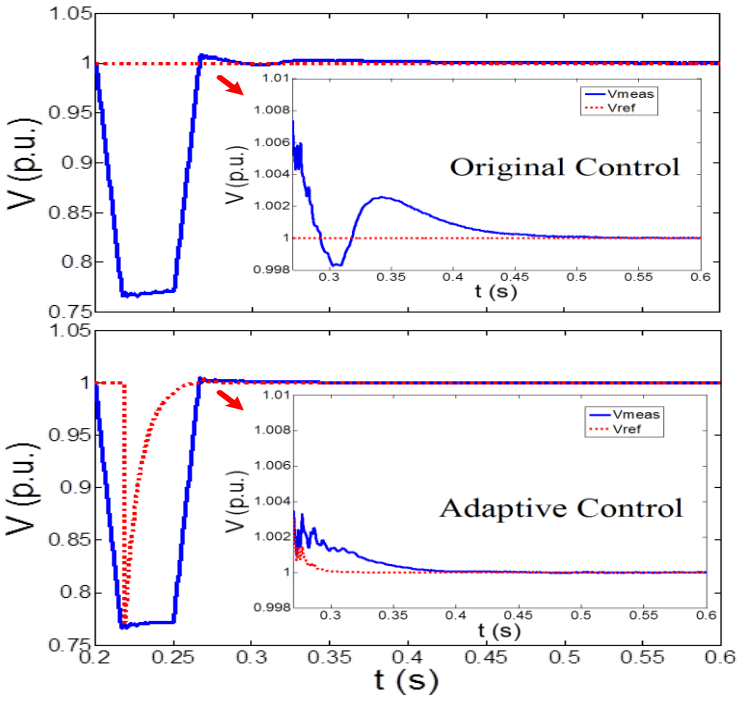

Figure 3.34 Results of measured voltage in a severe disturbance.

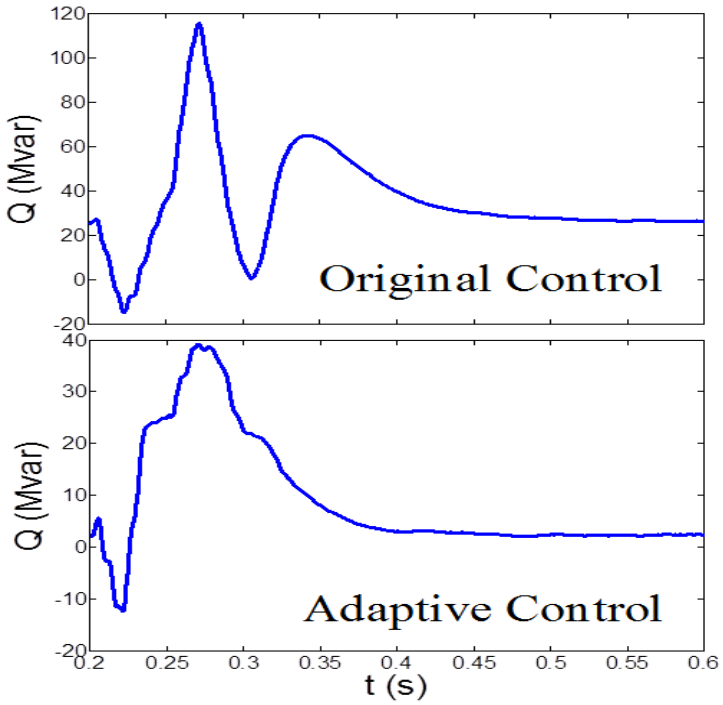

Figure 3.35 Results of output reactive power in a severe disturbance.

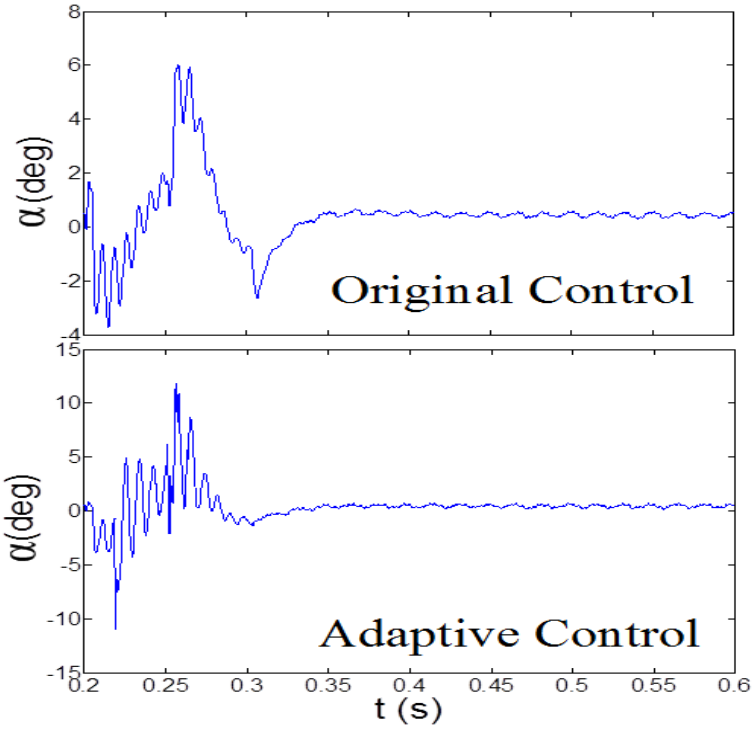

Figure 3.36 Results of α in a severe disturbance.

Due to the limit of the STATCOM capacity, the voltage cannot get back to 1.0 p.u. when there is a severe voltage drop from 1.0 p.u. to 0.6 p.u.. After the disturbance is cleared at 0.25 sec, from Figure 3.34 and Figure 3.35, it is obvious that the adaptive PI control can bring the voltage back to 1.0 p.u. with a quicker and smoother response than the original control.

3.5 Conclusions

From the above six case studies shown in subsections 3.4.2 to 3.4.7, it is evident that the adaptive PI control can achieve faster and more consistent response than the original control. The response time and the curve of the proposed adaptive PI control is almost identical under various conditions such as a change of (initial) control gains, a change of load, a change of network topology, consecutive disturbances and a severe disturbance. In contrast, the response curve of the original control model varies greatly under a change of system operating conditions and may fail to correct the voltage to the expected value.

The advantage of the proposed adaptive PI control approach is expected because the control gains are dynamically and autonomously adjusted during the voltage correction process, therefore, the desired performance can be achieved. In contrast, the original fixed PI controller may be well tuned for the given operating condition, but may be inefficient or incapable to correct voltage under other operating conditions.

CHAPTER 4

FLATNESS-BASED ADAPTIVE CONTROL OF STATCOM

4.1 Chapter Introduction

In this chapter, a flatness-based adaptive control (FBAC) method is proposed and applied to STATCOM for voltage control. By the flatness-based control (FBC), the trajectories of all system variables can be directly estimated by the flat output and its derivatives without solving differential equations. By the adaptive control, the control gains can be dynamically tuned to satisfy the time-varying operation condition requirement.

4.2 STATCOM Model and Control for Flatness-based Adaptive Control

The equivalent circuit of the STATCOM is shown in Figure 4.1. In this power system, the equivalent connecting impedance consists of R_s and L_s in series with the voltage source inverter. Here, the equivalent resistance R_s accounts for the sum of the transformer winding losses and the inverter conduction losses, and the equivalent inductance L_s represents the transformer leakage inductance. C represents the capacitance of the *dc* side capacitor. In Figure 4.1, V_{al}, V_{bl} , and V_{cl} are the three-phase STATCOM output voltages; V_{as}, V_{bs} , and V_{cs} are the three phase bus voltages; and i_{as}, i_{bs} , and i_{cs} are the three-phase currents [31, 66].

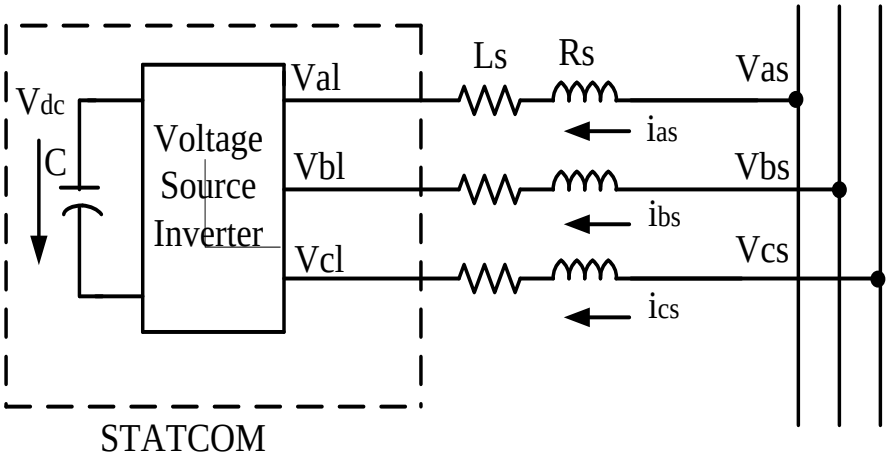

Figure 4.1 STATCOM Model.

The three-phase mathematical expressions of the STATCOM can be written similar to (3.1) to (3.4). By using the *abc/dq* transformation, the mathematical expressions can be rewritten as:

$$\begin{cases} L_s \frac{di_{ds}}{dt} = -R_s i_{ds} + \omega L_s i_{qs} + V_{ds} - V_{dl} \\ L_s \frac{di_{qs}}{dt} = -R_s i_{qs} - \omega L_s i_{ds} + V_{qs} - V_{ql} \\ \frac{d}{dt}\left(\frac{1}{2} C V_{dc}^2\right) = \frac{3}{2}\left(V_{dl} i_{ds} + V_{ql} i_{qs}\right) \end{cases} \tag{4.1}$$

$$V_{dl} = \frac{1}{2} V_{dc} m_\alpha cos\delta \tag{4.2}$$

$$V_{ql} = \frac{1}{2} V_{dc} m_\alpha sin\delta \tag{4.3}$$

where ω is the synchronously rotating angle speed of the voltage vector; i_{ds} and i_{qs} are the *d* and *q* axis currents corresponding to i_{as}, i_{bs}, and i_{cs}; V_{ds} and V_{qs} represent the *d* and *q* axis voltages corresponding to V_{as}, V_{bs} , and V_{cs}; V_{dl} and V_{ql} represent the *d* and *q* axis voltage corresponding to V_{al}, V_{bl} , and V_{cl}; m_a is the ratio between the peak amplitude of the phase

converter voltage to dc voltage and δ is the STATCOM voltage vector position in the *d-q* frame.

Based on the above equations, the traditional control strategy can be obtained, and the STATCOM control block diagram is shown in Figure 4.2 [35, 66].

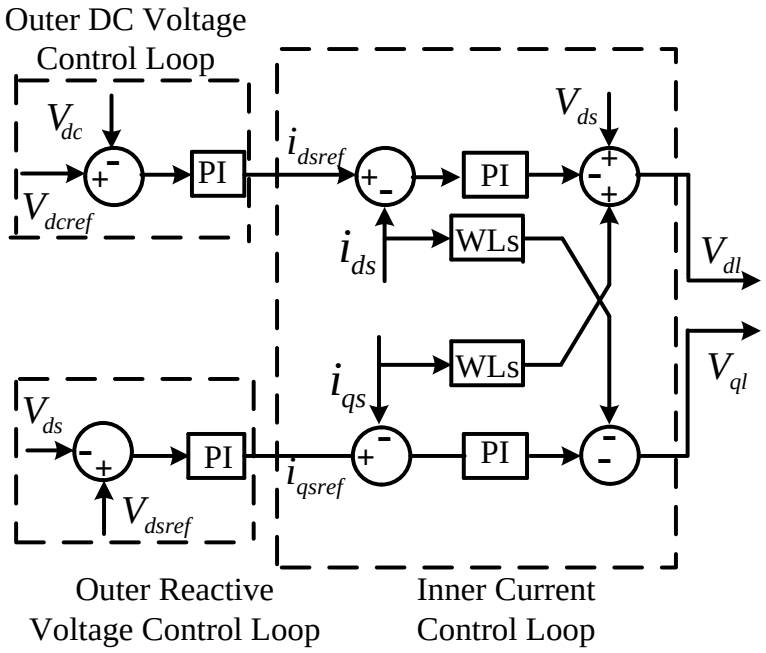

Figure 4.2 A typical double-loop control block of STATCOM.

In Figure 4.2, a typical double-loop control strategy is used in STATCOM. The outer loop forms the desired active and reactive current references to maintain the voltages at the point of common coupling (PCC), and the inner loop is to control inverter currents with zero steady-state errors. This control strategy needs four PI controllers in its control

systems. Therefore, it can be a tedious and time-consuming work for utility engineers to perform trial-and-error studies to find suitable parameters when a new STATCOM is connected or when the system operating condition has significant changes to demand new tuning of STATCOM control parameters. Moreover, this control system has a coupling relationship between the active current and the reactive current, and thus, it is hard to maintain the voltages at the PCC with small effects on the dc-link voltage. These are potential difficulties for a large-scale utilization of STATCOM. Therefore, the FBAC is proposed in this chapter.

4.3 Flatness-Based Control for STATCOM

4.3.1 Flatness-based Control Design for STATCOM

To realize flatness-based control (FBC) in STATCOM, we set the state variable as: $x=(x_1, x_2, x_3)^T=(i_{ds}, i_{qs}, V_{dc})^T$, and the input control variable as: $u=(u_1, u_2)^T=(m_a cos\delta, m_a sin\delta)^T$. Neglecting the inductance and converter losses and the change in the energy stored in the inductance [19, 39], we can rewrite (4.1) in standard form $\dot{x} = f(x) + g(x)u$ as follows:

$$\begin{cases} \dot{x}_1 = -\frac{R_s}{L_s}x_1 + \omega x_2 + \frac{V_{ds}}{L_s} - \frac{x_3 u_1}{2L_s} \\ \dot{x}_2 = -\frac{R_s}{L_s}x_2 - \omega x_1 + \frac{V_{qs}}{L_s} - \frac{x_3 u_2}{2L_s} \\ \dot{x}_3 = \frac{3}{2Cx_3}(x_1 V_{ds}) \end{cases} \tag{4.4}$$

Since all system variables can be determined if we know I_q and V_{dc}. Therefore, the flat output in this system can be set as:

$$\begin{cases} y_1 = x_2 \\ y_2 = x_3 \end{cases} \tag{4.5}$$

Based on (4.4) and (4.5), the following equation can be derived:

$$\begin{cases} \dot{y}_1 = \dot{x}_2 \\ \dot{y}_2 = \dot{x}_3 \\ \ddot{y}_2 = \frac{3(\dot{x}_1 x_3 V_{ds} - \dot{x}_3 x_1 V_{ds})}{2C x_3^2} \end{cases} \tag{4.6}$$

Using y and y's derivative to express $x=(x_1, x_2, x_3)^T$ and $u=(u_1, u_2)^T$, we have:

$$\begin{cases} x_1 = \frac{2C}{3V_{ds}} \dot{y}_2 y_2 \\ x_2 = y_1 \\ x_3 = y_2 \end{cases} \tag{4.7}$$

$$\begin{cases} u_1 = \frac{2}{y_2}\left(-L_S \frac{2C}{3V_{ds}}(y_2 \ddot{y}_2 + \dot{y}_2^2) + \omega L_S y_1 - R_S \frac{2C}{3V_{ds}} y_2 \dot{y}_2 + V_{ds}\right) \\ u_2 = \frac{2}{y_2}\left(-L_S \dot{y}_1 - \omega L_S \frac{2C}{3V_{ds}} y_2 \dot{y}_2 - R_S y_1 + V_{qs}\right) \end{cases} \tag{4.8}$$

Then the following equations can be obtained as (4.9) and (4.10).

$$\mathrm{m}_a = \sqrt{u_1^2 + u_2^2} \tag{4.9}$$

$$\delta = \arctan \frac{u_2}{u_1} \tag{4.10}$$

Based on (4.4)-(4.10), the flatness-based control can be implemented with the control block shown in Figure 4.3.

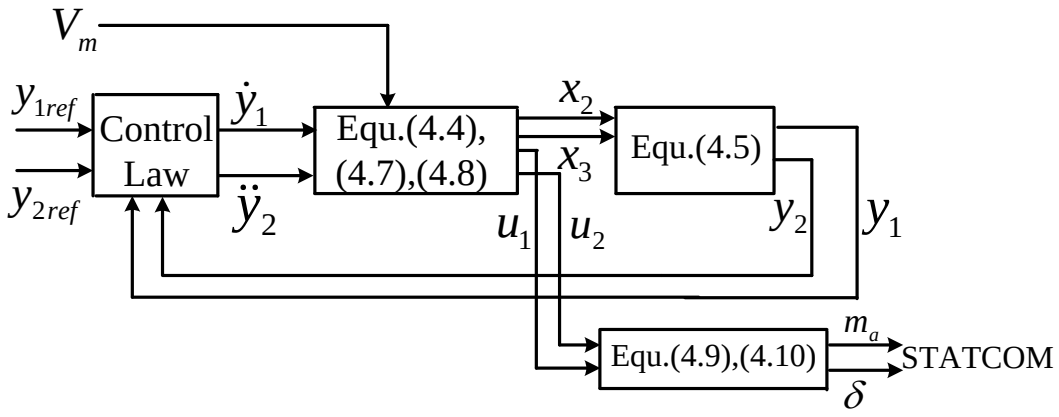

Figure 4.3 Flatness-based control block.

In Figure 4.3, y_{1ref} and y_{2ref} are defined by the system desired initial and final conditions. As shown in Figure 4.3, the nonlinear STATCOM system can be equivalent to a linear system, and the trajectories of all system variables can be directly estimated by flat output and its derivatives without solving differential equations. This is the advantage of flatness-based control when applied to STATCOM control.

4.3.2 Flat Output

Assume that the initial disturbance occurs at time t_0; the final time instant of the dynamic study is t_1; the desired initial states are $I_q(t_0)$ (or simply $I_q(0)$) and $V_{dc}(t_0)$ (or simply $V_{dc}(0)$); and the final states are $I_q(t_1)$ and $V_{dc}(t_1)$.

The initial and final conditions are modeled as follows:

$$\begin{cases} y_{1ref}(t_0) = I_q(t_0) \\ y_{1ref}(t_1) = I_q(t_1) \\ y_{2ref}(t_0) = V_{dc}(t_0) \\ y_{2ref}(t_1) = V_{dc}(t_1) \end{cases} \tag{4.11}$$

$$\begin{cases} \dot{y}_{1ref}(t_0) = 0 \\ \dot{y}_{1ref}(t_1) = 0 \\ \dot{y}_{2ref}(t_0) = 0 \\ \dot{y}_{2ref}(t_1) = 0 \\ \ddot{y}_{2ref}(t_0) = 0 \\ \ddot{y}_{2ref}(t_0) = 0 \end{cases} \tag{4.12}$$

In order to satisfy Eqs. (4.11) and (4.12), the desired trajectory for flat output can be expressed as:

(1) $0<t<t_0$

$$\begin{cases} y_{1ref}(t) = I_q(0) \\ y_{2ref}(t) = V_{dc}(0) \end{cases}$$

(2) $t_0 \leq t \leq t_1$

$$\begin{cases} y_{1ref}(t) = I_q(0) + \left(I_q(t_1) - I_q(0)\right) \times dd_1 \\ y_{2ref}(t) = V_{dc}(0) + \left(V_{dc}(t_1) - V_{dc}(0)\right) \times dd_2 \end{cases}$$

Without losing generality, in order to make the output curve as smooth as possible, we may set:

$$\begin{cases} y_{1ref}(t) = \sum_{j=0}^{N} \frac{a_j}{j!}(t - t_0)^j \\ y_{2ref}(t) = \sum_{j=0}^{N} \frac{b_j}{j!}(t - t_0)^j \end{cases}$$

Based on (4.11) and (4.12), dd_1 and dd_2 can be obtained as follows:

$$\begin{cases} dd_1 = \left(4 \times \left(\frac{t-t_0}{t_1-t_0}\right)^2 - 4 \times \left(\frac{t-t_0}{t_1-t_0}\right)^3 + \left(\frac{t-t_0}{t_1-t_0}\right)^4\right) \\ dd_2 = \left(9 \times \left(\frac{t-t_0}{t_1-t_0}\right)^3 - 12 \times \left(\frac{t-t_0}{t_1-t_0}\right)^4 + 3 \times \left(\frac{t-t_0}{t_1-t_0}\right)^5 + \left(\frac{t-t_0}{t_1-t_0}\right)^6\right) \end{cases}$$

(3) $t>t_1$

$$\begin{cases} y_{1ref}(t) = I_q(t_1) \\ y_{2ref}(t) = V_{dc}(t_1) \end{cases}$$

4.4 Control Law for Flatness-based Adaptive Control

The differential parameterization of the control input $u=(u_1,u_2)^T$ can be expressed by $(y_1, y_2, \dot{y}_1, \dot{y}_2, \ddot{y}_2)^T$. Also, the proposed flat output trajectory tracking is to control $\dot{y}_1$ and $\ddot{y}_2$. This can be accomplished by the following linear feedback control law:

$$\begin{cases} \dot{y}_1 = \dot{y}_{1ref} - (y_1 - y_{1ref})K_{11} \\ \ddot{y}_2 = \ddot{y}_{2ref} - K_{22}(\dot{y}_2 - \dot{y}_{2ref}) + K_{21}(y_2 - y_{2ref}) \end{cases} \quad (4.13)$$

In the previous work [44], the choice of the coefficients K_{11}, K_{21} and K_{22} is to guarantee the satisfaction of the Hurwitz polynomial condition (namely, to guarantee that the roots are located in the left part of the complex plane). Thus, the asymptotic exponential stability to zero of the tracking error is guaranteed.

However, the constant gains cannot ensure an optimized and consistently efficient performance for various external conditions. In order to achieve a control method that can ensure a fast and desirable response when the system operation condition varies, an adaptive control scheme is combined with flat control. Here, the flat control gains are

dynamically and adaptively adjusted based on the external condition. Thus, the proposed control method is termed flatness-based adaptive control (FBAC).

Set $err_1(t)=y_1(t)-y_{1ref}(t)$, $err_2(t)=y_2(t)-y_{2ref}(t)$, and $\dot{err}_2(t) = \dot{y}_2(t) - \dot{y}_{2ref}(t)$. The process of adaptive control design is described below with different scenarios of the error value.

Based on the system bus capacity and the STATCOM rating, ΔV_{max} can be obtained, which means any voltage change greater than ΔV_{max} cannot come back to 1 per unit. Based on [65], the sensitivity of di_{qs}/dV is around 1 p.u. /0.034 p.u. of voltage in this paper. For simplicity, we may assume the $\Delta i_{qs}/\Delta V$ sensitivity is a linear function. When the voltage error is $\varepsilon_2 = 0.0001$ p.u., Δi_{qs} is $\varepsilon_1 = 0.003$ p.u.. If the system voltage error is less than ε_2 p.u., the system is considered as stable and control gains are kept the same. Otherwise, the control gains need to be tuned to make system voltage get back to 1 p.u.. Since $y_1=i_{qs}$, err_1 is considered. If $|err_1(t)| < \varepsilon_1$, the system is considered as stable, and $K_{11}(t)$ can be set as initial values (such as 1). If $|err_1(t)| > \varepsilon_1$, the following approach is employed to tune control gains.

(1) When $0 < t < t_0$: $y_{1ref}(0)\neq 0$ and $y_1(t)$ needs to be increased to $y_{1ref}(t)$ as quickly as possible (i.e., in one sampling cycle Δt) to ensure $err_1=0$. Without losing generality, we can assume $y_1(t)=y_{1ref}(t)$ after Δt. Thus, we have $\mathrm{K}_{11}(t) = \frac{1}{\Delta t}$.

(2) When $t_0 \leq \mathrm{t} \leq t_1$: since the final ideal state $\dot{y}_1(t) = 0$, based on (4.13), we can

obtain:

$$0 = \dot{y}_{1ref}(t) - \left(y_1(t) - y_{1ref}(t)\right) K_{11}(t) \tag{4.14}$$

Therefore:

$$\mathrm{K}_{11}(t) = \left|\frac{\dot{y}_{1ref}(t)}{err_1(t)}\right| \tag{4.15}$$

(3) When $\mathrm{t} > t_1$: $y_1(t)$ needs to be increased to $y_{1ref}(t)$ as quickly as possible to ensure err_1=0. Since we consider $y_1(t)=y_{1ref}(t)$ after Δt, we have $\mathrm{K}_{11}(t) = \frac{1}{\Delta t}$.

Next, $err_2(t)$ is considered in a similar yet different way. Based on [65], ΔV_{dc} and the system voltage error are in the same range. Therefore, if $|err_2(t)| < \varepsilon_2$, $K_{21}(t)$ and $K_{22}(t)$ can be set as initial values (such as 1). If $|err_2(t)| > \varepsilon_2$, the approach listed below is employed to tune control gains.

(1) In the ideal state, $\ddot{y}_2(t) = \ddot{y}_{2ref}(t)$. Without losing generality, we can set $K_{22}(t)=K(t)K_{21}(t)$. Then, we have $\mathrm{K(t)} = \left|\frac{err_2(t)}{\dot{err}_2(t)}\right|$.

(2) When $0 < t < t_0$ or $\mathrm{t} > t_1$: $\ddot{y}_2(t)$ needs to be decreased to $\ddot{y}_{2ref}(t)$ as quickly as possible (i.e., in one sampling cycle Δt) to ensure err_2=0. Therefore, we have $K_{21}(t) = \left|\frac{\dot{err}_2(t)/\Delta t}{err_2(t)+K(t)\dot{err}_2(t)}\right|$ and $K_{22}(t) = \mathrm{K(t)}\left|\frac{\dot{err}_2(t)/\Delta t}{err_2(t)+K(t)\dot{err}_2(t)}\right|$.

(3) When $t_0 \le \mathrm{t} \le t_1$: the ideal state $\ddot{y}_2(t) = 0$. Set $tt=t-\Delta t$, and in a very short time control gains stay the same, such as $K_{21}(t)= K_{21}(tt)$ and $K_{22}(t) = K_{22}(tt)$. if the system stable, we have:

$$0 = \ddot{y}_{2ref}(t) - K_{22}(t)\dot{err}_2(t) - K_{21}(t)err_2(t) \tag{4.16}$$

$$0 = \ddot{y}_{2ref}(tt) - K_{22}(t)\dot{err}_2(tt) - K_{21}(t)err_2(tt) \qquad (4.17)$$

Based on (4.16) and (4.17), the following equation can be obtained:

$$\mathrm{K}(t) = \left|\frac{\ddot{y}_{2ref}(t)err_2(tt) - \ddot{y}_{2ref}(tt)err_2(t)}{\dot{err}_2(t)\ddot{y}_{2ref}(tt) - \dot{err}_2(tt)\ddot{y}_{2ref}(t)}\right| \qquad (4.18)$$

$$K_{21}(t) = \left|\frac{\ddot{y}_{2ref}(t)}{err_2(t) + K(t)\dot{err}_2(t)}\right| \qquad (4.19)$$

$$K_{22}(t) = K(t)K_{21}(t) \qquad (4.20)$$

Based on the proposed control law, the FBAC can be implemented as shown in Figure 4.4. This module is the "Control Law" block in Figure 4.3 which shows the FBAC diagram.

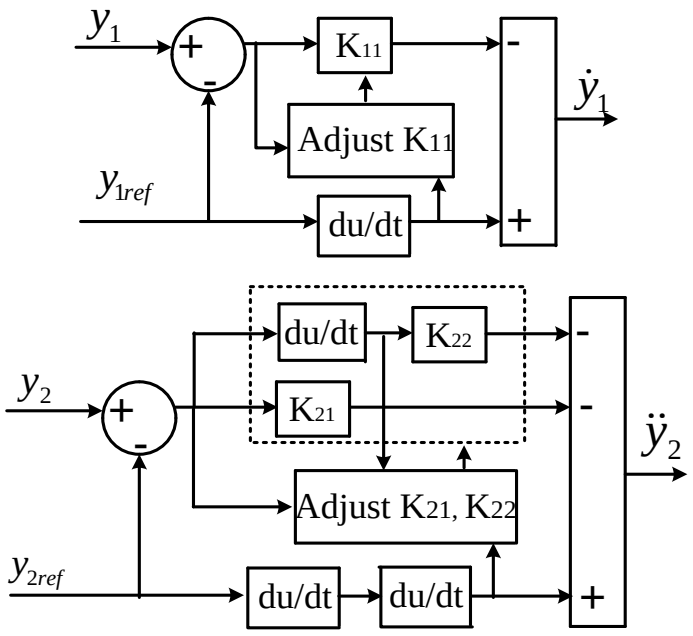

Figure 4.4 Implementation of the adaptive control module

Based on the flatness-based control logic and the adaptive control module shown in Figure 4.3 and Figure 4.4, respectively, the FBAC can be designed and implemented. Next, in Section 4.5, the simulation results from the original control, the FBC and the FBAC will be discussed and compared.

4.5 Simulation Results

4.5.1 System data

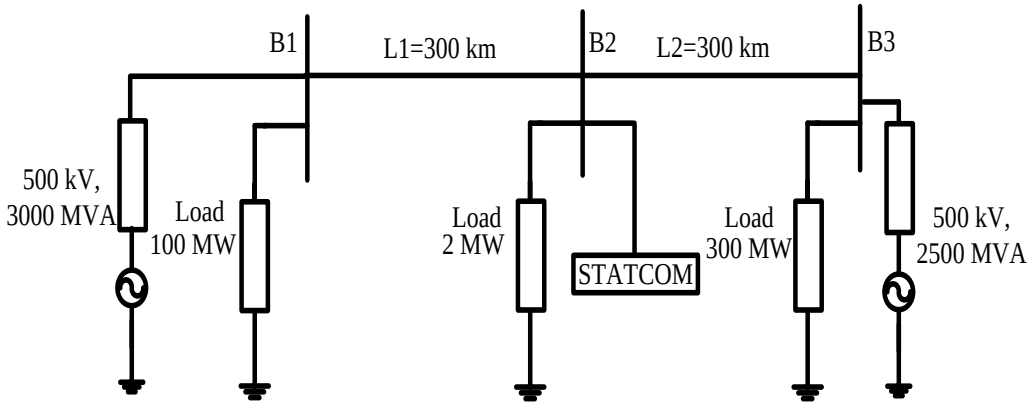

Figure 4.5 The test system for simulation study

In the system simulation diagram shown in Figure 4.5, the STATCOM is used for Bus B2 voltage regulation on a 500 kV transmission line. The power grid consists of two 500 kV equivalents (3000 MVA and 2500 MVA, respectively) connected by a 600-kilometer transmission line. In this study system, the STATCOM has a rating of +/- 100MVA. It is a phasor model of a typical three-level PWM STATCOM. DC link nominal voltage is 40 kV

with an equivalent capacitance of 375 uF. The transformer leakage reactance and the phase reactor of the IGBT bridge of an actual PWM STATCOM are 0.22 p.u. on 100 MVA in this system [65].

In the original model, the control system is realized by four PI controllers and referred to as the original control in this section. Note, the original control gains shown in literature [65] are well tuned. In the flatness-based control (FBC), which is elaborated in section 4.3, the control gains K_{11}, K_{21} and K_{22} are also well tuned based on the trial and error approach for the first case study (i.e., Subsection 4.5.2 below) and are set at 1.6, 0.9 and 0.9, respectively. In the proposed flatness-based adaptive control (FBAC), which is a combined model of sections 4.3 and 4.4, the initial control gains are set to 1's, and then the gains are dynamically adjusted based on the method described in section 4.4. The original control, the FBC and the FBAC are compared in this section. In the simulation, the reference voltage at Bus B2, shown in Figure 4.5, is 1.0 p. u. at the beginning, with the voltage base being 500 kV. Assume the initial disturbance occurs at t_0=0.2 *sec*; and the system is expected to reach back the desired normal state at t_1=0.3 *sec*.

4.5.2 Change of Reactive Load

Here, we keep all the parameters unchanged, as in the original studied system. At t_0=0.2 *sec*, a new reactive load of 80 MVar is added at B2 as a disturbance. The results of

Bus B2 voltage (V), STATCOM reactive power output (Q), the d and q axis currents are shown in Figure 4.6 to Figure 4.9 respectively. Observations are summarized in Table 4.1.

Table 4.1 Performance comparison for change of reactive load

	Original Ctrl.	Flatness based Ctrl. (FBC)	Flatness based adaptive Ctrl. (FBAC)
Lowest Voltage after disturbance	0.9713 p.u.	0.9713 p.u.	0.9713 p.u.
Time (sec) when V=1.0	0.4293 sec	0.3001 sec	0.2895 sec
Δt to reach V=1.0	0.2293 sec	0.1001 sec	0.0895 sec
Var Amount at steady state	-0.83 p.u.	-0.83 p.u.	-0.83 p.u.

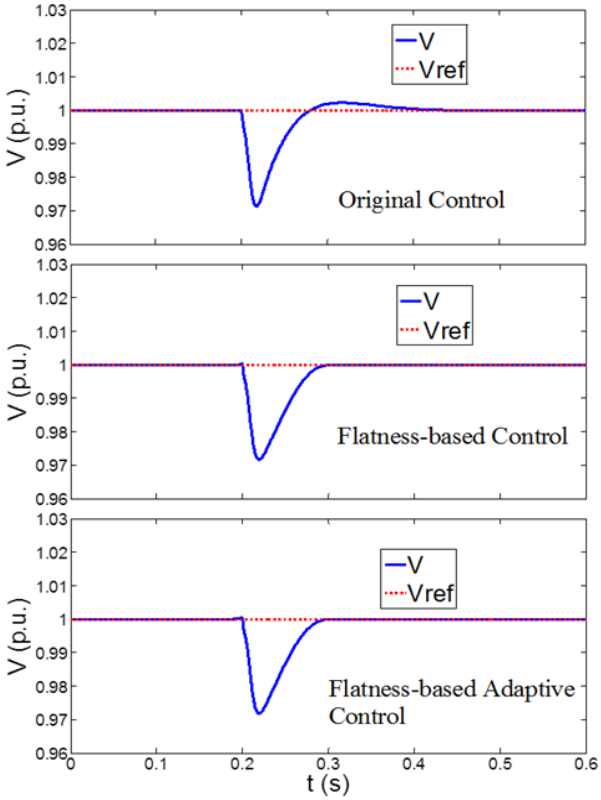

Figure 4.6 Results of V with change of reactive load

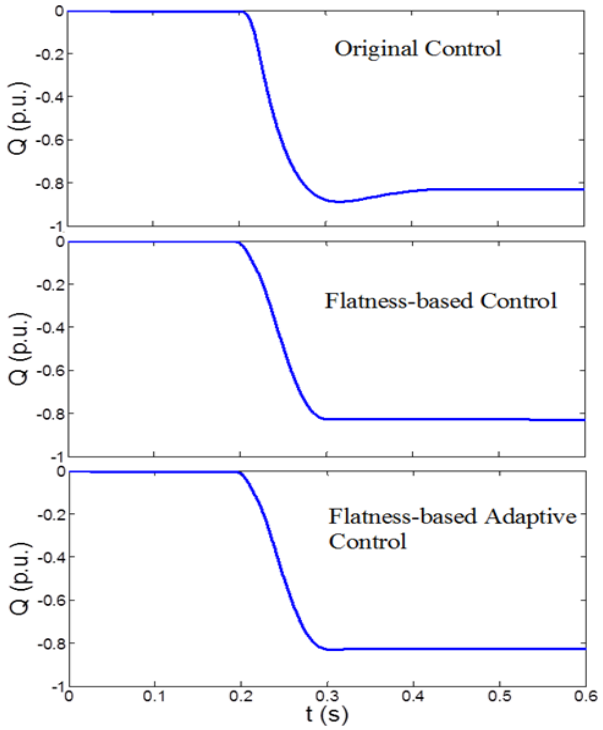

Figure 4.7 Results of Q with change of reactive load

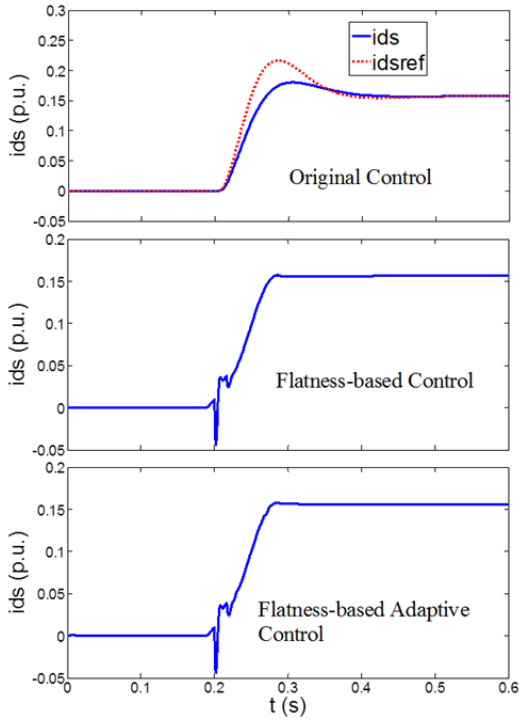

Figure 4.8 Results of I_d with change of reactive load

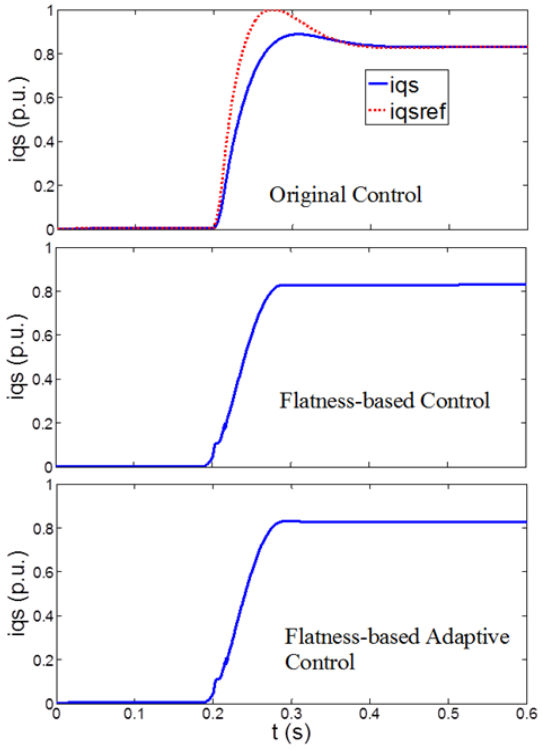

Figure 4.9 Results of I_q with change of reactive load

From the results, it is obvious that the FBC and the proposed FBAC can achieve quicker response than the original control. The needed reactive power, i_{ds}, and i_{qs} are the same while the FBC and the FBAC perform much faster to bring the voltage back to 1.0. Note, as previously mentioned, the control gains K_{11}, K_{21} and K_{22} in the FBC are well tuned based on this case using the trial and error approach and are set at 1.6, 0.9 and 0.9, respectively. Since the parameters are well tuned for this case, the FBC can give desirable responses very close to the response of the proposed FBAC in this case.

4.5.3 Change of Transmission Network

In this case, the original system parameters are kept. However, a new Line L3 of 125 km is added between bus B2 and B3 at the system to mimic a new operation topology. Then, Line L3 is switched off at t_0=0.2 *sec* to mimic a disturbance.

The results from the original control, the FBC and the proposed FBAC are shown in Figure 4.10 to Figure 4.14. Observations are summarized in Table 4.2.

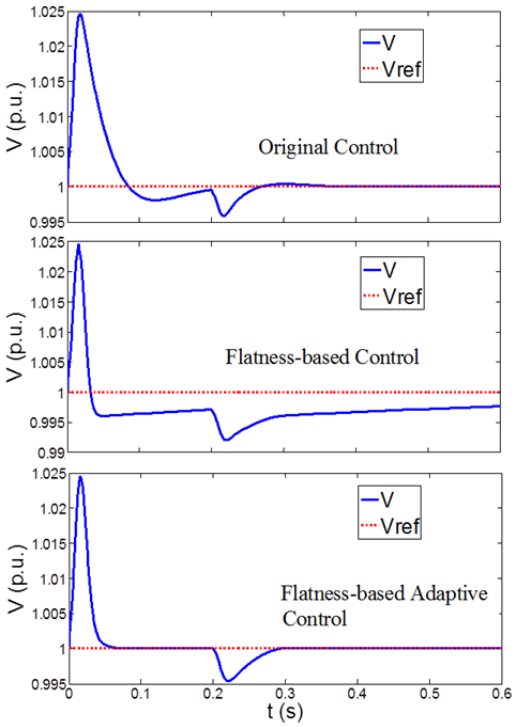

Figure 4.10 Results of *V* with change of transmission network.

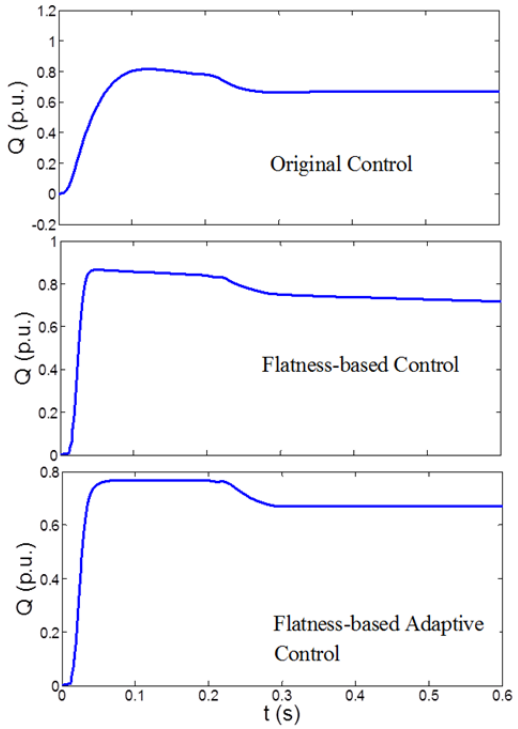

Figure 4.11 Results of Q with change of transmission network.

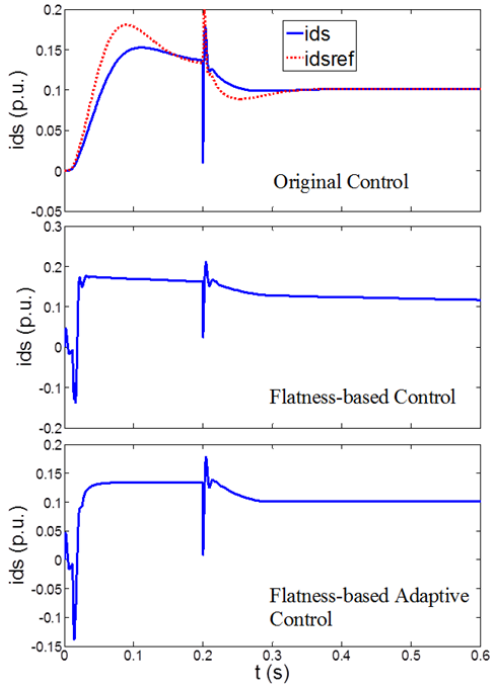

Figure 4.12 Results of I_d with change of transmission network.

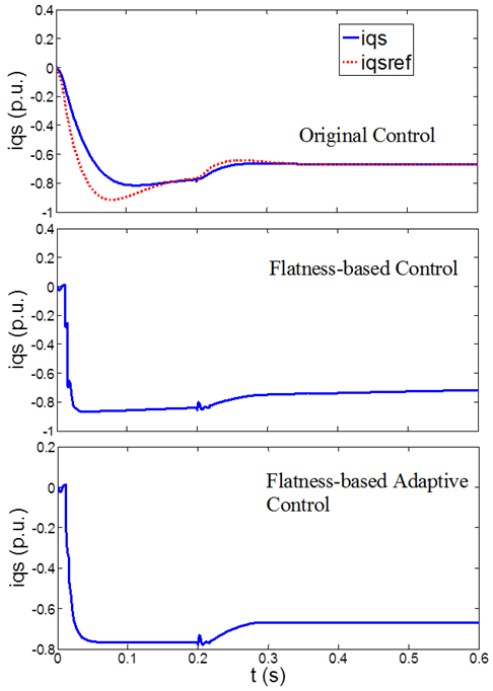

Figure 4.13 Results of I_q with change of transmission network.

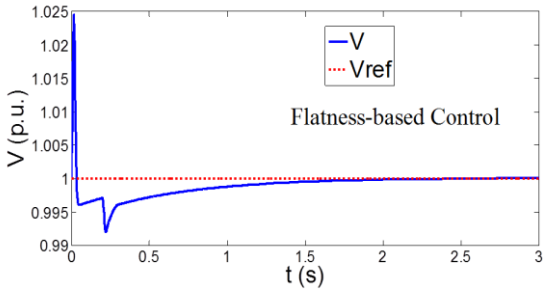

Figure 4.14 Results of FBC with change of transmission network.

Table 4.2 Performance comparison for change of transmission network

	Original Ctrl.	Flatness based Ctrl. (FBC)	Flatness based adaptive Ctrl. (FBAC)
Highest Voltage after change of transmission network	1.0245	1.0245	1.0245
Time (sec) when V=1.0 after change of transmission network	N/A	N/A	0.0765
Lowest Voltage after disturbance	0.9955 p.u.	0.992 p.u.	0.9955
Time (sec) when V=1.0 after disturbance	0.3824 sec	2.2863	0.2914 sec
Δt to reach V=1.0 after disturbance	0.1824 sec	2.0863	0.0914 sec
Var Amount at steady state	0.67 p.u.	0.67 p.u.	0.67 p.u.

From the results, we can find out that when the transmission network changes, the original control and the FBC cannot bring the system voltage back to 1 p.u. even during the initialization stage before the disturbance occurs at 0.2 sec. This also implies that the gains in the original PI control and FBC must be manually re-tuned to achieve a satisfying performance under a new topology.

After the disturbance (switching off Line L3) occurs at 0.2 sec, the FBC cannot make the system reach its steady-state voltage within 0.6 sec. Note, a separate diagram in Figure 4.14 with extended simulation time shows that the voltage eventually reaches back

to 1 p.u. at t=2.2863 sec, or 2.0863 sec after the disturbance of topology change. This is also shown in Table 4.2. The original control performs better, reaching 1.0 p.u. in 0.1824 sec after the topology change. However, this is still much slower than the proposed FBAC which brings the system voltage back to 1 p.u. in 0.0914 sec after the disturbance, as shown in Table 4.2.

The response time (i.e., Δt to reach V=1.0) of the FBAC is only 50% of the original control and 4.3% of the FBC. In other words, the FBAC shortens the response time by 0.1 sec and 2.0 sec respectively, as opposed to the original control and the FBC. Since 0.1 sec can be significant in modern STATCOM control and makes a big difference in STATCOM performance [31], the improved performance with FBAC is considerable. Therefore, the proposed FBAC can achieve a response quicker than the original control and even much quicker than the FBC. Thus, the control gains K_{11}, K_{21} and K_{22} in the original control and the FBC are not optimal under this new topology. Some form of gain tuning of K_{11}, K_{21} and K_{22} must be performed to achieve the same response as the proposed FBAC. Apparently, the tuning-free FBAC has an advantage over the other two controls.

4.5.4 Change of Transmission Network and Load

In this case, the original system parameters are kept. However, a 125km new Line L3 is added between bus B2 and B3 at the system to mimic the new operation system. Line 1 is switched off and a new load 200MW is added at B2 at 0.2 sec as a large disturbance. The

results of three controls are shown in Figure 4.15 to Figure 4.19. Again, it should be noted that the initial dynamics in these figures are due to the change of transmission network. Observations are summarized in Table 4.3.

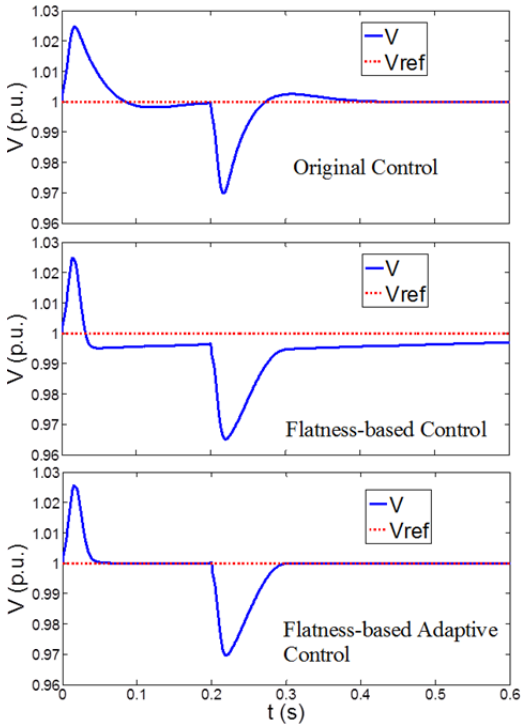

Figure 4.15 Results of *V* with change of transmission network and load.

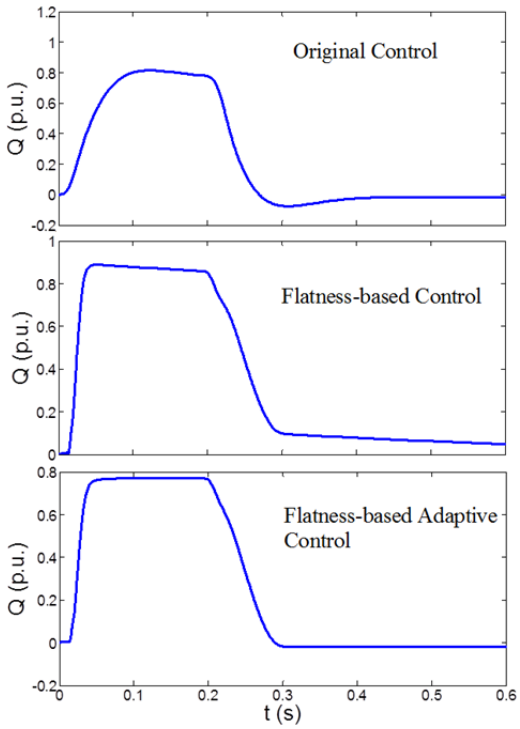

Figure 4.16 Results of Q with change of transmission network and load.

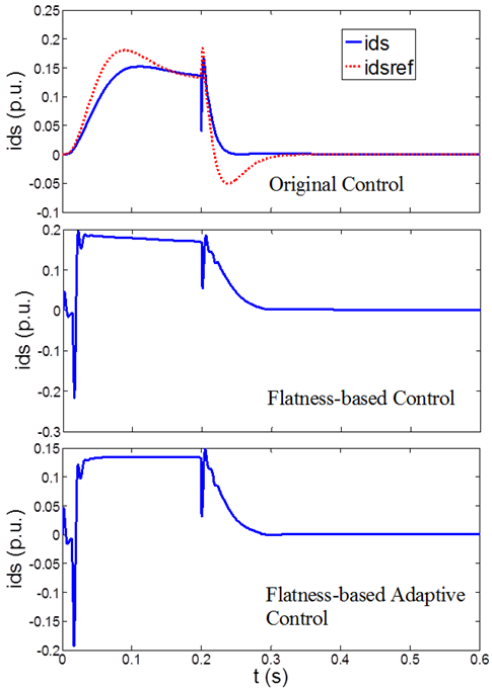

Figure 4.17 Results of I_d with change of transmission network and load.

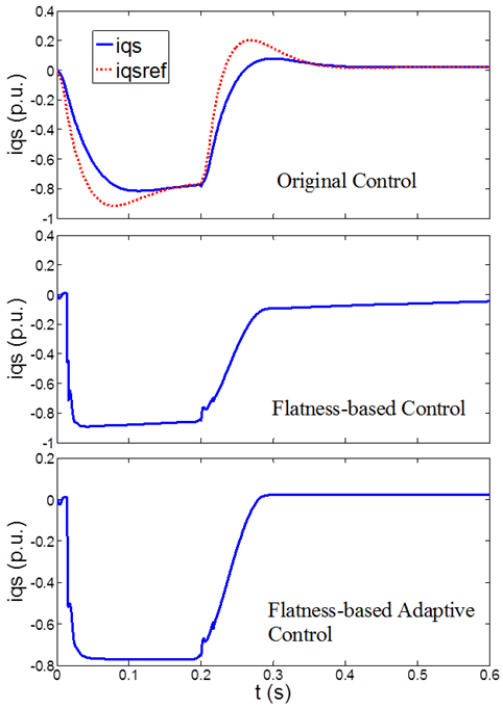

Figure 4.18 Results of I_q with change of transmission network and load.

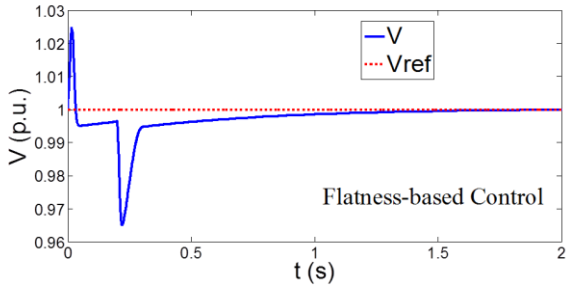

Figure 4.19 Results of FBC with change of transmission network and load.

Table 4.3 Performance comparison for change of transmission network and load.

	Original Ctrl.	Flatness based Ctrl. (FBC)	Flatness based adaptive Ctrl. (FBAC)
Highest Voltage after change of transmission network	1.0245	1.0245	1.0245
Time (sec) when V=1.0 after change of transmission network	N/A	N/A	0.0619
Lowest Voltage after disturbance	0.9698 p.u.	0.9652 p.u.	0.97 p.u.
Time (sec) when V=1.0 after disturbance	0.4166 sec	1.9082	0.3025 sec
Δt to reach V=1.0 after disturbance	0.2166 sec	1.7082	0.1025 sec
Var Amount at steady state	-0.02 p.u.	-0.02 p.u.	-0.02 p.u.

From the results, the FBAC response remains unchanged under this disturbance, while the original control method gives slower response and the FBC cannot bring the voltage back to steady-state in 0.6 sec. Note, a separate diagram in Figure 4.19 with extended simulation time shows that the voltage eventually reaches back to 1 p.u. at *t*=1.9082 sec, or 1.7082 sec after the disturbance. This is also shown in Table 4.3.

The observation is similar to the previous case. The response time (i.e., Δt to reach V=1.0) of the FBAC is only 47% of the original control and 6% of the FBC. Hence, similar to the previous case, the advantage of the proposed FBAC method is clearly demonstrated again.

4.6 Conclusions

The three case studies in Subsections 4.5.2 to 4.5.4 show the advantage of the proposed FBAC over the original control and the FBC. The original control and the FBC models may have a desirable response in a specific system. However, when the system operating condition changes, the FBC gains and traditional PI control gains need to be redesigned or re-tuned to obtain satisfying responses; otherwise, the original control and the FBC may be subject to slower response, as demonstrated in subsections 4.5.3 to 4.5.4. However, the proposed FBAC can consistently achieve fast, smooth, and desirable responses under various changes of system operating conditions such as a change of load and a change of network, and the response curves are almost identical in all cases.

CHAPTER 5

ADAPTIVE GAIN-TUNING CONTROL METHOD FOR AGC WITH EFFECTS OF WIND RESOURCES

5.1 Chapter Introduction

This chapter builds the wind power model on the partial load area. An adaptive gain-tuning control (AGTC) for AGC with effects due to wind resources is presented. By this control method, the PI control parameters can be automatically and dynamically calculated during different disturbances in a power system. In the proposed method, the initial gains will be calculated first. Then, the variable wind energy will be integrated into the power systems. Then, the PI control parameters for AGC will be computed automatically and will be adjusted in real time based on the area control error (ACE) signal to keep the frequency stable.

5.2 AGC Model and Control

A large, interconnected power system is usually divided into several control area for efficient operation and control. The control areas are connected by the tie-lines. In each control area, an automatic generation controller (AGC) monitors the system frequency and tie-line flows. To maintain stable operation of the system, both constant frequency and constant tie-line power exchange must be ensured. Also, area control error (ACE) for each

area will be calculated and kept in a low range. Therefore, ACE, which is defined as a linear combination of power net-interchange and frequency deviations, is generally taken as the controlled output of AGC. As the ACE is driven to zero by the AGC, both frequency and tie-line power errors will be forced to zeroes [5-6]. Figure 5.1 shows the studied n-area power system.

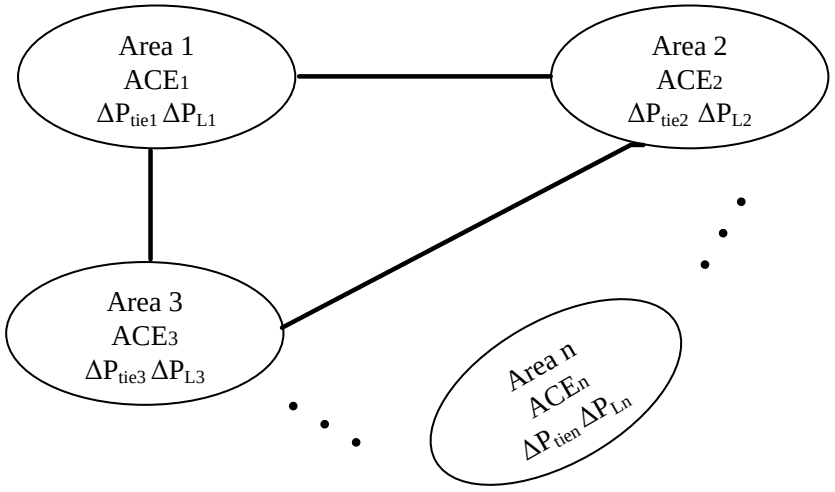

Figure 5.1 n-area power system.

The parameters for the n area power system are as follows:

$\mathrm{ACE_i} = \Delta \mathrm{P_{tiei}} + \mathrm{B_i}\Delta\omega_\mathrm{i}$ the area control errors for area *i*;

ΔP_{tiei} = tie line flow for area *i*;

ΔP_{Li} = load changes for area *i*;

$\Delta\omega_i$= the angular frequency deviations for area *i*;

$B_i = D_i + \frac{1}{R_i}$ frequency bias factors for area *i*;

R_j= the speed regulations for generator *j*;

D_j = damping constant for generator *j*;

H_j= inertia constants for generator *j*;

τ_{gj} = governor time constants for generator *j*;

τ_{Tj}= turbine time constants for generator *j*;

i=1, 2, 3,…, n; and

j=1, 2, 3,…, m;

m=the total number of generators;

In the original AGC control, the proportional integral (PI) controllers are used [12-13, 49, 75]. The control gains are usually designed by:

1) Trial and error approach;
2) Pole placement method; or
3) Population based search techniques.

The first method is very time-consuming and the second method is easily affected by the designer's experience. All these methods with fixed control gains may not obtain the desired response when the power system operation conditions change, especially when power systems operate with variable wind power. To ensure the desired response, an

adaptive gain-tuning control (AGTC) is presented for the AGC with wind power. A key feature of the proposed AGTC method is the dynamic, self-adjustment of control parameters to continuously follow the desired response, which is set to be ACE_i=0 in this work. The AGTC block for AGC in the area *i* is shown in Figure 5.2. In the figure, U_i is the output of the PI controller. K_{Pi}, K_{Ii} are PI controller gains for area *i* (*i*=1~n). The parameters K_{Pi}, K_{Ii} will be dynamically adjusted based on ACE_i. In this work, steam turbine with no heat type is modeled to realize the AGTC. The control gains in the system with steam turbine of reheat type and hydraulic turbine can be designed in a similar way.

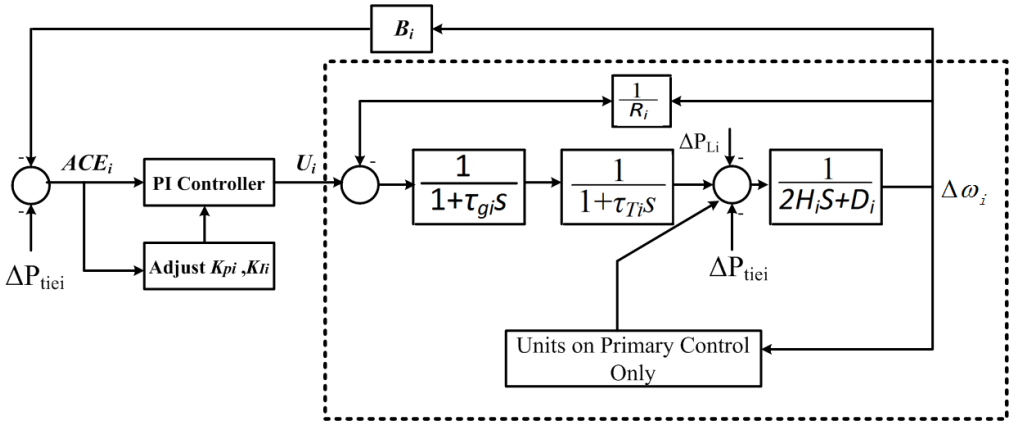

Figure 5.2 AGTC block for area *i*.

On one hand, larger values of K_{Pi} and K_{Ii} may induce the oscillation; on the other hand, smaller values of K_{Pi} and K_{Ii} may lead the slow response. These effects are also mentioned and analyzed in [29]. Therefore, the proper control parameters are highly important to

achieve better AGC responses. In the next section, the PI control gain design will be introduced.

5.3 Gain Design for AGC

5.3.1 Initial gains setting

Under the initial condition, we may assume that ΔP_{tiei}=0 and the power output of the units with only primary control will keep the same. Based on Figure 5.2, the closed-loop transfer function of the area *i* can be obtained [3].

$$-\frac{\Delta\omega_i(s)}{\Delta P_{Li}(s)} = \frac{(1+\tau_{gi}s)(1+\tau_{Ti}s)s}{(2H_iS+D_i)(1+\tau_{gi}s)(1+\tau_{Ti}s)s+B_i(K_{Pi}s+K_{Ii})+\frac{s}{R_i}} \tag{5.1}$$

Then, the characteristic polynomial equation for each area can be shown as:

$$a_4\mathrm{s}^4 + a_3\mathrm{s}^3 + a_2\mathrm{s}^2 + a_1\mathrm{s} + a_0\mathrm{s}^0 = 0 \tag{5.2}$$

where:

$a_4 = 2\mathrm{H}_i\tau_{gi}\tau_{Ti}$ (i=1~3)

$a_3 = \left(2\mathrm{H}_i\tau_{gi} + 2\mathrm{H}_i\tau_{Ti} + D_i\tau_{gi}\tau_{Ti}\right)$

$a_2 = \left(2\mathrm{H}_i + D_i\tau_{gi} + D_i\tau_{Ti}\right)$

$\mathrm{a}_1 = \left(\mathrm{D_i} + \mathrm{B_i}\mathrm{K_{pi}} + \frac{1}{\mathrm{R_i}}\right)$

$a_0 = B_iK_{Ii}$

Based on the Routh-Hurwitz criterion, if the system is stable, then we have

$$\begin{cases} a_4 > 0 \\ a_3 > 0 \\ b_{31} > 0 \\ b_{41} > 0 \\ a_0 > 0 \end{cases} \tag{5.3}$$

where $b_{31} = \frac{a_2 a_3 - a_4 a_1}{a_3}$; $b_{32} = a_0$; and $b_{41} = \frac{b_{31} a_1 - b_{32} a_3}{b_{31}}$.

Since K_{Pi}>0, and K_{Ii}>0, we can obtain that a_4>0, a_3>0 and a_0>0. If the system is stable, the following equations need to be satisfied.

$$\begin{cases} a_2 a_3 - a_4 a_1 > 0 \\ b_{31} a_1 - b_{32} a_3 > 0 \end{cases} \tag{5.4}$$

Based on (5.4), the initial value for K_{Pi} and K_{Ii} (i=1~3) can be obtained.

5.3.2 Control gain design during the disturbance

At arbitrary time instant $t=t_1$, set $t_2=t_1-\tau$, in which τ is set to be 0.1 sec. PI control gains stay the same within 0.1s, such that $K_{Pi}(t_1)= K_{Pi}(t_2) = K_{Pi}(t_0)$; $K_{Ii}(t_1)= K_{Ii}(t_2)= K_{Ii}(t_0)$. Under normal conditions, each area can carry out its control obligation, and steady-state corrective action of AGC is confined to the area that the deficit or excess generation occurs [3,11], [69-70]. Therefore, when the system is stable, we can obtain:

$$U_i(t_1) = A_{1i} K_{Pi}(t_0) + B_{1i} K_{Ii}(t_0) \tag{5.5}$$

$$U_i(t_2) = A_{2i} K_{Pi}(t_0) + B_{2i} K_{Ii}(t_0) \tag{5.6}$$

where $U_i(t_1)$, $U_i(t_2)$, A_{1i}, B_{1i}, A_{2i} and B_{2i} are known variable. $K_{Pi}(t_0)$ and $K_{Ii}(t_0)$ are unknown variables. $U_i(t_1)$ and $U_i(t_2)$ are equal to corresponding load changes at area i, namely $U_i(t_1)=|\Delta P_{Li}(t_1)|$ and $U_i(t_2)=|\Delta P_{Li}(t_1)|$ (here, $|\Delta P_{Li}(t_1)|$ >0 $|\Delta P_{Li}(t_2)|$ >0).

$$A_{1i} = ACE_i(t_1)$$

$$A_{2i} = ACE_i(t_2)$$

$$B_{1i} = \int_{t_0}^{t_1} ACE_i(t)\,dt$$

$$B_{2i} = \int_{t_0}^{t_2} ACE_i(t)\,dt$$

In case that (5.5) and (5.6) are singular, we can simply assume $K_{Pi}(t_0)=K_{Ii}(t_0)$ to reach a solution. Based on (5.5), we can obtain:

$$\mathrm{K}_{Pi}(t_0) = \frac{U_i(t_1)}{A_{1i}+B_{1i}} \tag{5.7}$$

Based on (5.6) and (5.7), the following equations can be obtained.

$$\mathrm{K}_{Ii}(t_0) = \frac{U_i(t_2)-A_{2i}\mathrm{K}_{Pi}(t_0)}{B_{2i}} \tag{5.8}$$

$$\mathrm{K}_{Pi}(t_0) = \frac{U_i(t_1)-B_{1i}\mathrm{K}_{Ii}(t_0)}{A_{1i}} \tag{5.9}$$

Based on (5.7) to (5.9), the control gains for each area can be calculated during the disturbance.

5.3.3 Flow Chart

Figure 5.3 is an exemplary flowchart of the proposed AGTC method for AGC.

The adaptive gain-tuning control (AGTC) process begins at Start. The initial PI control gains are calculated. The tie line flow ΔP_{tiei} and the angular frequency deviations $\Delta\omega_i$ (i=1~n) is sampled according to a desired sampling rate and ACE_i is calculated. If $|\Delta ACE_i|<\varepsilon_1$, (the tolerance threshold, ε_1, which is a very small value such as 0.0001 p.u.), then, there is no reason to change any of the identified parameters: $K_{Pi}(t)$ and $K_{Ii}(t)$ (i=1~n)

and the power system is under normal state. On the other hand, if $|\Delta ACE_i|>\varepsilon_1$, AGTC begins to work, then, $K_{Pi}(t)$ *and* $K_{Ii}(t)$ are adjusted based on (5.7), (5.8) and (5.9).

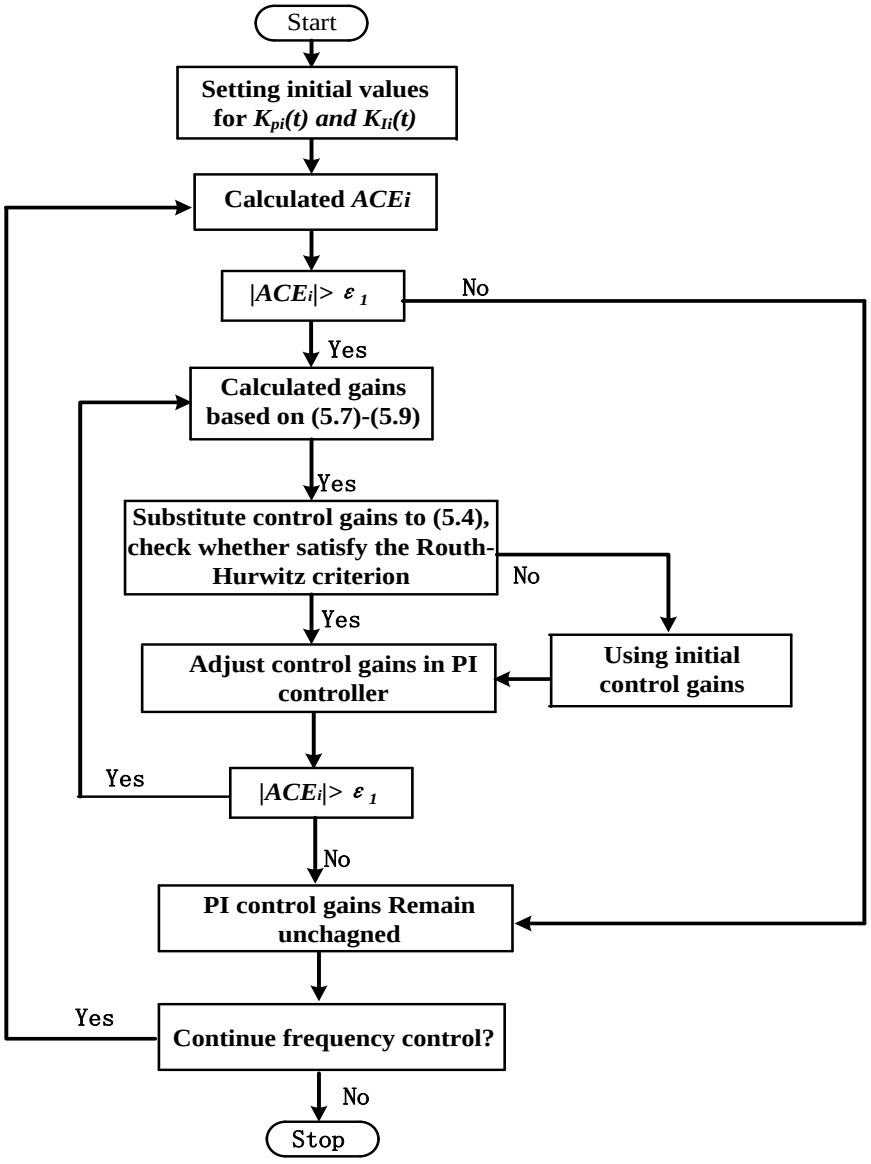

Figure 5.3 AGTC algorithm flow chart.

After obtaining the PI control gains, $K_{Pi}(t)$ and $K_{Ii}(t)$ need to be substituted to (5.4) to check whether the PI control gains satisfy the Routh-Hurwitz criterion. If satisfied, the PI control gains will be updated based on the calculated control gains; otherwise, the initial control gains will be selected instead of the calculated control gains to avoid system frequency oscillation.

After checking the Routh-Hurwitz criterion, ACE_i will be checked again to see whether it is within the tolerance threshold ε1. If it is not within the threshold, the PI control gains need to be recalculated until the ACE_i is less than the given threshold ε1. When ACE_i is less than ε1, the algorithm stops and the control gains remain the same.

Since it is necessary to continuously perform the frequency control process, the process returns to the block of measuring load changes.

5.4 Wind Power Model

The wind energy tends to be variable and uncertain due to the effects of the natural and topographical conditions. Based on the previous works [1, 71], wind speed can be modeled as (5.10) to mimic the real time wind speed.

$$V(t) = V_m(t) + V_e(t) \tag{5.10}$$

A normal distribution is applied to the wind speed forecast error in this paper. The model is written as follows:

$$V_e(t) = \mathrm{N}\left(\mu_e(t), \sigma_e^2(t)\right) \tag{5.11}$$

where

$V_m(t)$=forecast wind speed

$V_e(t)$= wind speed forecast error at time t;

N denotes normal distribution;

$\mu_e(t)$= mean value of $V_e(t)$;

$\sigma_e^2(t)$= variance of $V_e(t)$;

Then, the wind power output of the aerodynamic system can be expressed as equation as following,

$$P_t = C_p(\lambda, \beta)\frac{\rho\pi R^2}{2}V(t)^3 \tag{5.12}$$

where, P_t is the mechanical output power of the wind turbine; C_p is the performance coefficient of the wind turbine; ρ is the air density; R is the radius of wind turbine blades; $V(t)$ is the real time wind speed; λ is the tip speed ratio of the rotor blade tip speed to wind speed, $\lambda = \frac{R\omega_t}{V(t)}$ in which ω_t is the speed of the low-speed shaft; and β is the blade pitch angle.

A generic equation is used to model $C_p(\lambda, \beta)$:

$$C_p(\lambda, \beta) = 0.5176\left(\frac{116}{\lambda_i} - 0.4\beta - 5\right)e^{-\frac{21}{\lambda_i}} + 0.0068\lambda \tag{5.13}$$

with

$$\frac{1}{\lambda_i} = \frac{1}{\lambda + 0.08\beta} - \frac{0.035}{\beta^3 + 1} \tag{5.14}$$

Therefore, with given wind speed, the wind power output can be calculated. In this work, the wind energy conversion system (WECS) operating in partial load region is considered since this region contains considerable wind power variation. A maximum power point tracking (MPPT) algorithm is used in WECS such that the energy conversion efficiency is maximized in the partial load region. $C_p(\lambda, \beta)$ can be chosen as 0.45 and the other wind turbine system parameters are chosen in accordance with [72].

5.5 Simulation Results

5.5.1 Studied System

In this section, the adaptive gain-tuning control (AGTC) is tested on the IEEE 39-bus system with 3 areas, 10 machines and 3 wind farms as shown in Figure 5.4. The studied system is simulated based on MATLAB software. The intra-area lines are considered in the power flow calculation, and the tie-line flows are used for control studies. The simulation result is compared with the original control with fixed control gains. The system parameters are shown in Table 5.1 [49, 73].

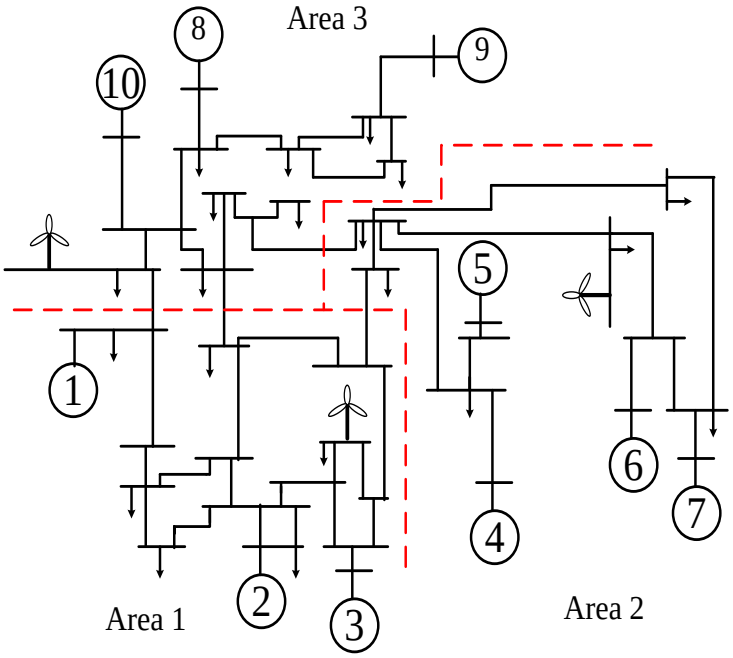

Figure 5.4 IEEE 39 bus system

Table 5.1 System Parameters

Area	Gen.	H	R	D	τ_g	τ_T
1	1	70.0	0.05	1	0.08	0.04
	2	30.3	0.05	1	0.08	0.04
	3	35.8	0.05	1	0.08	0.04
2	4	28.6	0.05	1	0.08	0.04
	5	26	0.05	1	0.08	0.04
	6	34.8	0.05	1	0.08	0.04
	7	26.4	0.05	1	0.08	0.04
3	8	24.3	0.05	1	0.08	0.04
	9	34.5	0.05	1	0.08	0.04
	10	20.0	0.05	1	0.08	0.04

In the simulation, the wind speeds at area 1, area 2 and area 3 are obtained from actual operational data at National Wind Technology Center M2 Meter on Mar. 27th 2014 [74]. The wind speed shown in Table 5.2 was measured per minute. The measured wind speed is considered as forecast wind speed $V_m(t)$. The mean value of the wind speed forecast error $\mu_e(t)$ is set at 0 and the deviation of the wind speed forecast error $\sigma_e^2(t)$ is set at $0.05V_m(t)$. In the simulation, the wind speed is sampled every second. The rated wind power output for areas 1, 2 and 3 is 150 MW.

Table 5.2 Wind Speed Data

Time (min)	Area 1(m/s)	Area 2(m/s)	Area 3(m/s)
1	7.1368	8.1652	5.7231
2	6.8243	7.5242	5.5949
3	5.5789	12.516	5.3815
4	5.5942	14.156	5.6022
5	5.0617	10.113	5.5912
6	5.6466	11.407	5.4507
7	5.2773	11.683	5.5002
8	5.6786	11.138	5.6437
9	5.0952	10.335	5.7857
10	5.3341	13.044	5.742
11	4.9394	11.198	5.9416
12	5.4907	8.8389	6.4208
13	5.466	10.234	6.4463
14	5.3939	12.642	6.4113
15	4.2183	9.3247	6.5934

Table 5.3 Initial PI control gains

Area	PI Controller	AGTC (Initial Gains)	Original (Well Tuned)
1	K_P	0.05	0.118
	K_I	0.05	0.118
2	K_P	0.07	0.118
	K_I	0.07	0.118
3	K_P	0.1	0.118
	K_I	0.1	0.118

Figure 5.5 shows the wind power profiles. In the system, the original control is conventional PI controller with fixed control gains. In this part, the proposed control method will be compared with the original control with wind energy sources in different areas. The initial PI control gains are shown in Table 5.3. Note, the initial gains shown in Table 5.3 are one of many choices from the solution scope. All the initial control gains satisfying the conditions in Section 5.3.1 can be chosen. However, in order to avoid possible overshooting, smaller control gains satisfying (5.4) are chosen for the PI controllers. The original control with fixed control gains in Table 5.3 are tuned based on the trial and error approach. The subsections from 5.5.2 to 5.5.4 compared the proposed control simulation results with the original control using the well-tuned control gains.

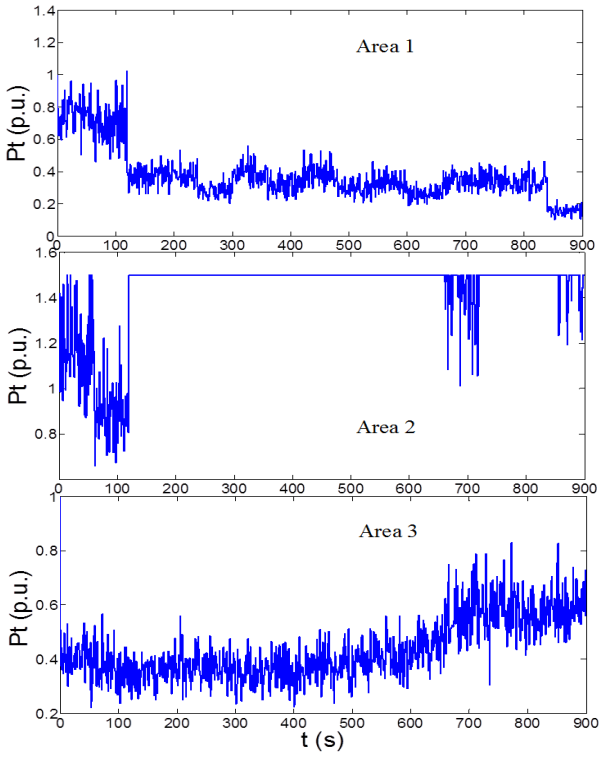

Figure 5.5 Wind power profile for the three areas.

5.5.2 Integrated Wind Power in Areas 1 and 3

All the parameters are kept unchanged. The wind power is added in areas 1 and 3. The results of the original control method and the proposed AGTC method are shown in Figures 5.6 and 5.7.

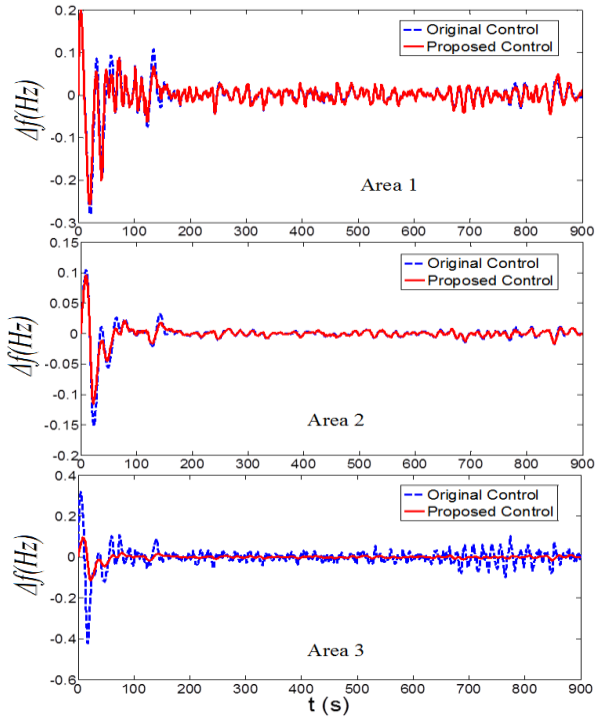

Figure 5.6 Results of frequency deviation with wind in Areas 1 and 3.

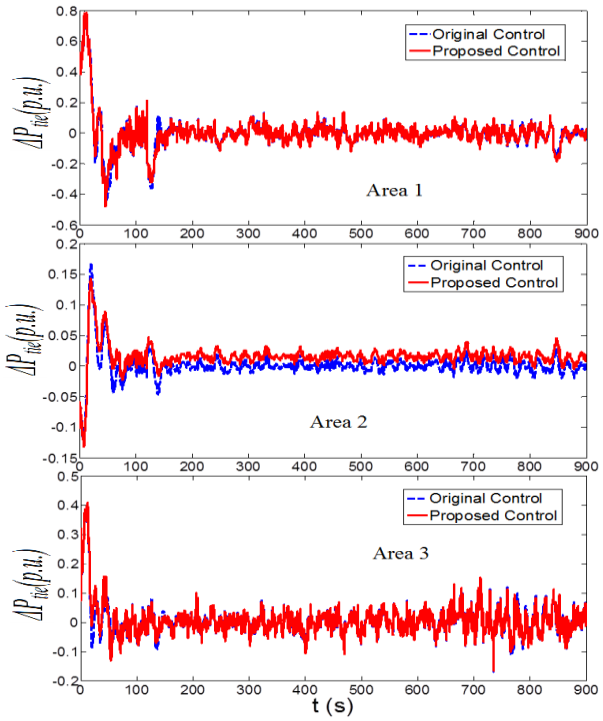

Figure 5.7 Results of tie power deviation with wind in Areas 1 and 3.

Figures 5.6 and 5.7 show the frequency deviations, Δf, and the tie line flow deviation, ΔP_{tie}, in each area, respectively. From the results, it is evident that the proposed AGTC can achieve a better and smoother response than the original PI control which has well-tuned control gains especially in Area 3. The reason is that the fixed PI control gains cannot guarantee the desirable response during variable wind power. However, with AGTC, the PI control gains are continually self-adjusted to meet the requirement of varying power system operation condition.

The PI control gains of the proposed control are also shown in Figures 5.8 and 5.9. It can be observed that with the proposed AGTC, the PI control parameters are no longer fixed under different wind speed over the studied time duration. They are dynamically self-adjusted in real time to keep system frequency at 60Hz under different wind speed. Also, with the proposed control method, the control parameter adaption is immediate and can be considered as no delay, because the computing time is around milliseconds which can be ignored and the hardware delay is also negligible.

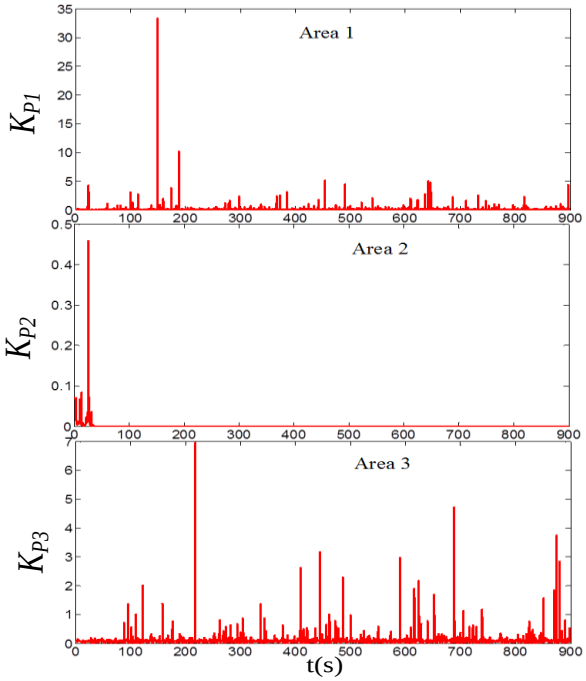

Figure 5.8 Results of K_P with wind in areas 1 and 3.

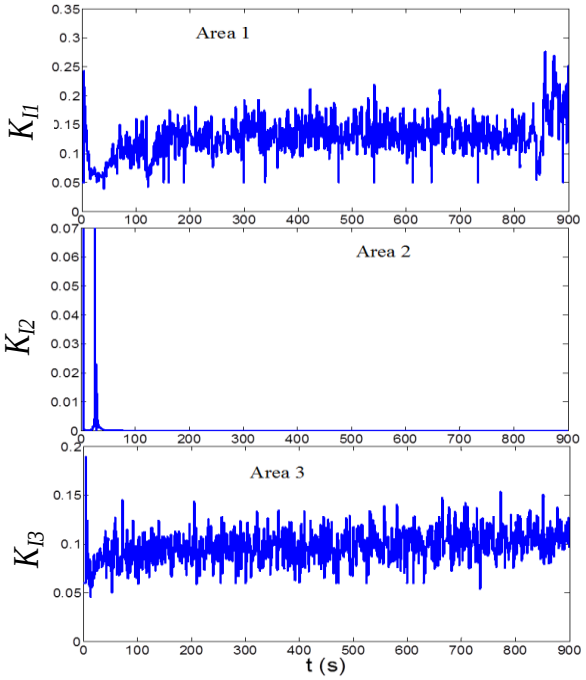

Figure 5.9 Results of K_I with wind in areas 1 and 3.

5.5.3 Integrated Wind Power in Areas 1 and 2

All the parameters are kept unchanged in this case study. The wind power is added in areas 1 and 2. The results of the original control method and the proposed AGTC method are shown in Figure 5.10 and Figure 5.11, respectively.

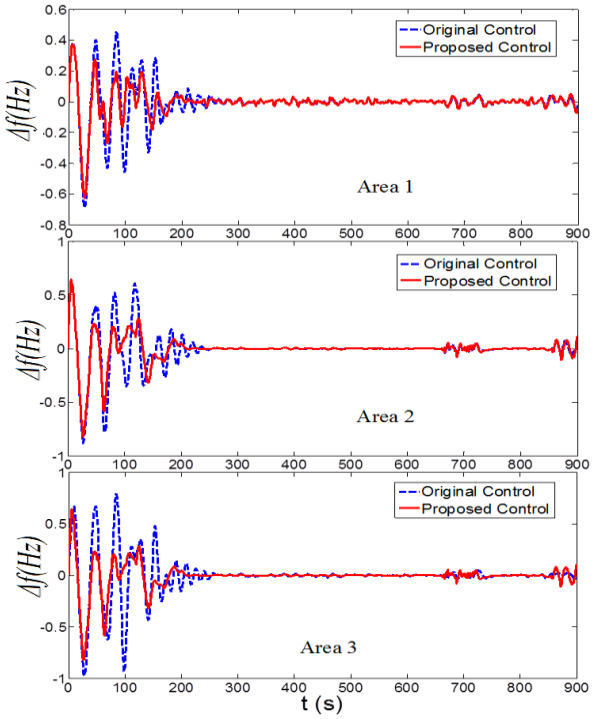

Figure 5.10 Results of frequency deviation with wind in areas 1 and 2.

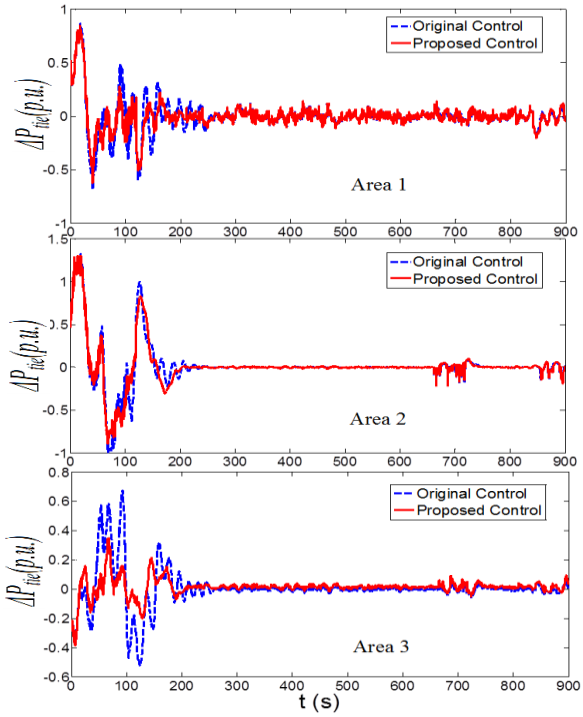

Figure 5.11 Results of tie power deviation with wind in areas 1 and 2.

Figure 5.10 and Figure 5.11 illustrate the frequency deviations Δf and the tie line flow deviation ΔP_{tie} in each area. From the results, it is evident that the proposed AGTC can achieve a better and smoother response than the original method with the well-tuned control gain. With AGTC, both frequency deviation and tie line flow deviation are reduced.

The PI control gains of the proposed control approach for each area are shown in Figure 5.12 and Figure 5.13. Similar to the study in the previous sub-section 5.5.2, with the proposed AGTC, the PI control parameters can be automatically and dynamically adjusted under different wind speeds during the disturbance to keep system frequency at 60Hz.

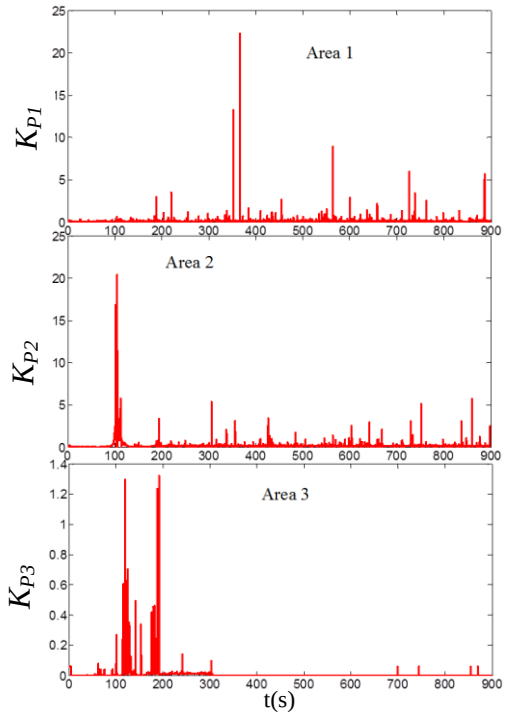

Figure 5.12 Results of K_P with wind in areas 1 and 2.

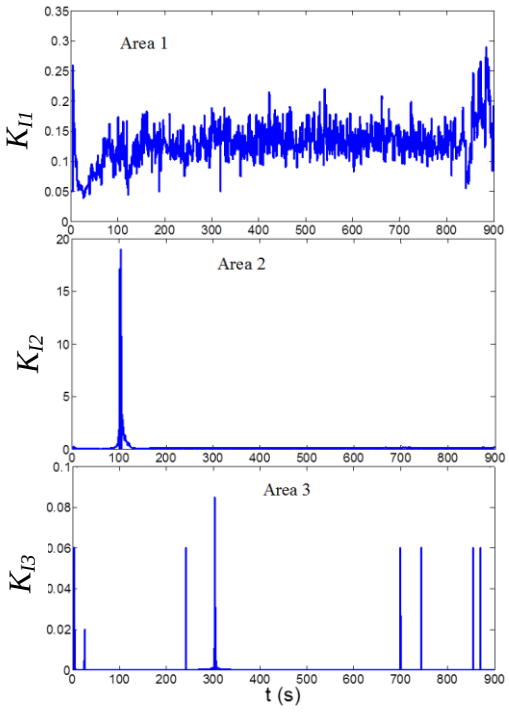

Figure 5.13 Results of K_I with wind in areas 1 and 2.

5.5.4 Integrate Wind Power in All Areas

In this simulation study, all the parameters are kept unchanged from the original one. The wind power sources are added in all three areas: areas 1, area 2, and area 3. The results of the original control method and the proposed AGTC are shown in Figures 5.14 and 5.15, which illustrate the frequency deviation Δf and the tie line flow deviation ΔP_{tie} in each area.

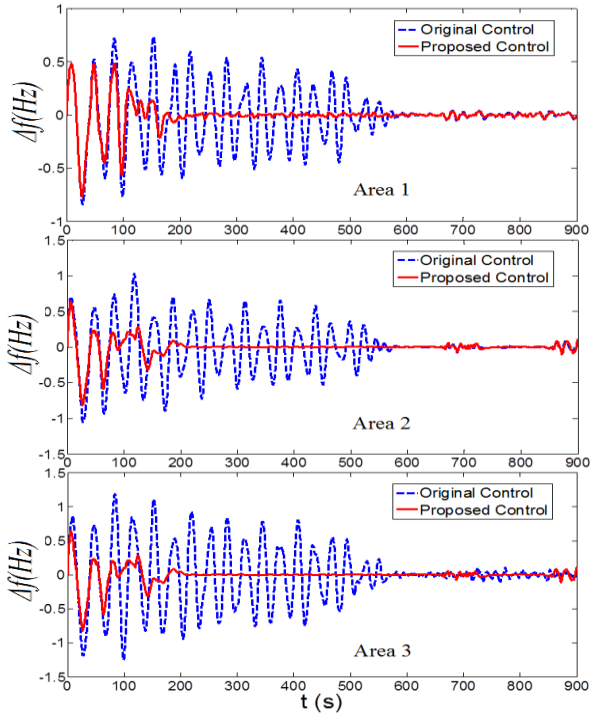

Figure 5.14 Results of frequency deviation with wind in all areas.

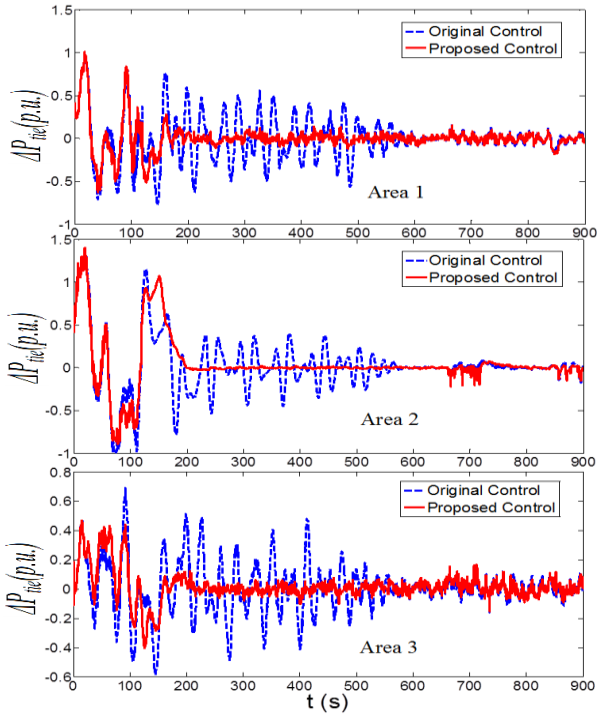

Figure 5.15 Results of tie power deviation with wind in all areas.

From the results, it is evident that the proposed AGTC can keep the system frequency stable. Since the fixed control gains cannot satisfy the requirements of the varying wind power, the AGC with original control cannot bring the system frequency back to 60 Hz and the AGC has a very poor response. However, with AGTC, both frequency deviations and tie line flow deviations are dramatically reduced.

The PI control gains of the proposed control for each area are shown in Figure 5.16 and Figure 5.17. Similar to the study in the previous sub-sections 5.5.2 and 5.5.3, with the proposed AGTC, the PI control parameters can be automatically and dynamically adjusted

under different wind speeds over the 900-second duration such that the control gains can be always dynamically adjusted and the AGC has much better responses.

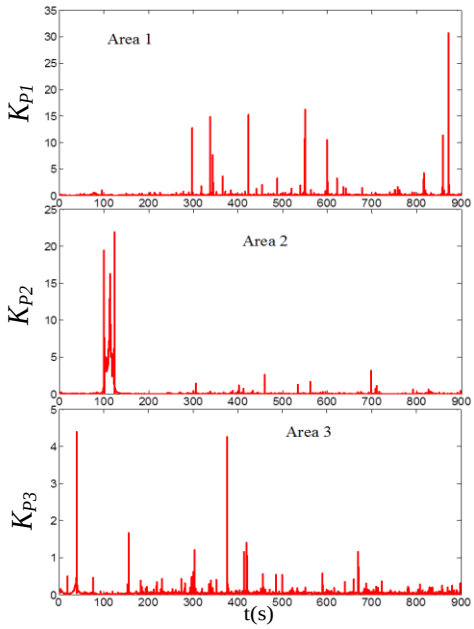

Figure 5.16 Results of K_P with wind in all areas.

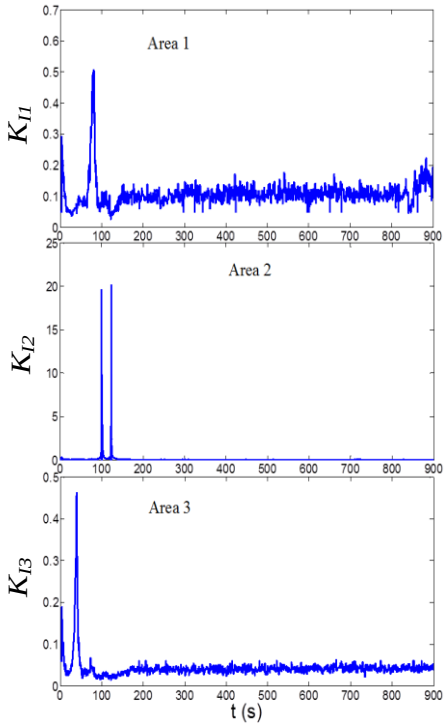

Figure 5.17 Results of K_I with wind in all areas.

5.6 Conclusions

The above AGC studies show convincing results that the proposed AGTC can achieve a better and more consistent response than the original control. With the proposed AGTC, the initial PI control gains are calculated in advance and kept the same for each specific area. Then, the PI control gains will be dynamically and autonomously adjusted during the frequency control process, based on the area control error (ACE) for area 1, area 2 and area 3, respectively. Therefore, a much better response for frequency regulation in real-time can always be obtained with the dynamic PI gains, and the desired performance can be

achieved. However, the original fixed-gain controller, which is well tuned for a specific given operating condition, may be inefficient or incapable of regulating the frequency under continuously varying operating conditions.

CHAPTER 6

CONCLUSIONS AND RECOMMENDATIONS

6.1 Summary of Contributions

Various STATCOM control methods have been reviewed including many applications of PI controllers. However, these previous works obtain the PI gains via a trial and error approach or extensive studies with a tradeoff of performance and applicability. Hence, control parameters for the optimal performance at a given operating point may not be effective at a different operating point.

To address the challenge, this work proposes a new control model based on adaptive PI control, which can self-adjust the control gains dynamically during a disturbance such that the performance always matches a desired response, regardless of the change of the operating condition. Since the adjustment is autonomous, this gives the "plug-and-play" capability for STATCOM operation. In the simulation study, the proposed adaptive PI control for STATCOM is compared with the conventional STATCOM control with pre-tuned fixed PI gains to verify the advantages of the proposed method. The results show that the adaptive PI control gives consistently excellent performance under various operating conditions such as different initial control gains, different load levels, changes of transmission network, consecutive disturbances and a severe disturbance. In contrast, the

conventional STATCOM control with fixed PI gains may perform acceptable in the original system, but may not perform as efficiently as the proposed control method when there is a change of the system conditions.

Next, this work proposes the flatness-based adaptive control (FBAC) method for STATCOM voltage regulation. By this method, the nonlinear STATCOM system is equivalent to a linear system, and the trajectories of all system variables can be directly and easily controlled by controlling flat output and its derivatives without solving differential equations. Further, the control gains can dynamically self-adjust during the voltage regulation after a disturbance. Thus, the performance from the FBAC always gives a consistent match to a desired response, regardless of the change of operating conditions. However, the original PI control and the flatness-based control (FBC), even if well-tuned for the given operating condition, may be inefficient or incapable to correct voltage when there is a change of the operating conditions.

Finally, an adaptive gain-tuning control (AGTC) for AGC with effects of wind resources is presented in this dissertation. By the proposed control method, the initial control gains are calculated first. Then, the wind energy with actual wind speed is integrated in power systems. During the disturbance, the control gains are dynamically adjusted such that the performance always matches a desired response. In the simulation study, the proposed control for AGC is compared with the conventional control with

pre-tuned PI gains to verify the advantages of the proposed method. The results show that the AGTC consistently provides excellent performance under variable wind power. Moreover, the deviation of angular frequency and tie line flow with the proposed control is much lower than the original control.

6.2 Future Works

The following directions may be considered as future works of this dissertation.

6.2.1 Develop a generic control method

- Extension to other power system control problems such as DFIG can be explored.
- More research work can focus on developing a generic control model with plug-and-play feature from the proposed method.

6.2.2 Test in a hardware test bed

- The proposed control methods may be tested in a hardware test bed, and a real system application can be explored.

LIST OF REFERENCES

[1] Y. Xu, Q. Hu, and F. Li, “Probabilistic model of payment cost minimization considering wind power and its uncertainty,” *IEEE Trans. Sustain. Energy*, vol. 4, no. 3, pp. 716-724, July 2013.

[2] S. Dahal, N. Mithulananthan, T. Saha, “Investigation of small signal stability of a renewable energy based electricity distribution system,” *IEEE PES General Meeting*, Minneapolis, Minnesota, 2010.

[3] P. Kundur, *Power System Stability and Control*. New York: McGraw-Hill, 1994.

[4] P. Kundur, J. Paserba, V. Ajjarapu, G. Andersson, A. Bose, C. Canizares, N. Hatziargyriou, D. Hill, A. Stankovic, C. Taylor, T. V. Custem, and V. Vittal, “Definition and classification of power system stability,” *IEEE Trans. Power Syst.*, vol. 19, no. 2, pp. 1387–1401, May 2004.

[5] Maria Hanley, Jovan Ilic, “Frequency Instability Problems in North American Interconnections,” *DOE/NETL-2011/1473*, Jun 2011.

[6] N. Mithulananthan, M. M. A. Salama, C. A. Canizares and J. Reeve, "Distribution system voltage regulation and var compensation for different static load models," *International Journal of Electrical Engineering Education*, vol. 37, pp. 384-395, 2000.

[7] S Musunuri, G Dhenavi, “Comparison of STATCOM, SVC, TCSC, and SSSC Performance in Steady State Voltage Stability Improvement”, *NAPS*, 2010.

[8] Mehrdad Ahmad, Mostafa Alinezhad, "Comparison of SVC and STATCOM in Static Voltage Stability Margin Enhancement", *Proceedings of World Academy of Science, Engineering and Technology*, vol. 38, Feb. 2009.

[9] A.H.M.A. Rahim, E.P. Nowicki, and J.M. Bakhashwain, "Fuzzy STATCOM Control Strategies for Power System Stabilization," *ICGST International Journal on Automatic Control and Systems Engineering*, ACSE, pp. 41-48, Feb. 2006.

[10] H. Saadat, *Power System Analysis*, 2nd Edition, McGraw-Hill, 2004.

[11] N. Jaleeli, L. S. VanSlyck, D. N. Ewart, L. H. Fink, and A. G. Hoffmann, "Understanding automatic generation control," *IEEE Trans. Power Syst.*, vol. 7, no. 3, pp. 1106–1122, Aug. 1992.

[12] J. Tlaq and F. Al-Basri, "Adaptive fuzzy gain scheduling for load frequency control," *IEEE Trans. Power Syst.*, vol. 14, no. 1, pp. 145–150, Feb. 1999.

[13] Pan, C. T., and Liaw, C. M., "An Adaptive Controller for Power System Load-Frequency Control," *IEEE Trans. Power Sys.*, vol. 4, no. 1, pp. 122-128, 1989.

[14] UCTE, *UCTE Operation Handbook*, Jul. 2004.

[15] Y. G. Rebours, D. S. Kirschen, M. Trotignon, and S. Rossignol, "A survey of frequency and voltage control ancillary services—Part I: Technical features," *IEEE Trans. Power Syst.*, vol. 22, no. 1, pp. 350–357, Feb. 2007.

[16] C.-H. Liu and Y.-Y. Hsu, "Design of a self-tuning PI controller for a STATCOM using particle swarm optimization," *IEEE Trans. Ind. Electron.,* vol. 57, no. 2, pp. 702–715, Feb. 2010.

[17] F. Li, J. D. Kueck, D. T. Rizy, T. King, "A preliminary analysis of the economics of using distributed energy as a source of reactive power supply," *Oak Ridge National Laboratory First Quarterly Report for Fiscal Year 2006*, Oak Ridge, TN, Apr. 2006.

[18] A. Jain, K. Joshi, A. Behal, and N. Mohan, "Voltage regulation with STATCOMs: Modeling, control and results," *IEEE Trans. Power Del.,* vol. 21, no. 2, pp. 726–735, Apr. 2006.

[19] D. Soto and R. Pena, "Nonlinear control strategies for cascaded multilevel STATCOMs," *IEEE Trans. Power Del.,* vol. 19, no. 4, pp. 1919–1927, Oct. 2004.

[20] F. Liu, S. Mei, Q. Lu, Y. Ni, F. F. Wu, and A. Yokoyama, "The nonlinear internal control of STATCOM: Theory and application," *Int. J. Elec. Power & Energy Syst.,* vol. 25, no. 6, pp. 421–430, 2003.

[21] C. Hochgraf and R. H. Lasseter, "STATCOM Controls for Operation with Unbalanced Voltage," *IEEE Trans. Power Del.,* vol. 13, no. 2, pp. 538–544, Apr. 1998.

[22] G. E. Valdarannma, P. Mattavalli, and A. M. Stankonic, “Reactive power and unbalance compensation using STATCOM with dissipativity based control,” *IEEE Trans. Control Syst. Technol.*, vol. 19, no. 5, pp. 598–608, Sep. 2001.

[23] Wang, H.F., “Phillips-Heffron model of power systems installed with STATCOM and applications,” *IEE Proc.-Gener. Transmi. Distib.*, vol. 146, no 5, pp. 521-527, Sep. 1999.

[24] H.F. Wang, "Applications of damping torque analysis to statcom control", *I. J. of Elec. Pwr & Energy Sys.*, vol. 22, pp. 197-204, 2000.

[25] Y. Han, Y.O. Lee and C.C. Chung, “Modified non-linear damping of internal dynamics via feedback linearization for static synchronous compensator”, *IET Gener. Transm. Distrib.*, vol. 5, no. 9, pp. 930–940, 2011.

[26] A. H. Norouzi and A. M. Sharaf, “Two control schemes to enhance the dynamic performance of the STATCOM and SSSC,” *IEEE Trans. Power Del.*, vol. 20, no. 1, pp. 435–442, Jan. 2005.

[27] M. S. E. Moursi and A. M. Sharaf, “Novel controllers for the 48-pulse VSC STATCOM and SSSC for voltage regulation and reactive power compensation,” *IEEE Trans. Power Syst.*, vol. 20, no. 4, pp. 1985–1997, Nov. 2005.

[28] http://www.mathworks.com/help/toolbox/physmod/powersys/ug/f8-8531.html, last access in Feb. 2012.

[29] H. Li, F. Li, J. D. Kueck, and D. T. Rizy "Adaptive Voltage Control with Distributed Energy Resources: Algorithm, Theoretical Analysis, Simulation and Field Test Verification," *IEEE Transactions on Power Systems*, vol. 25, no. 3, pp. 1638-1647, August 2010.

[30] H. Li, F. Li, Y. Xu, D.T. Rizy and S. Adhikari, "Autonomous and Adaptive Voltage Control using Multiple Distributed Energy Resources," *IEEE Transactions on Power Systems*, vol. 28, no. 2, pp. 718-730, May 2013.

[31] Pranesh Rao, M. L. Crow, and Zhiping Yang, "STATCOM Control for Power System Voltage Control Applications," *IEEE Trans. Power Del.*, vol. 15, no. 4, pp. 1311-1317, Oct. 2000.

[32] W. L. Chen and Y. Y. Hsu, "Controller design for an induction generator driven by a variable speed wind turbine," *IEEE Trans. Energy Convers.*, vol. 21, no. 3, pp. 625–635, Sep. 2006.

[33] Keyou Wang, and Mariesa L. Crow, "Power System Voltage Regulation via STATCOM Internal Nonlinear Control," *IEEE Trans. Power Syst.*, vol. 26, no. 3, pp. 1252-1262, Aug. 2011.

[34] V. Spitsa, A. Alexandrovitz, and E. Zeheb, "Design of a robust state feedback controller for a STATCOM using a zero set concept," *IEEE Trans. Power Del.*, vol. 25, no. 1, pp. 456–467, Jan. 2010.

[35] An Luo, Ci Tang, Zhikang Shuai, Jie Tang, Xian Yong Xu, and Dong Chen, "Fuzzy-PI-Based Direct-Output-Voltage Control Strategy for the STATCOM Used in Utility Distribution Systems, " *IEEE Trans. Ind. Electron.*, vol. 56, no. 1, pp. 2401-2411, July 2009.

[36] L. O. Mak, Y. X. Ni, and C. M. Shen, "STATCOM with fuzzy controllers for interconnected power systems," *Elect. Power Syst. Res.*, vol. 55, pp. 87–95, 2000.

[37] A. Gensior, H. Sira-Ramírez, J. Rudolph, and H. Güldner, "On some nonlinear current controllers for three-phase boost rectifiers," *IEEE Trans. Ind. Electron.*, vol. 56, no. 2, pp. 360–370, Feb. 2009.

[38] Q. Song, W. Liu, and Z. Yuan, "Multilevel optimal modulation and dynamic control strategies for STATCOMs using cascaded multilevel inverters," *IEEE Trans. Power Del.*, vol. 22, no. 3, pp. 1937–1937, Jul. 2007.

[39] D.-C. Lee, G.-M. Lee, and K.-D. Lee, "DC-bus voltage control of three phase ac/dc PWM converters using feedback linearization," *IEEE Trans. Ind. Applicat.*, vol. 36, pp. 826–833, May 2000.

[40] E. Song, "Experimental validation of a flatness-based control for a voltage source converter," M.S. thesis, Dept. Elect. Comput. Eng., Univ. Alberta, Edmonton, AB, Canada, 2006.

[41] E. Song, A. F. Lynch, and V. Dinavahi, “Experimental validation of nonlinear control for a voltage source converter,” *IEEE Trans. Control Syst. Technol.*, vol. 17, no. 5, pp. 1135–1144, Sep. 2009.

[42] A. Gensior, J. Rudolph, and H. Güldner, “Flatness based control of three-phase boost rectifiers,” *11th Eur. Conf. Power Electron. Appl. Rec. (EPE)*, Dresden, Germany, Sep. 2005.

[43] M. Fliess, J. Lévine, P. Martin, and P. Rouchon, “Flatness and defect of non-linear systems: Introductory theory and applications,” *Int. J. Control*, vol. 61, pp. 1327–1361, 1995.

[44] H. Sira Ram ŕez and S. K. Agrawal, *Differentially Flat Systems*. New York: Marcel Dekker, 2004.

[45] P. Thounthong, S. Pierfederici, and B. Davat, “Analysis of differential flatness-based control for a fuel cell hybrid power source,” *IEEE Trans. Energy Convers.*, vol. 25, no. 3, pp. 909–920, Sep. 2010.

[46] P. Martin, R. M. Murray, and P. Rouchon, “Flat systems, equivalence and trajectory generation,” *Ecole des Mines de Paris*, Technical report, April 2003.

[47] M. van Nieuwstadt and R. Murray. “Real-time trajectory generation for differentially at systems.” *Int. Journal of Robust and Nonlinear Control*, vol. 8, no. 11, pp. 995–1020, 1998.

[48] A. Khodabakhshian and R. Hooshmand, "A new PID controller design for automatic generation control of hydro power systems," *Elect. Power and Energy Systems,* vol. 32, pp. 375-382, 2010.

[49] Maryam Hassani Variani, Kevin Tomsovic, "Distributed Automatic Generation Control using Flatness-Based Approach for High Penetration of Wind Generation," *IEEE Trans. Power Sys.*, vol. 28, no. 3, pp. 3002-3009, 2013.

[50] E. C. Anene, U. O. Aliyu, J. Levine, and G. K. Venayagamoorthy, "Flatness-based feedback linearization of a synchronous machine model with static excitation and fast turbine valving," *in Proc. IEEE Power Eng. Soc. General Meeting,* pp. 1–6, Jun. 2007.

[51] E. Rakhshani and J. Sadeh, "A reduced-order estimator with prescribed degree of stability for two-area LFC system in a deregulated environment," *in Proc. IEEE Power Systems Conference and Exposition,* pp. 1–8, 2009.

[52] Y. Oguz, H. Erdal, and S. Taskin, "Design and simulation of a LQG robust controller for an electrical power system," *Journal of Electrical and Electronics Engineering,* vol. 8, no. 2, pp. 693–698, 2008.

[53] X. Yang and O. Marjanovic, "LQG Control with Extended Kalman Filter for Power Systems with Unknown Time-delays," *in Proc. 18th IFAC World Congress,* pp. 3708–3713, 2011.

[54] Mohanty, Banaja, Sidhartha Panda, and P. K. Hota. "Controller Parameters Tuning of Differential Evolution Algorithm and its Application to Load Frequency Control of Multi-source Power System." *International Journal of Electrical Power & Energy Systems*, vol. 54, pp. 77-85, 2014.

[55] G. A. Chown and R. C. Hartman, "Design & Experience of Fuzzy Logic Controller for Automatic Generation Control (AGC)," *IEEE Trans. Power Syst.*, vol. 13, no. 3, pp. 965–970, Aug. 1998.

[56] P.K. Dash, A.C. Liew, and B.R. Mishra, "An Adaptive PID Stabilizer for Power Systems using Fuzzy Logic," *Electric Power Systems Research*, vol. 44, pp. 213–222, 1998.

[57] Ibhan Kocaarslan, Ertugrul Cam, "Fuzzy Logic Controller in Interconnected Electric Power Systems For Load-Frequency Control", *Electrical Power and Energy Systems*, vol. 27, pp. 542-549, 2005.

[58] K.R.M. Vijaya Chandrakala, S. Balamurugan, K. Sankaranarayanan, "Variable structure fuzzy gain scheduling based load frequency controller for multi source multi area hydro thermal system," *Electrical Power and Energy Systems*, vol. 53, pp. 375–381, 2013.

[59] F. Beaufays, Y. Abdel-Magid, and B. Widrow, “Application of neural network to load frequency control in power systems,” *Neural Netw.*, vol. 7, no. 1, pp. 183–194, 1994.

[60] M. Djukanovic, M. Novicevic, D. J. Sobajic, and Y. P. Pao, “Conceptual development of optimal load frequency control using artificial neural networks and fuzzy set theory,” *Int. J. Eng. Intell. Syst. Elect. Eng. Commun.*, vol. 3, no. 2, pp. 95–108, 1995.

[61] M. A. Abido, “Optimal Design of Power System Stabilizers using Particle Swarm Optimization,” *IEEE Trans. Energy Convers.*, vol. 17, no. 3, pp. 406–413, Sep. 2002.

[62] Gozde H, Taplamacioglu MC, “Automatic generation control application with craziness based particle swarm optimization in a thermal power system,” *Int J Elect Power Energy Syst*., vol. 33, pp. 8-16, 2011.

[63] Panda S, Yegireddy NK. “Automatic Generation Control of Multi-area Power System using Multi-objective Non-dominated Sorting Genetic Algorithm-II,” *Int J Electr Power Energy Syst*., vol. 53, pp. 54–63, 2013.

[64] L. Nanda, S. Mishra, and L.C. Saikia, "Maiden Application of Bacterial Foraging-Based Optimization Technique in Multi-area Automatic Generation Control," *IEEE Trans. Power systems*, vol. 24, pp. 602 - 609, May 2009.

[65] http://www.mathworks.com/help/physmod/powersys/examples/statcom-phasor-model.html, last access in Apr. 2012.

[66] C. Schauder and H. Mehta, "Vector Analysis and Control of the Advanced Static Var Compensators," *Proc. Inst. Elect. Eng., Gen., Transm.*, Distrib., vol. 140, no. 4, pp. 299–306, Jul. 1993.

[67] Z.M. Ai-Hamouz and Y.L. Abdel-Magid, "Variable Structure Load Frequency Controllers for Multi Area Power Systems," *Int. J. Electr. Power Energy. Syst.*, vol. 15, no. 5, pp. 23-29, 1993.

[68] Yang Mi, Yang Fu, Chengshan Wang, and Peng Wang, "Decentralized Sliding Mode Load Frequency Control for Multi-Area Power Systems," *IEEE Transactions on Power Systems*, vol. 28, no. 4, pp. 4301-4309, Nov. 2013

[69] Elgerd OI. *Electric energy systems theory*. An introduction. New Delhi: Tata McGraw-Hill, 1983.

[70] K. S. S. Ramakrishna, Pawan Sharma, T. S. Bhatti, "Automatic Generation Control of Interconnected Power System with Diverse Sources of Power Generation," *International Journal of Engineering, Science and Technology*, vol. 2, no. 5, 2010, pp. 51-65.

[71] Jin, Z., Li, F., Ma, X., Djouadi, and S.M., "Semi-Definite Programming for Power Output Control in a Wind Energy Conversion System," *IEEE Transactions on Sustainable Energy*, vol. 5, no. 2, pp. 466-475, April 2014.

[72] M. Soliman, O. P. Malik, and D. T. Westwick, "Multiple model predictive control for wind turbines with doubly fed induction generators," *IEEE Trans. Sustain. Energy*, vol. 2, no. 3, pp. 215–225, Jul. 2011.

[73] V. Venkatasubramanian, M. Sherwood, V. Ajjarapu, and B. Leonardi, Real-Time Security Assessment of Angle Stability using Synchrophasors PSERC, Final Project Rep., May 2010.

[74] http://www.nrel.gov/midc/nwtc_m2/, last access on Sept. 5th, 2014.

[75] C. S. Chang and W. H. Fu, "Area load frequency control using fuzzy gain scheduling of PI controllers," *Elect. Power Syst. Res.*, vol. 42, no. 2, pp. 145–152, 1997.

APPENDIX

Publications

Journal

[1] **Yao Xu**, Qinran Hu and Fangxing Li, "Probabilistic Model of Payment Cost Minimization Considering Wind Power and its Uncertainty," *IEEE Transactions on Sustainable Energy*, vol. 4, no. 3, pp. 716-724, Jul. 2013.

[2] **Yao Xu** and Fangxing Li**,** "Adaptive Control of STATCOM for Voltage Regulation," *IEEE Transactions on Power Delivery*, vol. 29, no. 3, pp. 1002-1011, Jun. 2014.

[3] **Yao Xu**, Fangxing Li, Zhiqiang Jin, and Can Huang, "Flatness-based Adaptive Control of STATCOM," submitted to *Electric Power Systems Research*.

[4] **Yao Xu**, Fangxing Li, Zhiqiang Jin, and Maryam Hassani Variani, "Dynamic Gain-Tuning Control (DGTC) Approach for AGC with Effects of Wind Power," submitted to *IEEE Transactions on Power System*.

Patent

[5] Fangxing Li, **Yao Xu** and Kevin Tomsovic, "Adaptive Controller for STATCOM to Enhance Voltage Stability," U.S. Patent (8,836,163), issued on 09/16/2014.

VITA

Yao Xu joined The University of Tennessee at Knoxville in August 2010 to pursue the Ph.D. degree in Electrical Engineering. She received the B.S. and M.S. degrees in electrical engineering from Changsha University of Science and Technology, China, in 2006 and 2009, respectively. She was a recipient of the Min Kao Graduate Fellowship in Electrical Engineering. Her research interests include utility application of power electronics, power system control, and power markets.